SENSOR AND SIMULATION NOTES

NOTE 226

August 1976

Transient Analysis of a Finite Length Cylindrical Scatterer

Very Near a Perfectly Conducting Ground

T. H. Shumpert
Auburn University
Auburn, Alabama

D. J. Galloway
Dynetics, Inc.
Huntsville, Alabama

ABSTRACT

In attempting to model and predict the magnitude of the surface currents induced on aircraft in the ground-alert mode, it is necessary to examine the effects of the near proximity of the earth's surface. For thin cylindrical scatterers sufficiently far removed (several wavelengths) from the surface, these effects may be taken into account with filamentary currents on the scatterer and its image. However, if the scatterer is moved very near (a fraction of a wavelength) to the ground, the assumption of filamentary currents is invalidated. In this note a transmission line mode approximation is used to model the circumferential variations of the surface current induced on a finite length cylindrical scatterer very near a perfect ground. This solution is compared to previous solutions based on filamentary currents. The results give clear indications as to when the more sophisticated approach should be used to obtain valid solutions to the scattering problems of this type.

TABLE OF CONTENTS

I. INTRODUCTION

Previous investigations have considered the interactions of thin
cylinders with an electromagnetic pulse over perfectly conducting
grounds [1-5]. Limitations imposed by the so-called "thin-wire"
assumptions and approximations are inherent short-comings [6-8]. In
general, these approximations can be divided into three areas:
(1) current is assumed to flow only in the direction of the wire axis,
(2) boundary conditions are applied only to the axial component of the
electromagnetic field at the wire surface, (3) current and charge den-
sities are approximated by filaments of current and charge on the wire
axis [9-11]. The emphasis of this investigation is on the last of
these approximations. The first assumption ignores the induced current
in the circumferential direction, which is an appropriate approach [7],
[12] provided the length of the cylindrical scatterer is much greater
than its radius. With this restriction, the scattered field is deter-
mined primarily by the longitudinal component of the current so that
the significance of the circumferential component is minimal. It is
well known that for infinitely long cylinders, the axial component of
the incident electric field produces only currents in the axial direc-
tion and the component of the incident electric field in the circumfer-
ential direction results in only circumferential currents [13-21]. For
finite length cylinders, either component of the incident electric
field excites current in both the axial and circumferential directions

[22-25]. The second "thin-wire" approximation does not take into account that portion of the axial current contributed by the circumferential component of the incident electric field. The axial current caused by the axial component of the incident field is much more significant than that resulting from an incident electric field with a circumferential component. This restriction, that the cylindrical scatterer be thin, makes this approximation very reasonable [26]. Representing the current and charge densities induced on a thin cylindrical scatte by filaments of current and charge on the cylinder axis is in effc.t assuming that their circumferential variations are uniform [1-4]. This is well founded for a thin cylindrical scatterer many radii away from the ground plane [6], [27], but certainly not correct when the cylindrical scatterer is positioned near the ground plane - on the order of a radius away. In this analysis, the circumferential behavior of the induced currents on a thin cylinder is taken into account when the scatterer is near the ground plane.

A Pocklington type integro-differential equation [11] is formulated for the current induced on the thin cylinder and its image in terms of a complex frequency. This equation is reduced to a system of algebraic matrix equations through application of the method of moments [9], [11], [28-29]. This transient analysis problem employs the singularity expansion method, which was formalized and discussed in general by Baum, among others [30-33], and practically demonstrated by several researchers [1-3], [34-37]. The complex natural resonances, natural mode vectors, and normalization coefficients are calculated and compared to those found through enforcement of all the "thin-wire"

4

assumptions. As the cylinder approaches the ground plane, the trajec-

tories of certain singularities are presented and discussed. Induced

currents are calculated for various geometries and incident fields.

II. THEORY

Integro-differential Equation

Consider a finite length, infinitely thin-walled, perfectly conducting, right circular cylinder as shown in Figure 2-1. The cylinder is near and parallel to an infinite, perfectly conducting, ground plane. As indicated in the figure, the cylinder is of length L, radius a and height h above the ground plane. A combined cartesian and cylindrical coordinate system is centered on the cylinder as shown. The system, consisting of the cylinder and the ground plane, is illuminated by a transient incident field of electromagnetic radiation. The incident field is, by definition, that field which would exist if the cylinder and ground plane were absent. As shown in Figure 2-2, the incident electromagnetic field propagates in a general direction described by the angle θ^i with respect to the z axis and the angle ϕ^i with respect to the x axis. It is then desired to obtain the induced currents on the cylinder as a function of time.

By application of image theory [18], [38-39], the cylinder and incident TEM transient plane wave, in conjunction with the perfect ground plane, are transformed into an equivalent problem consisting of the "original cylinder" - to be called the object cylinder - and its image - to be named the image cylinder. According to image theory, the incident field must be imaged also - producing the equivalent two-body problem shown in Figure 2-3. Two individual coordinate systems are

6
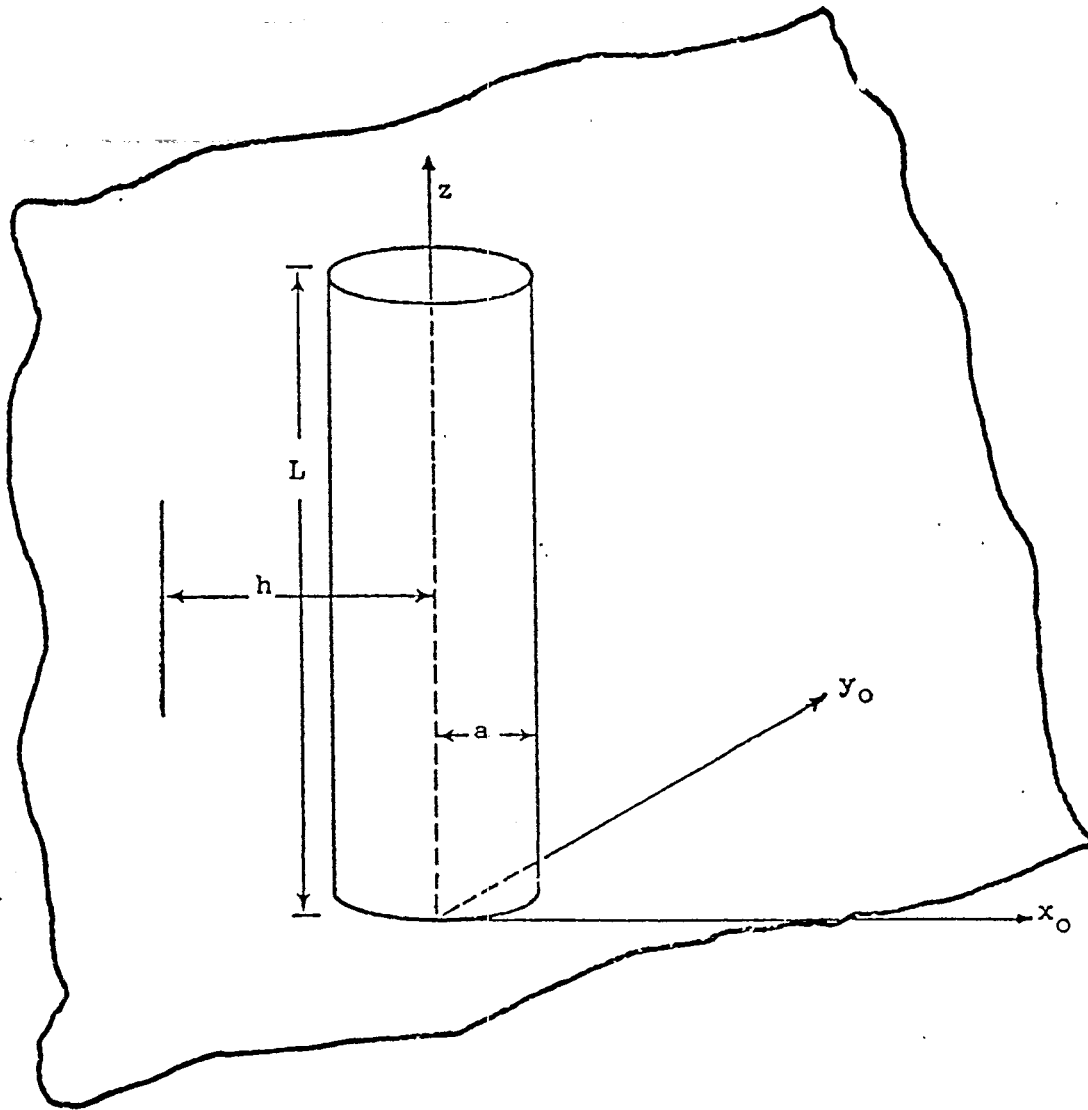
Figure 2-1.   Finite Length, Right Circular Cylinder -
Near and Parallel to Perfect Ground Plane
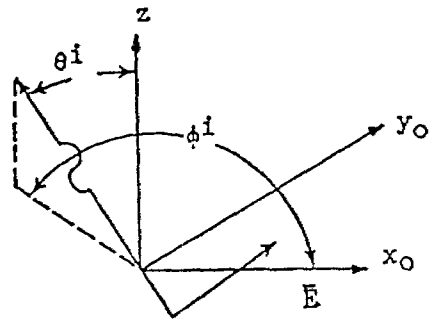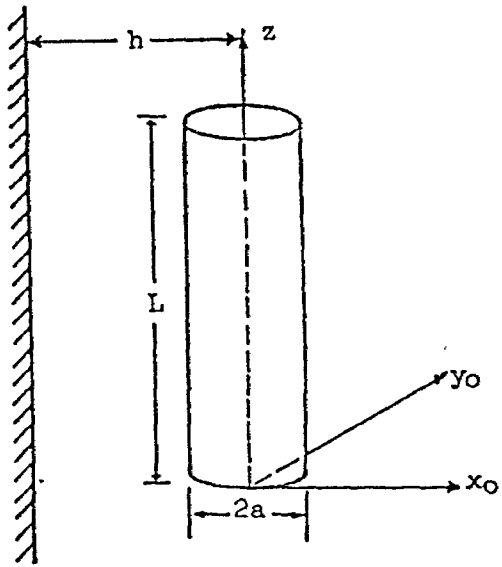
Figure 2-2.   Incident Field

IMAGE
CYLINDER

OBJECT
CYLINDER
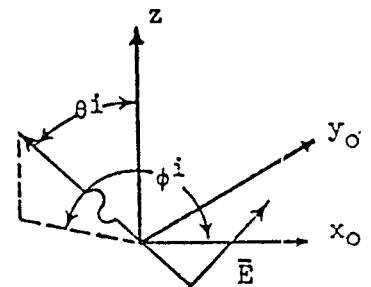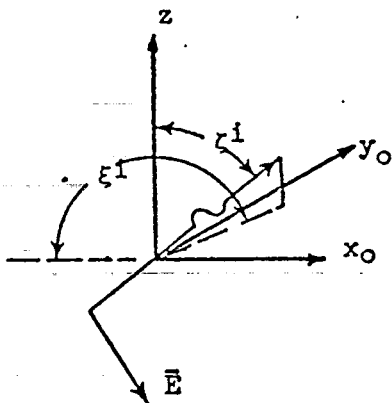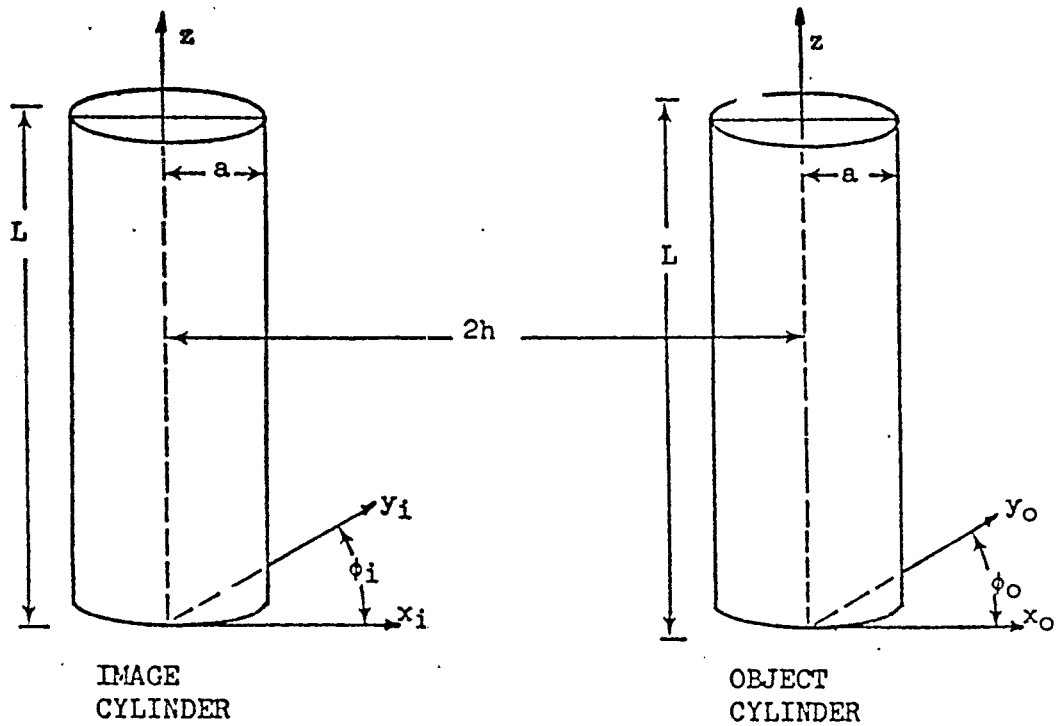
(Note: due to image theory, $\zeta^i = \theta^i$ and $\xi^i = \phi^i$; subscripts refer to
coordinate dependence and superscripts refer to incident field
dependence.)

Figure 2-3. Equivalent Image Theory Problem

defined by Figure 2-3, indicated by the subscripts "o" and "i", representing the object and image coordinate systems respectfully. Note the redundancy of defining a z_o and z_i axis since the cylinders are identical and parallel. With respect to the electromagnetic excitation, the term "incident field" shall now be understood to represent the field plus its reflection from the ground plane. The surface currents induced on the object and its image by this incident TEM plane wave are considered as equivalent source currents radiating in free space [ ]. Thus, the principles of free space Green's functions may be used to compute the scattered field at an arbitrary field point in space.

Referring to Figure 2-4, define appropriate magnetic vector potentials for the object and its image as follows:

$\bar{A}_o(\bar{R}_o)$ = the magnetic vector potential of the object in object coordinates

$\bar{A}_i(\bar{R}_i)$ = the magnetic vector potential of the image in image coordinates

$\bar{R}_o$ = a general field point in space measured from the object coordinate system

$\bar{R}_o{}'$ = a general source point on the object cylinder with respect to its coordinate system

$\bar{R}_i{}'$ = a general source point on the image cylinder with respect to its coordinate system

$\bar{R}_i$ = the same general field point in terms of the image coordinates

Thus, the magnetic vector potential of the object is expressed as

$$\bar{A}_o(\bar{R}_o) = \frac{\mu_o}{4\pi} \int_{S_o'} \bar{K}_o(\bar{R}_o{}') \ G_o(\bar{R}_o;\bar{R}_o{}') \ dS_o{}' , \qquad (2.1)$$

where primed indicates source points, unprimed indicates field points,

10

z

IMAGE
CYLINDER

z OBJECT
   CYLINDER

General
Source Point
on Object

General
Source Point
on Image

$\bar{R}_o{}'$

$\bar{R}_o - \bar{R}_o{}'$

y_i

$\bar{R}_i{}'$

$\bar{R}_i - \bar{R}_i{}'$

y_o

x_i

x_o

$\bar{R}_i$

$\bar{R}_o$
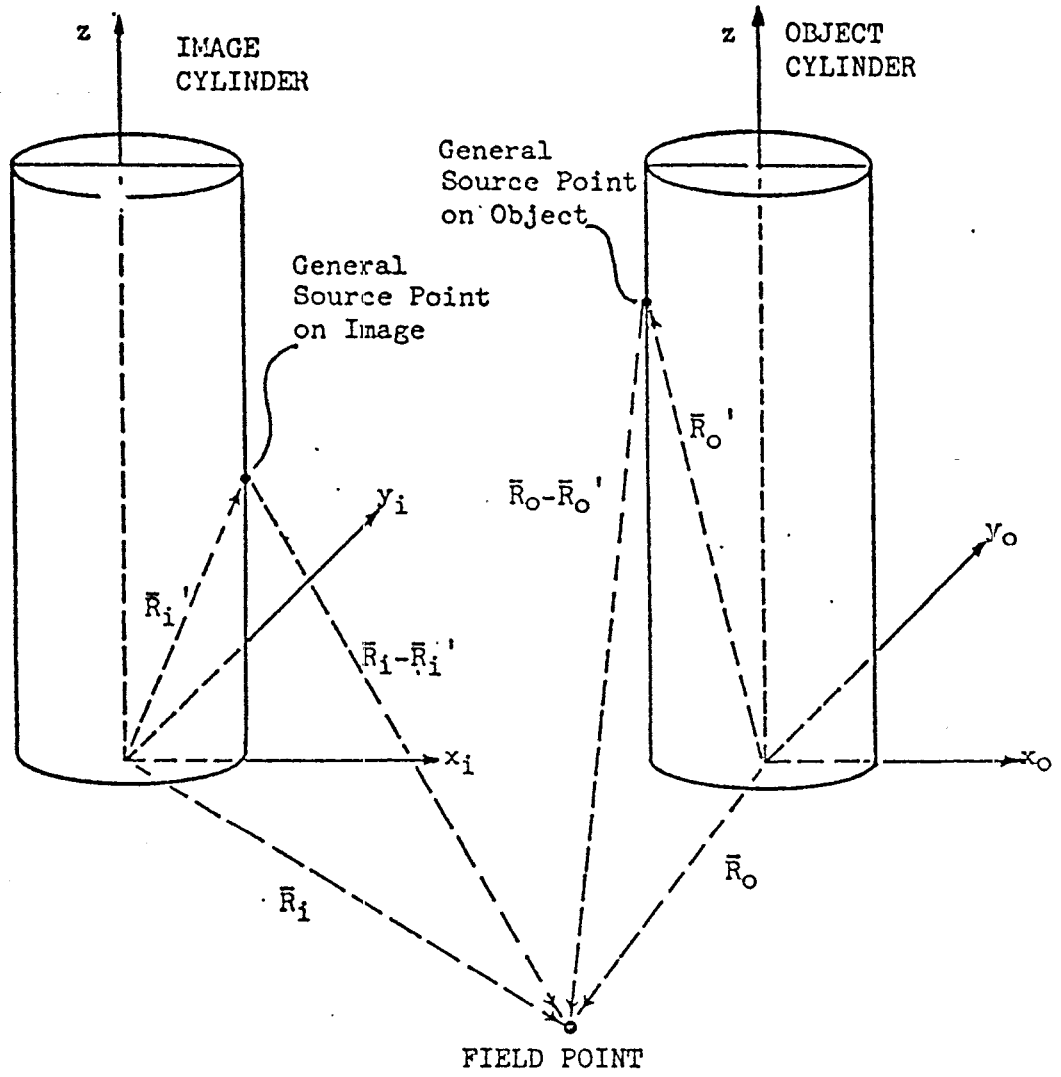
FIELD POINT

Figure 2-4. General Source and Field Points

11

and

$G_o(\bar{R}_o;\bar{R}_o') =$ the free space Green's function in object coordinates

$\bar{K}_o(\bar{R}_o') =$ the surface current density radiating in free space.

This Green's function has the general form of

$$G_o(\bar{R}_o;\bar{R}_o') = \frac{e^{-\gamma|\bar{R}_o-\bar{R}_o'|}}{|\bar{R}_o-\bar{R}_o'|} \qquad . \qquad (2.2)$$

Implicit in this equation is the assumption that the temporal variation of the fields is e^{st}, where

$$s = \sigma + j\omega, \qquad (2.3)$$

the complex frequency variable, with

$$\gamma = s/c \qquad (2.4)$$

$c =$ the speed of light in free space.

From Figure 2-4, define a cylindrical coordinate system superimposed upon the cartesian coordinate system in the usual manner. Through simple geometry,

$$|\bar{R}_o-\bar{R}_o'| = [\rho_o^2+\rho_o'^2-2\rho_o\rho_o' \cos(\phi_o-\phi_o') + (z-z')^2]^{1/2} \quad (2.5)$$

and for this circular cylinder, $\rho_o' = a$.

Therefore,

$$\bar{A}_o(\bar{R}_o) = \bar{A}_o(\rho_o, \phi_o, z) \qquad (2.6)$$

$$\bar{A}_o(\bar{R}_o) = \frac{\mu_o}{4\pi} \int_o^L \int_o^{2\pi} \bar{K}_o(\rho_o',\phi_o',z') \cdot G_o(\rho_o,\phi_o,z;\rho_o'\phi_o',z')a \, d\phi_o' \, dz' \quad (2.7)$$

12

$$\bar{A}_o(\bar{R}_o) = \frac{\mu_o}{4\pi} \int_0^L \int_0^{2\pi} \bar{K}_o(\phi_o{}',z') G_o(\rho_o,\phi_o,z;\phi_o{}',z') a \, d\phi_o{}' dz'$$

$$(2.8)$$

$$\bar{A}_o(\rho_o,\phi_o,z) = \frac{\mu_o}{4\pi} \int_0^L \int_0^{2\pi} \bar{K}_o(\phi_o{}',z') \frac{e^{-\gamma R_1}}{R_1} a \, d\phi_o{}' dz' \quad , \quad (2.9)$$

where $\quad R_1 = [\rho_o{}^2 + a^2 - 2\rho_o a \cos(\phi_o-\phi_o{}') + (z-z')^2]^{1/2} \quad . \quad (2.10)$

Upon accepting the first "thin-wire" approximation,

$$\bar{K}_o(\phi_o{}',z') = K_o(\phi_o{}',z') \hat{a}_z \quad , \quad\quad\quad (2.11)$$

such that

$$\bar{A}_o(\rho_o,\phi_o,z) = A_o(\rho_o,\phi_o,z) \hat{a}_z \quad\quad\quad\quad (2.12)$$

and

$$\bar{A}_o(\rho_o,\phi_o,z) = \hat{a}_z \frac{\mu_o}{4\pi} \int_0^L \int_0^{2\pi} K_o(\phi_o{}',z') \frac{e^{-\gamma R_1}}{R_1} a \, d\phi_o{}' dz', \quad (2.13)$$

or simply

$$A_{o_z}(\rho_o,\phi_o,z) = \frac{\mu_o}{4\pi} \int_0^L \int_0^{2\pi} K_o(\phi_o{}',z') \frac{e^{-\gamma R_1}}{R_1} a \, d\phi_o{}' \, dz' \quad .$$

$$(2.14)$$

This process can be repeated for the image cylinder, producing the similar equation

$$A_{i_z}(\rho_i,\phi_i,z) = \frac{\mu_o}{4\pi} \int_0^L \int_0^{2\pi} K_i(\phi_i{}',z') \frac{e^{-\gamma R_2}}{R_2} a \, d\phi_i{}' dz' \quad ,$$

$$(2.15)$$

13

where

$$R_2 = |\bar{R}_i - \bar{R}_i'| = [\rho_i{}^2 + a^2 - 2\rho_i a \cos(\phi_i - \phi_i') + (z-z')^2]^{1/2}. \quad (2.16)$$

Up to this point, the kernels of (2.14) and (2.16) are exact, in that the integrations are over the surface of the cylinders. The current has not been assumed to exist only on the cylinder axis, which would result in an approximate kernel.

As pointed out by others [1-4], [6], the circumferential variation of the currents can be described as uniform when the cylinder is m ↓↗ radii away from the ground plane, but this approximation becomes poor when the cylinder is near the ground plane. Taylor [40] has derived expressions for the circumferential variations of the axial current on an infinitely long cylinder over a ground plane in a static mode. As pointed out by Taylor, these resulting equations are also applicable to electrically thin cylinders separated a short distance from the ground plane and to finite length cylinders, provided the length is much greater than the height above the ground plane. Utilizing the equations of Taylor [40],

$$\bar{K}_o(\phi_o', z') = \frac{I_o(z')}{2\pi a} f_o(\phi_o')\hat{a}_z, \quad (2.17)$$

where

$$f_o(\phi_o') = \frac{[1 - (a/h)^2]^{1/2}}{1 + (a/h)\cos\phi_o'}, \quad (2.18)$$

$I_o(z') = $ axial variation of object surface current.

Separability of the current into its two distinct functional variations

becomes a better approximation as the cylinder becomes longer with respect to its radius. Note that as h becomes large, the circumferential variation of the axial current becomes uniform, as desired for a cylinder far removed from a ground plane [1-3]. Therefore, by assuming the current to behave in this manner, the magnetic vector potentials are composed of exact kernels, in the sense that the current resides upon the cylinder surface as opposed to the cylinder axis; the current is uniformly distributed about this surface when the cylinder is at a far distance from the ground plane; and the current becomes nonuniformly distributed as the cylinder draws near the ground plane. The results of these two approaches - approximate kernel with uniform circumferential variation of the axial current and exact kernel with an assumed circumferential variation of the axial current - will be examined and compared.

Returning to (2.17), the image currents are similarly

$$\bar{K}_i(\phi_i',z') = \frac{I_i(z')}{2\pi a} \ f_i(\phi_i')\hat{a}_z \ ; \tag{2.19}$$

where

$$f_i(\phi_i') = \frac{[1 - (a/h)^2]^{1/2}}{1 + (a/h)\cos(\phi_i'+\pi)} \ , \tag{2.20}$$

or

$$f_i(\phi_i') = \frac{[1 - (a/h)^2]^{1/2}}{1 - (a/h)\cos\phi_i'} \tag{2.21}$$

and

$I_i(z')$ = axial variation of image surface current.

Note the difference in f_i (2.21) and f_o (2.18) due to the coordinate references chosen. The magnetic vector potentials become

15

$$\bar{A}_o(\rho_o,\phi_o,z) = \hat{a}_z \frac{\mu_o}{4\pi} \int_0^L \int_0^{2\pi} \frac{I_o(z')}{2\pi a} f_o(\phi_o') \frac{e^{-\gamma R_1}}{R_1} a\, d\phi_o'\, dz'$$

$$(2.22)$$

$$\bar{A}_i(\rho_i,\phi_i,z) = \hat{a}_z \frac{\mu_o}{4\pi} \int_0^L \int_0^{2\pi} \frac{I_i(z')}{2\pi a} f_i(\phi_i') \frac{e^{-\gamma R_2}}{R_2} a\, d\phi_i'\, dz' \, .$$

$$(2.23)$$

Define two functions, F_o and F_i, as

$$F_o(\rho_o,\phi_o,z,z') = \int_0^{2\pi} f_o(\phi_o') \frac{e^{-\gamma R_1}}{R_1} a\, d\phi_o' \qquad \cdot 24)$$

$$F_i(\rho_i,\phi_i,z,z') = \int_0^{2\pi} f_i(\phi_i') \frac{e^{-\gamma R_2}}{R_2} a\, d\phi_i' \, , \qquad (2.25)$$

such that

$$\bar{A}_o(\rho_o,\phi_o,z) = \hat{a}_z \frac{\mu_o}{4\pi} \int_0^L \frac{I_o(z')}{2\pi a} F_o(\rho_o,\phi_o,z,z') dz' \qquad (2.26)$$

$$\bar{A}_i(\rho_i,\phi_i,z) = \hat{a}_z \frac{\mu_o}{4\pi} \int_0^L \frac{I_i(z')}{2\pi a} F_i(\rho_i,\phi_i,z,z') dz' \, . \qquad (2.27)$$

Drawing upon the principles of image theory, the currents on the object and image are related. At equivalent points on the object cylinder and its image, the currents are equal in magnitude, but opposite in sign. Stated simply,

$$I_o(z') = -I_i(z') \equiv I(z'). \qquad (2.28)$$

Therefore

$$\bar{A}_o(\rho_o,\phi_o,z) = \hat{a}_z \frac{\mu_o}{4\pi} \int_0^L \frac{I(z')}{2\pi a} F_o(\rho_o,\phi_o,z,z') dz' \qquad (2.29)$$

16

$$\bar{A}_i(\rho_i,\phi_i,z) = -\hat{a}_z \frac{\mu_o}{4\pi} \int_0^L \frac{I(z')}{2\pi a} F_i(\rho_i,\phi_i,z,z')dz'. \qquad (2.30)$$

Locate the field point at some general point on the surface of the object cylinder as illustrated in Figure 2-5. From the law of sines,

$$\rho_i \sin \phi_i = a \sin \alpha = a \sin \phi_o, \qquad (2.31)$$

and from the law of cosines,

$$\rho_i^2 = a^2 + 4h^2 + 4ah \cos \phi_o . \qquad (2.32)$$

Therefore, when $\bar{A}_i$ is evaluated on the object surface,

$$\rho_i = [a^2 + 4h^2 + 4ah \cos \phi_o]^{1/2} \qquad (2.33)$$

and

$$\phi_i = \sin^{-1} \left\{ \frac{a \sin \phi_o}{[a^2 + 4h^2 + 4ah \cos \phi_o]^{1/2}} \right\} . \qquad (2.34)$$

Note that when $\bar{A}_o$ is evaluated on the surface of the object,

$$\rho_o = a . \qquad (2.35)$$

Thus,

$$\bar{A}_o (\rho_o,\phi_o,z) \bigg]_{S_o} = \bar{A}_o(\phi_o,z) \qquad (2.36)$$

and

$$\bar{A}_i(\rho_i,\phi_i,z) \bigg]_{S_o} = \bar{A}_i (\phi_o,z), \qquad (2.37)$$

which demonstrates their functional dependence, upon this evaluation.

17
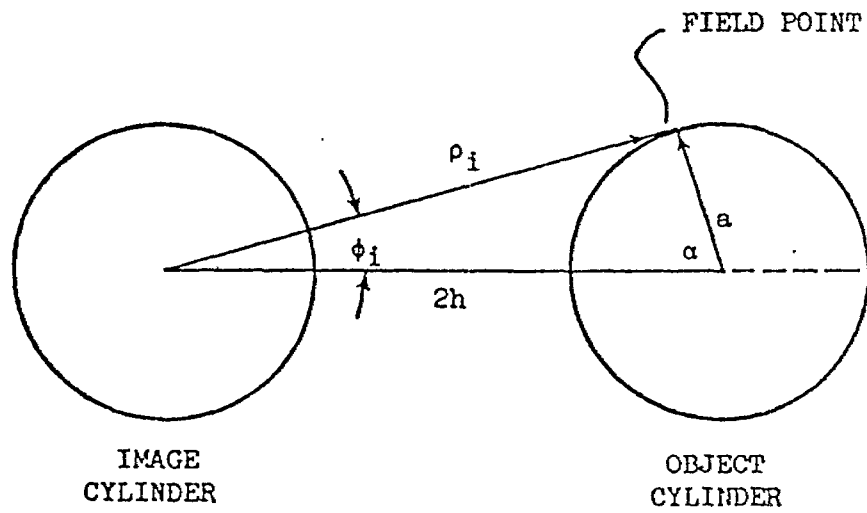
Figure 2-5.   Field Point on the Object Surface

Therefore, on the object cylinder surface

$$\bar{A}_o(\phi_o, z) = \hat{a}_z \frac{\mu_o}{4\pi} \int_0^L \frac{I(z')}{2\pi a} F_o(\phi_o, z, z') dz' \quad , \qquad (2.38)$$

with

$$F_o(\phi_o, z, z') = \sqrt{1-a/h} \int_0^{2\pi} \frac{1}{1+(a/h)\cos \phi_o'} \frac{e^{-\gamma R_1}}{R_1} a \, d\phi_o' \qquad (2.39)$$

$$R_1 = [2a^2 - 2a^2 \cos(\phi_o - \phi_o') + (z-z')^2]^{1/2} \qquad (2.40)$$

and

$$\bar{A}_i(\phi_o, z) = -\hat{a}_z \frac{\mu_o}{4\pi} \int_0^L \frac{I(z')}{2\pi a} F_i(\phi_o, z, z') dz', \qquad (2.41)$$

with

$$F_i(\phi_o, z, z') = \sqrt{1-a/h} \int_0^{2\pi} \frac{1}{1-(a/h)\cos \phi_i'} \frac{e^{-\gamma R_2}}{R_2} a \, d\phi_i' \qquad (2.42)$$

$$R_2 = \left\{ 2a^2 + 4h^2 + 4ah \cos \phi_o - 2[a^2 + 4h^2 + 4ah \cos \phi_o]^{1/2} \cdot \right.$$
$$\left. a \cos(\phi_i - \phi_i') + (z-z')^2 \right\}^{1/2} \qquad (2.43)$$

$$\phi_i = \sin^{-1} \left\{ \frac{a \sin \phi_o}{[a^2 + 4h^2 + 4ah \cos \phi_o]^{1/2}} \right\} \quad . \qquad (2.44)$$

The current, $I(z')$, induced by the incident field produces a scattered field. The total field, composed of the superposition of incident and scattered fields, must obey certain boundary conditions, which enforce uniqueness [18]. The total field is defined as

$$\begin{aligned} \bar{E}^t &= \text{incident field} + \text{scattered field} \\ &= \bar{E}^{inc} + \bar{E}^s \quad . \end{aligned} \qquad (2.45)$$

19

The scattered field is related to the induced currents and charges by

$$\bar{E}^s(\bar{R}) = -s\bar{A}^s(\bar{R}) - \nabla\phi^s(\bar{R}), \tag{2.46}$$

where

$\bar{A}^s(\bar{R})$ = the total "scattered" magnetic vector potential

ϕ^s = the total "scattered" electric scalar potential,

which can be related to $\bar{A}^s$ through the Lorentz gauge condition,

$$\phi^s(\bar{R}) = \frac{\nabla \cdot \bar{A}^s(\bar{R})}{-\mu_0\varepsilon_0 s} \quad . \tag{2.47}$$

Equation (2.46) becomes

$$\bar{E}^s(\bar{R}) = -s\left[\bar{A}^s(\bar{R}) - \frac{1}{\mu_0\varepsilon_0 s^2} \cdot \nabla[\nabla \cdot \bar{A}^s(\bar{R})]\right] \quad . \tag{2.48}$$

The charge distribution need not be known since the charges have been related to the current through the Lorentz gauge condition. Note that since $\gamma = s/c$ and $c = 1/\sqrt{\mu_0\varepsilon_0}$, $\gamma^2 = s^2\mu_0\varepsilon_0$. Thus,

$$\bar{E}^s(\bar{R}) = -s\left[\bar{A}^s(\bar{R}) - \frac{1}{\gamma^2} \nabla[\nabla \cdot \bar{A}^s(\bar{R})]\right] \quad . \tag{2.49}$$

On the surface of the object cylinder, the boundary condition is

$$\hat{n} \times \bar{E}^T = 0, \tag{2.50}$$

with $\hat{n}$ being the outward normal unit vector on the cylinder surface. This boundary condition can also be represented by

$$E^{inc}_{tan}\Big|_{S_0} = -E^s_{tan}\Big|_{S_0} \quad , \tag{2.51}$$

which merely states that the tangential components of the incident and scattered fields must cancel on the object surface in order to produce

20

the appropriate boundary condition. Combining (2.49) and (2.51) results in

$$E^{inc}_{tan} \Big]_{S_O} = s\left[\bar{A}^s(\bar{R}) - \frac{1}{\gamma^2} \nabla[\nabla \cdot \bar{A}^s(\bar{R})]\right]\Big]_{S_O} . \tag{2.52}$$

Since

$$\bar{A}^s(\bar{R}_O) = \bar{A}_O{}^s + \bar{A}_i{}^s = A_{0_z}\hat{a}_z + A_{i_z}\hat{a}z , \tag{2.53}$$

$$\bar{A}^s(\bar{R})\Big]_{S_O} = \hat{a}_z \frac{\mu_0}{4\pi} \int_0^L \frac{I(z')}{2\pi a} \left[F_0(\phi_0,z,z')-F_i(\phi_0,z,z')\right] dz' . \tag{2.54}$$

Incorporating the ideas proposed by (2.52) and (2.54), one arrives at

$$E^{inc}_{tan} \Big]_{S_O} = s\left[1-\frac{1}{\gamma^2}\nabla(\nabla\cdot)\right] \hat{a}_z\frac{\mu_0}{4\pi} \int_0^L \frac{I(z')}{2\pi a} \Big[F_0(\phi_0,z,z') - F_i(\phi_0 z,z')\Big] dz' . \tag{2.55}$$

Since

$$(-4\pi\epsilon_0 s)s[1-\frac{1}{\gamma^2}\nabla(\nabla\cdot)]\frac{\mu_0}{4\pi} = -\mu_0\epsilon_0 s^2[1-\frac{1}{\gamma^2}\nabla(\nabla\cdot)]$$

$$= \frac{-s^2}{c^2}[1-\frac{1}{\gamma^2}\nabla(\nabla\cdot)] = -\gamma^2[1-\frac{1}{\gamma^2}\nabla(\nabla\cdot)]$$

$$= [\nabla(\nabla\cdot) - \gamma^2], \tag{2.56}$$

(2.55) becomes

$$-4\pi\epsilon_0 s\left[E^{inc}_{tan}\Big]_{S_O}\right] = [\nabla(\nabla\cdot) - \gamma^2] \hat{a}_z\int_0^L \frac{I(z')}{2\pi a} \cdot$$
$$[F_0(\phi_0,z,z')-F_i(\phi_0,z,z')]dz' . \tag{2.57}$$

The differential operator [41] readily reduces since it acts on a vector with only a z component.

21

$$\text{grad div } V = \nabla(\nabla \cdot V) \qquad (2.58)$$

$$[\nabla(\nabla \cdot) - \gamma^2] = \frac{\partial^2}{\partial\rho\partial z} \hat{a}_\rho + \frac{1}{\rho}\frac{\partial^2}{\partial\phi_0\partial z} \hat{a}_\phi + \frac{\partial^2}{\partial z^2}\hat{a}_z - \gamma^2 \quad . \qquad (2.59)$$

The boundary conditions implied through (2.57) are simply

$$E_z^{inc} = -E_z^s \text{ on } S_0 .$$

$$E_\phi^{inc} = -E_\phi^s \text{ on } S_0 \qquad . \qquad (2.60)$$

Through application of these two equations, it is apparent that f·· finite length cylinders an axial component of current is created by both an axial and a circumferential component of the incident field [22-25]. Nevertheless, accepting the second "thin-wire" approximation, boundary conditions will only be enforced on the axial component of the incident field. This leaves the integro-differential equation

$$(-4\pi\epsilon_0 s)E_z^{inc}\Big|_{S_0} = \left(\frac{\partial^2}{\partial z^2} - \gamma^2\right) \int_0^L \frac{I(z')}{2\pi a} [F_0(\phi_0,z,z') - F_i(\phi_0,z,z')]dz' \quad . \qquad (2.61)$$

Referring to Figure 2-6, the total incident field can be formulated on a general basis. $\bar{E}_1$ is shown in the plane of the two descriptive coordinate directions a and b. An electric field normal to this plane will not produce a z component. Thus,

$$\bar{E}^{inc} = \bar{E}_1 e^{-\gamma b} + \bar{E}_2 e^{-\gamma d}$$

$$= \bar{E}_1 \exp\left\{-\gamma\left[z \cos\theta^i + a \cos[(\pi/2)-\theta^i]\right]\right\}$$
$$+ \bar{E}_2 \exp\left\{-\gamma\left[z \cos\theta^i + c \cos[(\pi/2)-\theta^i]\right]\right\} \qquad (2.62)$$

22
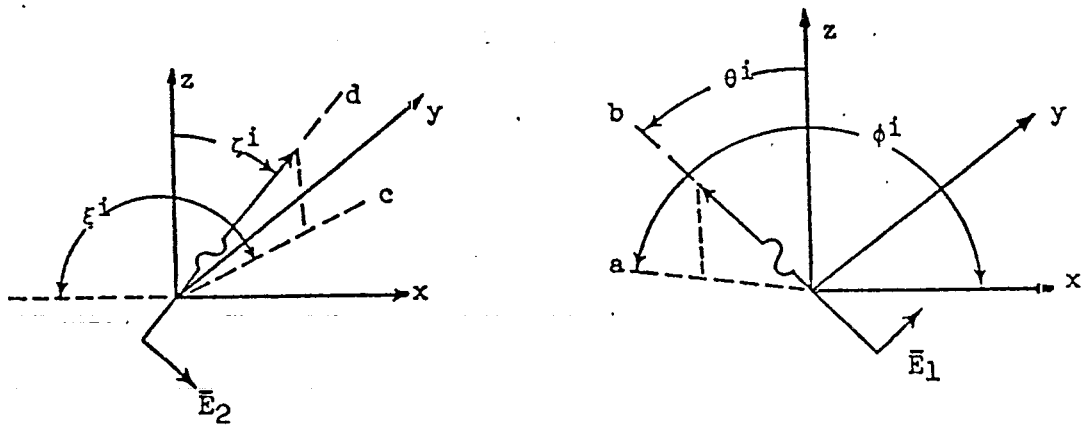
(Note: due to image theory, $\zeta^i = \theta^i$ and $\xi^i = \phi^i$)

Figure 2-6. General Incident Field

$$E^{inc} = \bar{E}_1 \exp\left\{ -\gamma \left[z \cos \theta^i + a \sin \theta^i \right] \right\}$$

$$+ \bar{E}_2 \exp\left\{ -\gamma \left[z \cos \theta^i + c \sin \theta^i \right] \right\}$$

$$= \bar{E}_1 \exp\left\{ -\gamma z \cos \theta^i - \gamma \sin \theta^i \left[x \cos \phi^i + y \cos(\phi^i - \pi/2) \right] \right\}$$

$$+ \bar{E}_2 \exp\left\{ -\gamma z \cos \theta^i - \gamma \sin \theta^i \left[x \cos (\pi-\phi^i) + y \cos(\phi^i - \pi/2) \right] \right\}, (\ \text{63})$$

where the principle of direction cosines [42] has been forwarded.
Simplification gives

$$E^{inc} = \bar{E}_1 e^{-\gamma z \cos \theta^i - \gamma \sin \theta^i [x \cos \phi^i + y \sin \phi^i]}$$

$$+ \bar{E}_2 e^{-\gamma z \cos \theta^i - \gamma \sin \theta^i [-x \cos \phi^i + y \sin \phi^i]} \quad (2.64)$$

Since only the axial component of the incident field is to be used,

$$E_{z_1} = |\bar{E}_1| \sin \theta^i = E_1 \sin \theta^i \tag{2.65}$$

$$E_{z_2} = -|\bar{E}_2| \sin \theta^i = -E_2 \sin \theta^i , \tag{2.66}$$

such that

$$E_z^{inc} = E_1 \sin \theta^i e^{-\gamma z \cos \theta^i - \gamma \sin \theta^i [x \cos \phi^i + y \sin \phi^i]}$$

$$-E_2 \sin \theta^i e^{-\gamma z \cos \theta^i - \gamma \sin \theta^i [-x \cos \phi^i + y \sin \phi^i]}$$

$$\tag{2.67}$$

On the ground plane, E_z must satisfy the boundary condition

$$E_z^{inc} {}_{(\text{Ground Plane})} = E_z^{inc} {}_{(x = -h)} = 0. \tag{2.68}$$

24

Enforcing this requirement on (2.67) necessitates that

$$E_1 = E_2 e^{-2\gamma h \sin \theta^i \cos \phi^i} \qquad (2.69)$$

Defining

$$E_o = -E_1 , \qquad (2.70)$$

then

$$E_2 = -E_o e^{2\gamma h \sin \theta^i \cos \phi^i} , \qquad (2.71)$$

such that

$$E_z^{inc} = -E_o \sin \theta^i e^{-\gamma z \cos \theta^i} \left[e^{-\gamma \sin \theta^i [x \cos \phi^i + y \sin \phi^i]} \right.$$
$$\left. -e^{2\gamma h \sin \theta^i \cos \phi^i - \gamma \sin \theta^i [-x \cos \phi^i + y \sin \phi^i]} \right] \qquad (2.72)$$

or

$$E_z^{inc} = -E_o \sin \theta^i e^{-\gamma z \cos \theta^i - \gamma y \sin \theta^i \sin \phi^i} .$$
$$\left[e^{-\gamma x \sin \theta^i \cos \phi^i} - e^{\gamma x \sin \theta^i \cos \phi^i + 2\gamma h \sin \theta^i \cos \phi^i} \right] . \qquad (2.73)$$

Comparison of this incident field to that of Umashankar, et. al. [3], is favorable. Letting $\phi^i = 180^o$,

$$\left. E_z^{inc} \right|_{\phi^i = \pi} = -E_o \sin \theta^i e^{-\gamma z \cos \theta^i} \left[e^{\gamma x \sin \theta^i} - \right.$$
$$\left. e^{-\gamma \sin \theta^i (x + 2h)} \right] , \qquad (2.74)$$

and evaluating E_z^{inc} on the cylinder axis (approximate kernel) instead of on its surface,

$$E_z^{inc}\bigg|_{\substack{\phi^i = \pi \\ x = 0}} = -E_0 \sin \theta^i e^{-\gamma z \cos \theta^i}\left[1 - e^{-\gamma 2h \sin \theta^i}\right] \quad (2.75)$$

which is identical to Umashankar's [3] field. This comparison is made note of since the induced current found by Umashankar shall be compared to the current found through this exact kernel formulation.

Before evaluating the incident field on the cylinder surface, the integro-differential equation (2.61) needs to be examined mor. closely. The unknown quantity, $I(z')$, is not a function of ϕ_0. It is apparent that by letting $\phi_0 = \alpha_1$, any particular angle, solving for $I(z')$ and letting $\phi_0 = \alpha_2$, a different particular angle, again solving for $I(z')$ – the two solutions must be identical. The implication is that in order to determine the unknown induced current, boundary conditions need not be enforced all over the object cylinder surface, but just at one particular value of ϕ_0. The circumferential variation of the current has already been assumed to be of the form expressed by (2.18) and (2.21), such that a solution for $I(z')$ at any particular value of ϕ_0 will readily result in a general solution for $I(z',\phi_0)$. Through examination, $\phi_0 = 0^0$ seems as profitable as any other choice. Thus, the integro-differential equation reduces to

$$(-4\pi\epsilon_0 s)E_z^{inc}\bigg|_{\substack{S_0 \\ \phi_0 = 0^0}} = \left(\frac{\partial^2}{\partial z^2} - \gamma^2\right)\int_0^L \frac{I(z')}{2\pi a}\left[F_0(z,z')-\right.$$
$$\left. F_i(z,z')\right]dz' \quad , \quad (2.76)$$

where

$$F_0(z,z') = F_0(\phi_0,z,z') \Big|_{\phi_0 = 0^\circ} = \sqrt{1-a/h} \int_0^{2\pi} \frac{1}{1+(a/h)\cos\phi_0} \cdot$$

$$\frac{e^{-\gamma r_1}}{r_1} \, a \, d\phi_0' \qquad (2.77)$$

$$r_1 = R_1 \Big|_{\phi_0 = 0^\circ} = [2a^2(1 - \cos\phi_0') + (z - z')^2]^{1/2} \qquad (2.78)$$

$$F_i(z,z') = F_i(\phi_0,z,z') \Big|_{\phi_0 = 0^\circ} = \sqrt{1-a/h} \cdot$$

$$\int_0^{2\pi} \frac{1}{1-(a/h)\cos\phi_i'} \, \frac{e^{-\gamma r_2}}{r_2} \, a \, d\phi_i' \qquad (2.79)$$

$$r_2 = R_2 \Big|_{\phi_0 = 0^\circ} = [(2a^2 + 4\,ah)(1- \cos\phi_i') + 4h^2 +$$

$$(z-z')^2]^{1/2} \qquad . \qquad (2.80)$$

Evaluation of the incident field results in

$$E_z^{inc} \Big|_{\substack{S_0 \\ \phi_0 = 0^\circ}} = E_z^{inc} \Big|_{\substack{y = 0 \\ x = a}} =$$

$$-E_0 \sin\theta^i e^{-\gamma z \cos\theta^i} \Big[e^{-\gamma a \sin\theta^i \cos\phi^i} -$$

$$e^{\gamma a \sin\theta^i \cos\phi^i + 2\gamma h \sin\theta^i \cos\phi^i} \Big] \qquad (2.81)$$

By defining

$$\beta^i = \sin\theta^i \cos\phi^i \quad , \qquad (2.82)$$

the incident field is simply

$$E_z^{inc} \Big|_{\substack{S_0 \\ \phi_0 = 0^\circ}} = -E_0 \sin\theta^i e^{-\gamma(z \cos\theta^i + \beta^i a)} \cdot$$

$$\Big[1-e^{\gamma 2\beta^i(a + h)}\Big] \qquad . \qquad (2.83)$$

27

Through examination of this equation, the appearance of a phase difference between the two terms inside the brackets is obviously that caused by the "original" incident field and the same field reflected from the ground plane arriving at some later time.

The integro-differential equation (2.76) can be altered slightly in form and notation in order to better represent the problem. Since the differential operator does not operate on z',

$$(-4\pi\epsilon_0 s)E_z^{inc}\bigg|_{\substack{S_0\\ \phi_0 = 0^\circ}} = \int_0^L \frac{I(z')}{2\pi a}\left(\frac{\partial^2}{\partial z^2} - \gamma^2\right)[F_0(z,z') - F_i(z,z')]\, dz'. \qquad (2.84)$$

In order to better represent the complex frequency dependence,

$$(-4\pi\epsilon_0 s)E_z^{inc}(s)\bigg|_{\substack{S_0\\ \phi_0 = 0^\circ}} = \int_0^L \frac{I(z',s)}{2\pi a}\left(\frac{\partial^2}{\partial z^2} - \gamma^2\right)[F_0(z,z',s) - F_i(z,z',s)]\, dz'. \qquad (2.85)$$

Let $\qquad 1 - \cos\phi_0' = 2\sin^2\frac{\phi_0'}{2}$ \qquad\qquad (2.86)

and $\qquad d$ = diameter of the cylinder
$\qquad\qquad = 2a$ \qquad\qquad (2.87)

in F_0, such that

$$[2a^2(1 - \cos\phi_0') + (z-z')^2]^{1/2} = [d^2 \sin^2\frac{\phi_0'}{2} + (z-z')^2]^{1/2}, \qquad (2.88)$$

with a similar substitution in F_i.

The final results are summarized for reference:

$$(-4\pi\epsilon_0 s)E_z^{inc}(s)\bigg|_{\substack{\phi_0 = 0^\circ\\ S_0}} = \int_0^L \frac{I(z',s)}{2\pi a}\left(\frac{\partial^2}{\partial z^2} - \gamma^2\right) \cdot [F_0(z,z',s)-F_i(z,z',s)]\, dz' \qquad (2.89)$$

28

$$E_z^{inc}(s)\Big|_{\substack{\phi=0^\circ\\S_0}} = -E_0(s)\sin\theta^i e^{-\gamma(z\cos\theta^i + \beta^i a)}.$$

(2.90)

$$F_0(z,z',s) = \sqrt{1-(a/h)^2}\int_0^{2\pi} \frac{\left(1-e^{\gamma\beta^i(a+h)}\right)}{1+(a/h)\cos\phi_0'}\frac{e^{-\gamma r_1}}{r_1}\, a\, d\phi_0'$$

(2.91)

$$F_i(z,z',s) = \sqrt{1-(a/h)^2}\int_0^{2\pi} \frac{1}{1-(a/h)\cos\phi_0'}\frac{e^{-\gamma r_2}}{r_2}\, a\, d\phi_i'$$

(2.92)

$$r_1 = [d^2\sin^2\tfrac{\phi_0'}{2} + (z-z')^2]^{1/2}$$

(2.93)

$$r_2 = ([d^2 + 8ah]\sin^2\tfrac{\phi_i'}{2} + 4h^2 + (z-z')^2]^{1/2}.$$

(2.94)

This integro-differential equation is to be solved for the unknown induced current on the cylinder. ·

Application of the Method of Moments

The integro-differential equation shall be cast into matrix form suitable for a numerical solution. This general process has come to be known as the method of moments [9], [11], [28-29]. Generally, the "wire" along the cylinder surface at $\phi_0 = 0^\circ$ is broken into segments, integrals approximated by the sum of integrals over N small segments, and the current assumed to be constant over each individual segment.

With regard to Figure 2-7, expand the current in a set of basis functions such that

$$I(z',s) = \sum_n \alpha_n(s)I_n(z'),$$

(2.95)

where

$\quad \alpha_n(s) =$ unknown coefficient of constant current in the nth subsection

29

MATCH POINTS ON CYLINDER
SURFACE AT $\phi_o = 0°$

z^{N+1} ___

$z_N = L$

z^N ___

z^{n+1} ___

z_m

z^n ___

z^3 ___

z_2

z^2 ___

$z_1 = 0$

z^1 ___

| "WIRE"

___ SUBSECTION ENDS

X MATCH POINTS

$z_m = (m-1)\Delta$ (MATCH POINTS)
$\quad m = 1,2,\ldots N$

$z^n = (n-2/3)\Delta$ (SUBSECTION ENDS)
$\quad n = 1,2,\ldots N+1$

$\Delta = L/(N-1)$ LENGTH OF ZONE

$N = $ NUMBER OF SUBSECTIONS
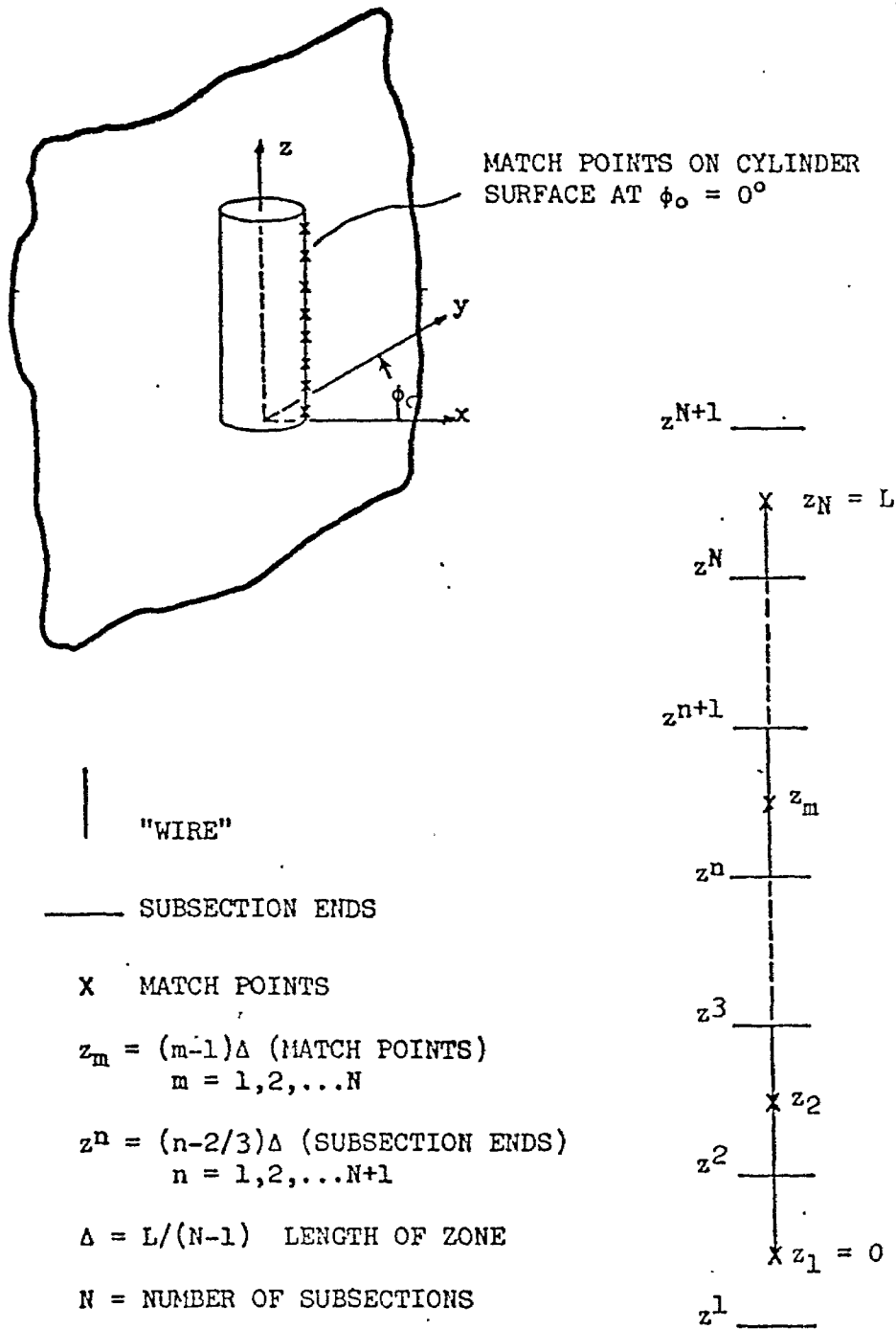
Figure 2-7. Moment Method Partitioning of Geometry

$$I_n(z') = \begin{cases} 1 & \text{for } z^n < z < z^{n+1} \\ 0 & \text{elsewhere} \quad n = 2,3,\ldots.N-1 \end{cases}. \qquad (2.96)$$

Thus, use is made of a pulse function expansion described by Harrington [9]. This representation is chosen such that the boundary conditions,

$$I(0) = I(L) = 0, \qquad (2.97)$$

are satisfied automatically by allowing the two end subsections or zones to extend past the surface of the cylinder and assuming the current on these zones to be zero. As shown on Figure 2-7, each zone is of length Δ, where

$$\Delta = \frac{L}{N-1} = \text{length of a zone} \qquad (2.98)$$

N = number of subsections or zones

$$z^n = (n-3/2)\Delta \qquad n = 1,2,\ldots.N+1 \qquad (2.99)$$
$$= \text{subsection ends.}$$

Applying these concepts to the integro-differential equation (2.89) produces

$$(-4\pi\epsilon_0 s)\left\{ -E_0(s)\sin\theta^i e^{-\gamma z}\cos\theta^i\left[e^{-\gamma\beta^i a} - e^{\gamma\beta^i(a+2h)}\right]\right\}$$
$$= \sum_n \alpha_n(s)\int_{z^n}^{z^{n+1}} \frac{1}{2\pi a}\left(\frac{\partial^2}{\partial z^2} - \gamma^2\right)\left[F_0(z,z',s) - F_i(z,z',s)\right]\,dz'.$$
$$(2.100)$$

Forcing this equation to be satisfied at discrete match points amounts to choosing delta functions as testing functions [9]. The match points are the center of subsections as shown in Figure 2-7, where

31

$$z_m = (m-1)\Delta \qquad m = 1,2,\ldots.N$$
$$= \text{match points.} \tag{2.101}$$

As pointed out by Harrington [9], the derivatives may be carried out analytically or approximated by finite difference techniques. Both avenues of approach were investigated, with the decision going to finite differences due to its ease of evaluation and simplicity. Using finite difference approximations, where

$$\frac{d^2F}{dz^2} = \frac{1}{(\Delta z)^2} \left[F(z + \Delta z) - 2F(z) + F(z-\Delta z) \right] , \tag{2.102}$$

the integro-differential equation is

$$(-4\pi\epsilon_0 s) \left\{ -E_0(s) \sin \theta^i e^{-\gamma z_m} \cos \theta^i \left[e^{-\gamma\beta^i a} - e^{\gamma\beta^i(a + 2h)} \right] \right\}$$

$$= \sum_n \frac{\alpha_n(s)}{2\pi a} \frac{1}{\Delta^2} \int_{z^n}^{z^{n + 1}} \left[F_0(z_{m+1},z',s) -(\gamma^2\Delta^2 + 2)\cdot \right.$$

$$F_0(z_m,z',s) + F_0(z_{m-1},z',s) -F_i(z_{m+1},z',s) + (\gamma^2\Delta^2 + 2)\cdot$$

$$\left. F_i(z_m,z',s) -F_i(z_{m-1},z',s) \right] dz' \qquad \begin{array}{l} n = 2,3,\ldots N-1 \\ m = 2,3,\ldots N-1. \end{array} \tag{2.103}$$

This equation is placed in the form of a matrix equation,

$$\bar{V}(s) = \bar{\bar{Z}}(s) \, \bar{I}(s), \tag{2.104}$$

where a single bar represents a column matrix or vector and double bars indicate a square matrix. Let the matrices be defined as

$$\bar{V}(s) = \text{the source vector} = [v_m],$$

where

32

v_m = the matrix elements of $\bar{V}(s)$

$$= (-4\pi\varepsilon_0 s) \left[-E_0(s) \sin \theta^i e^{-\gamma z_m} \cos \theta^i \left[e^{-\gamma\beta^i a} - e^{\gamma\beta^i(a+2h)} \right] \right]$$

$$m = 2,3,\ldots N-1 \qquad (2.105)$$

$\bar{I}(s)$ = the response vector = $[i_n]$,

where

i_n = the matrix elements of $\bar{I}(s)$
  = α_n, unknown coefficient of constant current in the nth zone

$$n = 2,3,\ldots N-1 \quad ; \qquad (2.106)$$

$\bar{\bar{Z}}(s)$ = the impedance matrix = $[z_{mn}]$,

where

z_{mn} = the matrix elements of $\bar{\bar{Z}}(s)$

$$= \frac{1}{\Delta^2} \int_{z^n}^{z^{n+1}} \frac{1}{2\pi a} \left[F_0(z_{m+1},z',s) - (\gamma^2\Delta^2 + 2) F_0(z_m,z',s) \right.$$

$$+ F_0(z_{m-1},z',s) - F_i(z_{m+1},z',s)$$

$$\left. + (\gamma^2\Delta^2 + 2) F_i(z_m,z',s) - F_i(z_{m-1},z',s) \right] dz'.$$

$$n = 2,3\ldots N-1$$
$$m = 2,3\ldots N-1 \qquad (2.107)$$

With simplification in mind, let

$$H_{mn}(z_m,s) = \int_{z^n}^{z^{n+1}} \int_0^{2\pi} \frac{1}{1 + (a/n)\cos \phi_0'} \frac{e^{-\gamma r_1}}{r_1} d\phi_0' dz' ,$$

$$(2.108)$$

with

$$r_1 = [d^2 \sin^2 \frac{\phi_0'}{2} + (z_m - z')^2]^{1/2} , \qquad (2.109)$$

33

and

$$H^i_{\overline{m}n}(z_m,s) = \int_{z^n}^{z^{n+1}} \int_0^{2\pi} \frac{1}{1-(a/h)\cos\phi_i} \overline{}$$

$$\frac{e^{-\gamma r_2}}{r_2} \, d\phi_i' \, dz' \, , \qquad (2.110)$$

with

$$r_2 = [(d^2 + 8ah)\sin^2\frac{\phi_i'}{2} + 4h^2 + (z_m - z')^2]^{1/2} \, . \qquad (2.111)$$

Thus, z_{mn} may be redefined as

$$z_{mn} = \frac{\sqrt{1-(a/h)}^2}{2\pi\Delta^2} \Big\{ H_{\underline{0}n}(z_{n+1},s) - (\gamma^2\Delta^2 + 2) H_{\underline{0}n}(z_m,s) +$$

$$H_{\underline{0}n}(z_{m-1},s) - H^i_{\overline{m}n}(z_{m+1},s) + (\gamma^2\Delta^2 + 2) H^i_{\overline{m}n}(z_m,s) -$$

$$H^i_{\overline{m}n}(z_{m-1},s) \Big\} \qquad (2.112)$$

The integrals defined by (2.108) and 2.110) present problems in numerical evaluation — but these can be overcome. Tesche [43] provides methods of treating integrals of this type. Note that the integrand of $H^i_{\overline{m}n}$ is never singular due to the obvious fact that all terms in the radical (2.11) are greater than or équal to zero except the term $4h^2$ which is never zero. Therefore, numerical evaluation of $H^i_{\overline{m}n}$ offers no problem. However, $H_{\underline{0}n}(z_m,s)$ presents some problems; in that, when $\phi_0' = 0^o$ and $z' = z_m$, the integrand is singular. $H_{\underline{0}n}(z_m,s)$, $H_{\underline{0}n}(z_{m-1},s)$, and $H_{\underline{0}n}(z_{m+1},s)$ shall be examined separately.

At $\phi_0' = 0^o$, the integrand of $H_0(z_{m+1},s)$ is singular when $z_{m+1} = z'$, where $z^n \le z' \le z^{n+1}$. Hence, at this point,

$$z^n \le z_{m+1} \le z^{n+1} \quad . \qquad (2.113)$$

34

Utilizing (2.99) and (2.101), reproduced here

$$z_m = (m-1)\Delta \qquad m = 1,2,\ldots.N+1$$

$$z^n = (n-3/2)\Delta \qquad n = 1,2,\ldots.N+1 \quad ,$$

the singularity occurs when

$$(n - 3/2)\Delta \leq [(m+1) -1]\Delta \leq [(n+1) -3/2]\Delta \qquad (2.114)$$

or when

$$-3/2 \leq (m-n) \leq - 1/2.$$

Since m and n are integers, "m-n" must be an integer between these two fractions. Thus, $H_{\Omega n}(z_{m+1},s)$ is singular when m-n = -1 or when m = n-1.

In a like manner, $H_{\Omega n}(z_m,s)$ is singular when $\phi_0' = 0^o$ and $z_m = z'$. Thus, the singularity occurs when

$$z^n \leq z_m \leq z^{n+1} , \qquad (2.115)$$

which can be expressed as

$$(n - 3/2)\Delta \leq (m-1)\Delta \leq [(n+1) - 3/2]\Delta \qquad (2.116)$$

or

$$- 1/2 \leq (m-n) \leq 1/2.$$

Through the same reasoning, $H_{\Omega n}(z_m,s)$ is singular when m = n.

It is apparent that $H_{\Omega n}(z_{m-1},s)$ is singular when m = n+1.

When these respective conditions do not exist, the integrals are readily amenable to numerical integration techniques, but at a singular point,

35

numerical techniques become suspect at best. Following general procedures outlined by Tesche [43], let the integral of $H_{\phi n}(z_m,s)$ at its singularity be T_1.

$$T_1 = H_{\phi n}(z_m,s) \quad \text{when } m = n \,, \tag{2.117}$$

with $H_{\phi n}$ defined by (2.108). Transform variables in (2.108) as follows:

let
$$\phi = \phi_0{}'$$
$$z = z_m - z'$$
$$dz = -dz' \tag{2.118}$$

and as for limits of integration

$$z^n \bigg|_{m=n} = z_m - z^n \bigg|_{m=n} = +\frac{\Delta}{2}$$

$$z^{n+1} \bigg|_{m=n} = z_m - z^{n+1} \bigg|_{m=n} = \frac{-\Delta}{2} \,. \tag{2.119}$$

Thus,

$$T_1 = \int_{-\frac{\Delta}{2}}^{\frac{\Delta}{2}} \int_0^{2\pi} \frac{1}{1 + (a/h)\cos\phi} \frac{e^{-\gamma r}}{r} \, d\phi \, dz \,, \tag{2.120}$$

with
$$r = [z^2 + d^2 \sin^2 \tfrac{\phi}{2}]^{1/2} \,, \tag{2.121}$$

which is one of the singular integrals to be evaluated. In a like manner, let

$$T_2 = H_{\phi n}(z_{m+1},s) \quad \text{when } m = n-1 \tag{2.122}$$

and after transforming by allowing

36

$$\phi = \phi_0{}'$$

$$z = z_{m+1} - z'$$

$$dz = -dz'$$

$$z_{m+1} - z^n \Big|_{m = n-1} = \frac{\Delta}{2} \qquad z_{m+1} - z^{n+1} \Big|_{m = n-1} = -\frac{\Delta}{2} \quad ,$$

$$T_2 = \int_{-\frac{\Delta}{2}}^{\frac{\Delta}{2}} \int_0^{2\pi} \frac{1}{1 + (a/h)\cos\phi} \; \frac{e^{-\gamma r}}{r} \; d\phi \; dz \quad , \qquad (2.123)$$

with r defined as in (2.121). A comparison of (2.120) and (2.123) obviously shows that

$$T_2 = T_1.$$

In addition, T_3 could be defined as $H_{\underline{m}n}(z_{m-1}, s)$ when $m = n+1$ and the end product would be that

$$T_1 = T_2 = T_3.$$

Therefore, the integral of the singular integrand of $H_{\underline{m}n}(z_{m+1}, s)$ when $m = n-1$, $H_{\underline{m}n}(z_m, s)$ for $m = n$, and $H_{\underline{m}n}(z_{m-1}, s)$ with $m = n+1$ is

$$T = \int_{-\frac{\Delta}{2}}^{\frac{\Delta}{2}} \int_0^{2\pi} \frac{1}{1 + (a/h)\cos\phi} \; \frac{e^{-\gamma r}}{r} \; d\phi \; dz \quad , \qquad (2.124)$$

with r given by (2.121).

This integral is further pursued in Appendix A, which concludes with the result that

$$T \simeq \frac{-2\pi\gamma\Delta}{[1-(a/h)^2]^{1/2}} + \frac{4\pi}{[1-(a/h)^2]^{1/2}}\left\{\ln 2 - \right.$$

$$\left. \ln\left[h/a + 1 - [(h/a)^2 - 1]^{1/2}\right]\right\} + 2\int_0^{2\pi}\frac{1}{1+(a/h)\cos\phi}\cdot$$

$$\ln\left\{\frac{\Delta}{4a} + \left[(\frac{\Delta}{4a})^2 + \sin^2\frac{\phi}{2}\right]^{1/2}\right\}\, d\phi \quad . \qquad (2.125)$$

The function is numerically evaluated easily, as the integrand is not singular.

The integro-differential equation has been cast as a system of matrices, which must be solved for the unknown induced current.

Application of the Singularity Expansion Method

The singularity expansion method (SEM) was introduced by Baum [31-33] and formalized and applied by many others [1-3], [30], [34-37] as a method for characterizing the response of scattering objects when illuminated by either transient or steady-state electromagnetic radiation. Before applying SEM to this transient problem, a brief survey of the general theory is appropriate – highlighting the areas of particular interest.

The complex natural frequencies of the scattering system, denoted by s_α, are those such that (2.104), when expressed as the homogeneous equation,

$$\bar{\bar{Z}}(s_\alpha)\, \bar{I}(s_\alpha) = 0, \qquad (2.126)$$

has a nontrivial solution for $\bar{I}(s_\alpha)$. The implication is that the determinant of $\bar{\bar{Z}}$ must vanish at these complex natural frequencies. Thus, the equation for determination of these natural resonances of the

induced current is

$$\det \bar{\bar{Z}}(s_\alpha) = 0 \quad . \tag{2.127}$$

As required by well-known linear circuit theory and Laplace transform theory, these natural resonances must occur in the left half portion of the complex s $(s = \sigma + j\omega)$ plane, defined in the usual manner by Laplace transform theory [44-45]. In addition, these natural resonances can not appear on the $j\omega$ axis and must consist of complex conjugate pairs. These facts are obvious, in order to produce real currents in the time domain which eventually go to zero due to the radiation of energy. It has been shown [35] that for bodies of finite extent, the response function has only poles and no branch cuts. Speculation has been put forth [37] that only simple poles exist for perfectly conducting bodies. The assumption that only simple poles exist is accepted without proof - although this has been substantiated numerically. Other researchers have made wide use of the simple pole assumption [1-3], [31], [34-37].

The matrix equation,

$$\bar{\bar{Z}}(s) \, \bar{I}(s) = \bar{V}(s), \tag{2.128}$$

has as a solution

$$\bar{I}(s) = \bar{\bar{Z}}(s)^{-1} \bar{V}(s). \tag{2.129}$$

Through the inverse Laplace transform, the current in the time domain is

$$I(t) = \frac{1}{2\pi j} \int_{\sigma_0 - j\infty}^{\sigma_0 + j\infty} \bar{\bar{Z}}(\tfrac{1}{s}) \bar{V}(s) e^{st} \, ds, \tag{2.130}$$

39

which could be evaluated numerically along the Bromwich path. SEM, an extension of well-founded techniques in classical circuit theory, is based upon the idea that the time domain response of the induced current is determined through knowledge of the complex natural frequencies of the system in addition to their corresponding residues. The time domain current is described by a sum over all the residues, times exponentially damped sinusoids.

Based upon this concept, SEM assumes that

$$\bar{\bar{Z}}(s)^{-1} = \sum_\alpha \frac{\bar{\bar{R}}_\alpha}{s-s_\alpha} \quad (+ \text{ entire functions, etc.}) \qquad (2.131)$$

which is a summation over all poles in the complex s plane. Define $\bar{\bar{R}}_\alpha$ as the system residue matrix at the pole s_α. Note that $\bar{\bar{R}}_\alpha$ is a constant matrix, in the sense that it is not a function of s. This residue matrix is a dyadic and can be represented as the outer product of two vectors independent of s as

$$\bar{\bar{R}}_\alpha = \bar{M}_\alpha \bar{C}_\alpha^T \quad , \qquad (2.132)$$

where $\bar{M}_\alpha$ is the natural mode vector and is a solution to

$$\bar{\bar{Z}}(s_\alpha)\bar{M}_\alpha = 0 \qquad (2.133)$$

and $\bar{C}_\alpha$ is the coupling vector, which satisfies the equation

$$\bar{\bar{Z}}(s_\alpha)^T \bar{C}_\alpha = 0$$

(T denotes transpose). For the electric field formulation, where symmetric matrices are encountered, these two vectors are identical [37].

Thus,

$$\bar{\bar{R}}_\alpha = \bar{C}_\alpha \ \bar{C}_\alpha{}^T \ . \tag{2.134}$$

Progressing one step further, let $\bar{\bar{C}}_\alpha$ be normalized such that its max-imum element is real and equal to unity.

$$\bar{C}_\alpha = \sqrt{\beta_\alpha} \quad [C_\alpha \text{ normalized}] \tag{2.135}$$

and define

$$\bar{C}_\alpha \text{ normalized} = \bar{C}_{\alpha_0},$$

such that

$$\bar{\bar{R}}_\alpha = \beta_\alpha \ \bar{C}_{\alpha_0} \ \bar{C}_{\alpha_0}{}^T \ , \tag{2.136}$$

where β_α is the normalization coefficient.

Since

$$\bar{\bar{Z}}(s)^{-1} = \sum_\alpha \frac{\beta_\alpha \bar{C}_\alpha \bar{C}_\alpha{}^T}{s-s_\alpha} \ , \tag{2.137}$$

the normalization coefficient is determined through consideration of a particular singularity [2], s_p, such that

$$\bar{C}_p{}^T \bar{\bar{Z}}(s) \bar{\bar{Z}}(s)^{-1} \bar{C}_p = \bar{C}_p{}^T \bar{\bar{U}} \bar{C}_p = \bar{C}_p{}^T \bar{C}_p \tag{2.138}$$

(Note: $\bar{\bar{U}}$ is the identity matrix.)

$$\bar{C}_p{}^T \bar{\bar{Z}}(s) \sum_\alpha \beta_\alpha \frac{\bar{C}_\alpha \bar{C}_\alpha{}^T}{s-s_\alpha} \ \bar{C}_p = \bar{C}_p{}^T \bar{C}_p$$

$$\sum_\alpha \beta_\alpha \frac{\bar{C}_p{}^T \bar{\bar{Z}}(s) \bar{C}_\alpha \bar{C}_\alpha{}^T \bar{C}_p}{s-s_\alpha} = \bar{C}_p{}^T \bar{C}_p \ . \tag{2.139}$$

41

Noting that

$$\bar{c}_p^T \bar{\bar{Z}}(s_p)\bar{c}_\alpha = \bar{c}_p^T \bar{\bar{Z}}(s_p)^{TT}\bar{c}_\alpha = (\bar{\bar{Z}}(s_p)^T \bar{c}_p)^T \bar{c}_\alpha = \bar{0}, \qquad (2.140)$$

$$\sum_\alpha \beta_\alpha \frac{\bar{c}_p^T[\bar{\bar{Z}}(s) - \bar{\bar{Z}}(s_p)]\bar{c}_\alpha \bar{c}_\alpha^T \bar{c}_p}{s - s_\alpha} = \bar{c}_p^T \bar{c}_p \quad . \qquad (2.141)$$

By definition,

$$\lim_{s \to s_p} \frac{\bar{\bar{Z}}(s) = \bar{\bar{Z}}(s_p)}{s - s_\alpha} = \bar{\bar{Z}}'(s_p) \, \delta_{p\alpha} \quad , \qquad (2.142)$$

where

$$\bar{\bar{Z}}'(s_p) = \frac{d\bar{\bar{Z}}}{ds} \bigg]_{s = s_p}$$

and $\delta_{p\alpha}$ is the Kronecker delta function. Taking the limit as s approaches s_p in (3.141) results in

$$\beta_\alpha \bar{c}_p^T \bar{\bar{Z}}'(s_p)\bar{c}_p \bar{c}_p^T \bar{c}_p = \bar{c}_p^T \bar{c}_p \, , \qquad (2.143)$$

from which we conclude that

$$\beta_p = \frac{1}{\bar{c}_p^T \bar{\bar{Z}}'(s_p)\bar{c}_p} \quad . \qquad (2.144)$$

Therefore,

$$\bar{i}(t) = \frac{1}{2\pi j} \int_{\sigma_0 - j\infty}^{\sigma_0 + j\infty} \sum_\alpha \nu_\alpha c_{\alpha_0} \frac{e^{st}}{s - s_\alpha} \, ds \qquad (2.145)$$

where $\quad \eta_\alpha = \beta_\alpha \bar{c}_{\alpha_0}^T \bar{v}_\alpha \qquad\qquad (2.146)$

is defined as the coupling coefficient. With the matrix elements of $\bar{V}(s)$ defined by (2.105), let the incident field be a step-function plane wave, such that

$$E_0(s) = E_0/s.$$

The matrix elements of $\bar{V}(s)$ are then defined as

42

$$v_m = 4\pi\varepsilon_0 E_0 \sin\theta^i e^{-\gamma z_m} \cos\theta^i \left[e^{-\gamma\beta^i a} - e^{\gamma\beta^i(a+2h)} \right]$$

$$m = 2,3,\ldots N-1. \qquad (2.147)$$

Evaluating (2.145) through the residue theorem will produce appropriate Heaviside functions, which are viewed as enforcing causality [37], [1-3].

The exponential dependence of (2.145) is expressed by

$$v_m e^{st} = D e^{-\gamma z_m} \cos\theta^i \left[e^{-\gamma\beta^i a} - e^{\gamma\beta^i(a+2h)} \right] e^{st}, \qquad (2.148)$$

where

$$D = 4\pi\varepsilon_0 E_0 \sin\theta^i. \qquad (2.149)$$

(2.148) can be written as

$$v_m e^{st} = D \left[e^{s\left[t - \frac{z_m \cos\theta^i + \beta^i a}{c}\right]} - e^{s\left[t - \frac{z_m \cos\theta^i - \beta^i(a+2h)}{c}\right]} \right] \qquad (2.150)$$

such that (2.145) becomes

$$\bar{I}(t) = \frac{1}{2\pi j} \int_{\sigma_0 - j\infty}^{\sigma_0 + j\infty} \sum_\alpha \frac{\beta_\alpha \bar{C}_{\alpha_0} \bar{C}_{\alpha_0}^T}{s - s_\alpha} \bar{V}_\alpha(s) \, ds \qquad (2.151)$$

with $\bar{V}_\alpha(s)$ a vector with matrix elements defined by (2.150). In other words,

$$\bar{V}_\alpha(s) = [v_m e^{st}] = \bar{V}(s)e^{st}. \qquad (2.152)$$

For the sake of simplicity, let

$$\tau_1 = \frac{z_m \cos\theta^i + \beta^i a}{c} \qquad (2.153)$$

43

and

$$\tau_2 = \frac{z_m \cos \theta^i - \beta^i(a + 2h)}{c} \quad , \qquad (2.154)$$

such that the matrix elements of $\bar{V}_\alpha(s)$ are

$$v_m e^{st} = D \left[e^{s(t-\tau_1)} - e^{s(t-\tau_2)} \right] . \qquad (2.155)$$

Since the integrand of (2.151) has only poles at $s = s_\alpha$, evaluation

through the residue theorem produces

$$\bar{I}(t) = \sum_\alpha \beta_\alpha \bar{C}_{\alpha_0} \bar{C}_{\alpha_0}^T \bar{v}_\alpha(t) \qquad (2.156)$$

where

$$\bar{v}_\alpha(t) = [v_{m_\alpha}(t)] \qquad (2.157)$$

with

$$v_{m_\alpha}(t) = D \left(u(t-\tau_1) e^{s_\alpha(t-\tau_1)} - u(t-\tau_2) e^{s_\alpha(t-\tau_2)} \right) \quad .$$
$$m = 2,3,\ldots N-1 \qquad (2.158)$$

Note that the complex natural frequencies, natural mode vectors,

and normalization coefficients are not functions of the incident field.

Only $\bar{v}_\alpha(t)$ is altered upon a change in the angles of incidence. There-

fore, once s_α, β_α, and $\bar{C}_{\alpha_0}$ are found for a particular L, h, and a,

the current excited by any incident field is easily found. This is

perhaps the greatest utility of SEM.

The singularity expansion method, applied to this transient elec-

tromagnetic problem, produces a system of matrices, which are solved for

the induced current on the object cylinder as a function of time.

Heuristic study into the nature of these complex natural frequencies,

44

natural mode vectors, and normalization coefficients is justified

through a better understanding of the two-body transient scattering

problem.

Approximations and Limitations Imposed

The approximations and assumptions which are accepted throughout

this thesis are of prime importance. Whether analytical or numerical

solutions to problems are exercised, final results must be evaluated in

light of limitations placed upon their very existence. Therefore, this

section brings together all of these approximations and assumptions

with the purpose of examination and evaluation.

The assumptions and approximations are as follows:

a) Current is assumed to flow only in the direction of the
cylinder axis (2.11).

b) Boundary conditions are enforced only to the axial
component of the tangential electric field (2.61).

c) End caps on the cylinders are ignored (2.8).

d) The current is assumed to be separable (2.17).

e) Taylor's [40] equations are adapted for the circumferen-
tial variation of the currents (2.18).

f) The moment method introduces an approximate numerical
solution (2.95).

g) The exponential $e^{-\gamma r}$ is expanded in a two term Taylor
series for the solution of T (A1.5).

As previously outlined in the introduction, the first two assumptions

restrict the cylinder to be thin, L >> a. Ignoring the endcaps amounts

to letting the cross sectional surface area be small, a << λ, so that

any current induced on the endcaps will not significantly contribute to

the scattered field [46]. By assuming the current to be separable, the

45

restriction that L >> a is again necessary, since this approximation is poor only near the ends of the cylinders.

Up to this point, the most restrictive clause placed upon this formulation is that the length of the cylinder must be much greater than its radius. Thus, the cylinders must be thin.

Taylor [40] states that the equation for circumferential variations of the axial current (2.18) is applicable to electrically thin cylinders separated a short distance from the ground plane and provided the length is much greater than the height above the ground plane, the expressions can be used for finite length cylinders. Concerning the separation from the ground plane, this restriction is linked to approximating the two parallel cylinders as supporting a transmission line mode (TEM). Typically, this TEM mode requires that $h \ll \lambda$, $a \ll \lambda$, and $L \gg h$. Nevertheless, note that when $a \ll h$, (2.18) approaches unity and the circumferential variations of the axial current becomes uniform − as would be the case for a thin cylinder far from the ground plane [1-4]. The current is uniformly distributed in ϕ at a far distance from the ground plane and only becomes nonuniformly distributed as the cylinder draws near the ground plane. Therefore, when (2.18) is actually affecting the distribution of the currents, these typical TEM mode restrictions are satisfied. More importantly, when the cylinder is far removed, circumferential variation of the currents is uniform, (2.18) doesn't significantly affect the equations, and the typical transmission line restrictions need not be satisfied.

With reference to (A1.5), the Taylor series expansion of $e^{-\gamma r}$ about $r = 0$ is truncated after two terms:

46

$$e^{-\gamma r} = 1 - \gamma r + \frac{r^2\gamma^2}{2!} - \frac{r^3\gamma^3}{3!} + \ldots \frac{(-1)^n r^n \gamma^n}{n!} + \ldots \qquad (2.159)$$

$$= \sum_{n=o}^{\infty} \frac{(-r\gamma)^n}{n!} \quad ,$$

where

$$r = [z^2 + d^2 \sin^2 \phi/2]^{1/2} \quad -\frac{\Delta}{2} < z < \frac{\Delta}{2} \quad . \qquad (2.160)$$

The maximum of γr is

$$\text{max of } \gamma r = \gamma \sqrt{z^2 + d^2} \quad , \qquad (2.161)$$

where

$$d = 2a.$$

Thus

$$\text{max of } \gamma r = \gamma \sqrt{z^2 + 4a^2}$$

$$= \gamma \sqrt{\frac{\Delta^2}{4} + 4a^2}$$

$$= 2 \sqrt{\frac{(\gamma\Delta)^2}{16} + (\gamma a)^2} \quad . \qquad (2.162)$$

If

$$\gamma\Delta \ll 1 \qquad (2.163)$$

and

$$\gamma a \ll 1, \qquad (2.164)$$

it follows that

47

$$\text{max of } \gamma r \ll 1. \tag{2.165}$$

Therefore,

$$e^{-\gamma r} \approx 1 - \gamma r \tag{2.166}$$

provided (2.163) and (2.164) are satisfied. This does not place any restrictions on the relative zone size, Δ, with respect to the radius as pointed out by Tesche [43]. By momentarily letting $\gamma = 2\pi/\lambda$, (2.163) and (2.164) are implied by

$$\Delta \ll \lambda \tag{2.167}$$

$$a \ll \lambda. \tag{2.168}$$

The restriction, (2.167), is a necessity whenever a numerical technique is forthcoming. Accurate reconstruction of the current on an object couldn't be expected if the zone size was on the order of a wavelength. As for (2.160), the cylinder has already been assumed thin with respect to L and this must now require that the cylinder be thin with respect to wavelength. Since this is not a steady-state problem but one involving transients composed of an infinite number of frequencies, (2.168) indicates that this formulation is not applicable to high frequency response analysis. In conclusion, the "most" restrictive sentence encountered is that this formulation applies to thin cylinders.

III. NUMERICAL METHODS AND RESULTS

A computer code has been written to implement the equations developed in the previous section and thereby determine the natural resonances, natural mode vectors, normalization coefficients, and transient current response. The cylindrical scatterer is described by a general length, radius, and height above the ground plane. Illumination is provided by a step-function plane wave with arbitrary angles of incidence. Brief mention of some of the numerical methods used is warranted.

In order to better adapt the equations for z_{mn} (2.112), $H_{0_{mn}}$(2.108), and $H_{i_{mn}}$(2.110) to numerical evaluation, their form can be altered. After suppressing the functional dependence and highlighting the matrix notation, these equations are

$$z_{mn} = \frac{\sqrt{1-(a/h)^2}}{2\pi\Delta^2}\Big[H_0(m+1,n) - (\gamma^2\Delta^2+2)H_0(m,n) + H_0(m-1,n)$$

$$-H_i(m+1,n) + (\gamma^2\Delta^2+2)H_i(m,n) - H_i(m-1,n)\Big]$$

$$\text{(3.1)}$$

$$H_0(m,n) = \int_{(n-3/2)\Delta}^{(n-1/2)\Delta} \int_0^{2\pi} \frac{1}{1+(a/h)\cos\phi_0} \frac{e^{-\gamma r_1}}{r_1} d\phi_0{}' \, dz'$$

$$\text{(3.2)}$$

$$H_i(m,n) = \int_{(n-3/2)\Delta}^{(n-1/2)\Delta} \int_0^{2\pi} \frac{1}{1-(a/h)\cos\phi_i} \frac{e^{-\gamma r_2}}{r_2} d\phi_i{}' \, dz',$$

$$\text{(3.3)}$$

where

$$r_1 = [d^2 \sin^2 \frac{\phi_0'}{2} + ((m-1)\Delta - z')^2]^{1/2} \tag{3.4}$$

$$r_2 = [(d^2 + 8ah) \sin^2\frac{\phi_i'}{2} + 4h^2 + ((m-1)\Delta - z')^2]^{1/2} \quad . \tag{3.5}$$

Knowledge of the symmetries occuring in these matrix equations can significantly reduce the amount of computer time required for this numerical solution. In (3.2), let

$$u = z' - (n-3/2)\Delta \;, \tag{3.6}$$

such that

$$H_0(m,n) = \int_0^\Delta \int_0^{2\pi} \frac{1}{1 + (a/h)\cos \phi_0'} \frac{e^{-\gamma r}}{r} d\phi_0' \; du \tag{3.7}$$

with

$$r = [d^2 \sin^2 \frac{\phi_0'}{2} + (\Delta(m-n+1/2) - u)^2]^{1/2} \quad . \tag{3.8}$$

Obviously,

$$H_0(m,n) = H_0(m+i, n+i) \qquad i = 0,1,2,3\ldots \tag{3.9}$$

since r is determined by the difference between m and n – not their actual values. Note also that a similar change of variables in (3.3) leads to the same conclusion with regard to H_i. On relating this symmetry to (3.1), it is apparent that

$$z_{mn} = z_{m+i \; n+i} \qquad i = 0,1,2\ldots \quad . \tag{3.10}$$

Thus, every element in any diagonal of the impedance matrix, $\bar{\bar{Z}}(s)$, is identical. This reduces the number of matrix elements, z_{mn}, which have

to be calculated fron $(N-2)^2$ to only 2N-5. Furthermore, upon numerical evaluation it was found that

$$H_0(m,n) = H_0(n,m) \tag{3.11}$$

and likewise that this symmetry existed in H_i. Through (3.1), it follows that

$$z(m,n) = z(n,m). \tag{3.12}$$

Proving (3.11) analytically was pursued at length, but not established. However, this symmetry was used to conserve computer time in calculating $z(m,n)$. These simplifications require that only $H_0(m,n)$ and $H_i(m,n)$ for m = 1 and n = 2,3,...N-1 be determined along with T (2.125) in order to form the entire impedance matrix.

Since both single and double numerical integrations were necessary, a n-dimensional Romberg integration routine [47] was modified for dealing with complex functions.

Other researchers [1-3] have considered the interactions of thin cylinders with an electromagnetic pulse over perfectly conducting grounds. The "thin-wire" assumptions and approximations have been incorporated into an SEM analysis. One of several computer programs written by Shumpert [1], [3] was secured and data obtained concurrently with the computer code written by this author. In this manner, the number of zones used, accuracy requested, and geometrical parameters were insured to be identical. The numerical results produced by Shumpert's [1] computer program, shall be associated with the title "approximate" kernel, in the sense that the "thin-wire" approximations were incorporated; and in particular, the current was approximated by

51

filaments of current on the cylinder axis. Data found through equations developed in this paper shall be associated with the label "exact" kernel, for obvious reasons.

Before presenting da:a related to the cylindrical scatterer over the ground plane, a brief analysis of the cylinder in free space is appropriate. By setting the image terms (2.110) equal to zero and letting h >> a, the impedance matrix (2.112) reduces to one characteristic of a cylindrical scatterer in free space with uniform circumf··en-tial variation of the axial current. The kernel is still "exact", in the sense that the current resides on the cylinder surface. Figure 3-1 illustrates the position of some of the complex natural resonances, or singularities, for both the "exact" and "approximate" kernel. Only the second quadrant is shown - the complex conjugates appearing in the third quadrant. As noted by Tesche [37], the singularities occur in layers and can be described by two subscripts, $s_{\ell n}$: "ℓ" denoting the layer of the pole and "n" referring to the pole within that layer. The natural frequencies are presented as having mode distributions that are either even or odd with respect to the scatterer center. Figure 3-1 illustrates the soundness of the third "thin-wire" approximation - currents might as well be approximated by filaments of current on the cylinder axis, since singularity locations for the "exact" and "approximate" kernels occur at essentially the same points. Computer time required to locate the singularities through the "exact" kernel was roughly twice that necessary with Shumpert's [1] program. Table 3-1 gives the numerical data depicted in Figure 3-1. Figure 3-2 points out the well-known fact that as the cylinder becomes fatter, the singularities must move to the

left and down [37]. From circuit theory, this movement points to a decreased quality factor, Q, [48], which is expected as the radius of the cylinder becomes larger with respect to its length. Data shown in Figure 3-2 for the case of $L/a = 10$ can only be considered as a "first-cut" approximation because of the thin cylinder restrictions that have been imposed upon the "exact" kernel. Nevertheless, one would expect the results, displayed in Figure 3-2, for the "exact" kernel to be more accurate as the cylinder approaches $L/a = 10$ than the trajectory produced by the "approximate"kernel Table 3-2, presenting Figure 3-2 in tabular form, shows the divergence of correlation between the "approximate" and "exact" kernels as the cylinder becomes fatter. Note that in this figure and table, the commonly used shape parameter is defined by

$$\Omega = 2 \ln(L/a). \tag{3.13}$$

Suppose a cylinder with a shape parameter of 10.6 ($L/a = 200$) is now placed in proximity to and parallel to a perfectly conducting ground plane of infinite extent. As the cylinder approaches the ground plane, the circumferential variation of the current becomes nonuniform and one would expect the singularities nearest the imaginary axis to approach the theoretical resonances of the ideal two-wire transmission line. As displayed in Figure 3-3 the singularity associated with the first resonance of the scatterer itself, s_{11}, moves toward its expected destination, $\omega L/c = \pi$. Both the "approximate" and the "exact" kernel yield the same trajectory until $h/L \cong .1$ or when the scatterer is approximately twenty radii

53

away from the ground plane. The "exact" kernel continues on its upward arc toward the first resonance of the transmission line as the "approximate" kernel falls rapidly toward the origin. The increasing difference between the s_{11} singularity locations predicted by the two different formulations is highlighted in Table 3.3. With the cylinder two radii away from the ground plane, the "approximate" kernel was ill conditioned and the singularity could not be located. Figures 3-4, 3-5, 3-6, and 3-7 present similar trajectories of the s_{11} singularity for L/a = 100, 30, 20, and 10 respectively. Tables 3-4, 3-5, 3-6, and 3-7 exhibit the numerical data observed in the figures of the same number. It should be pointed out that in each of these trajectories, the "exact" and "approximate" kernel data seem to begin diverging when the spacing (h/L) is approximately equal to ten. This fact seems to be rather independent of the particular L/a ratio. The trajectories of the singularities associated with the second resonance of the scatterer itself with L/a = 200, 100, 30, 20, and 10 are found in Figures 3-8 through 3-12. As was the case with the s_{11} trajectories, the path traversed by s_{12} in these figures is predicted by both kernels, until some point of divergence. The exact kernel natural resonance continues to advance towards the imaginary axis while the approximate kernel breaks downward. Note that when L/a is equal to 200, the point of departure between the two formulations occurs when the cylinder axis is slightly closer than L/10 to the ground plane, or when its axis is 20 radii away. With L/a = 100, the last point of agreement in singularity locations between the exact and approximate kernels occurs when h/L = .1 and with the cylinder as close as 10 radii away from the

ground plane. The ratio of height to radius is apparently not as critical as the ratio of height to cylinder length. Tables 3-8 through 3-12 present in tabular form the trajectories of s_{12} corresponding Figures 3-8 through 3-12.

The real and imaginary parts of the normalized natural modes associated with the first three resonances of the scatterer for $L/a = 30$ and $h/L = 0.05$ are found in Figure 3-13. It may be pointed out that these distributions are essentially indentical to those found previously for scatterers isolated in free space.

With the coupling coefficient as defined in eq. (2.146), calculations of this coefficient versus the angle θ^i were made for the case $L/a = 30$ and $h/L = 0.05$. These calculations are shown in Figure 3-14. (Note the angle ϕ^i was held constant at $\phi^i = 180°$.) As would be expected, the η_{11} and η_{13} peak for broadside incidence. However it is more difficult to interpret the behavior of η_{12}. Figure 3-15 presents similar data for η_α for the case $L/a = 20$ and $h/L = 0.075$.

With the thin cylindrical scatterer far removed from the ground plane, let the direction of propagation of the incident field be such that $\theta^i = 30°$ and $\phi^i = 180°$ (see Fig. 2-2). The current on the cylinder at $z/L = .75$ is presented in Figure 3-16 for both the exact and approximate kernel. Data for the approximate kernel was found by Umashankar [2], [3] and is made note of only to illustrate correlation between the two kernels when the circumferential variation of the axial current is uniform. All of the current plots in this note were constructed using the first three singularities nearest the imaginary axis, which is a valid approach [1-3] when considering "late time", low frequency

response. Obviously, the utility of the exact kernel formulation is with the scatterer near the ground plane. With the scatterer 1/20 of its length away from the cylinder broadside ($\theta^i = 90°$) and from above ($\theta^i = 180°$). As shown in Figure 3-17, the transient current on the cylinder at three different positions is presented for the case when $L/a = 30$, $\frac{h}{L} = 0.05$, $\theta^i = 90°$, and $\phi^i = 180°$. As indicated, the low damping constant results in considerable ringing of this current. A similar transient current was obtained for the case $L/a = 20$, $h/a = 0.075$, $\theta^i = 90°$, and $\phi^i = 180°$. Again, considerable ringing is evidneced as indicat.d by the close proximity of the poles to the $j\frac{\omega L}{c}$ axis in the trajectory curves. Since both time histories presented in the previous two figures represented behavior for broadside incidence from above the scatterer, another more general case is included in Figure 19 where $L/a = 30$, $h/L = 0.05$, $\theta^i = 30°$, $\phi^i = 180°$, and $/L = 0.25, 0.5, 0.75$.

Note: Due to the small difference between singularity locations
for the exact and approximate kernels with respect
to graph dimensions, they are shown at the
same point.

L/a = 200 (Ω=10.6)

x EVEN MODES
● ODD MODES
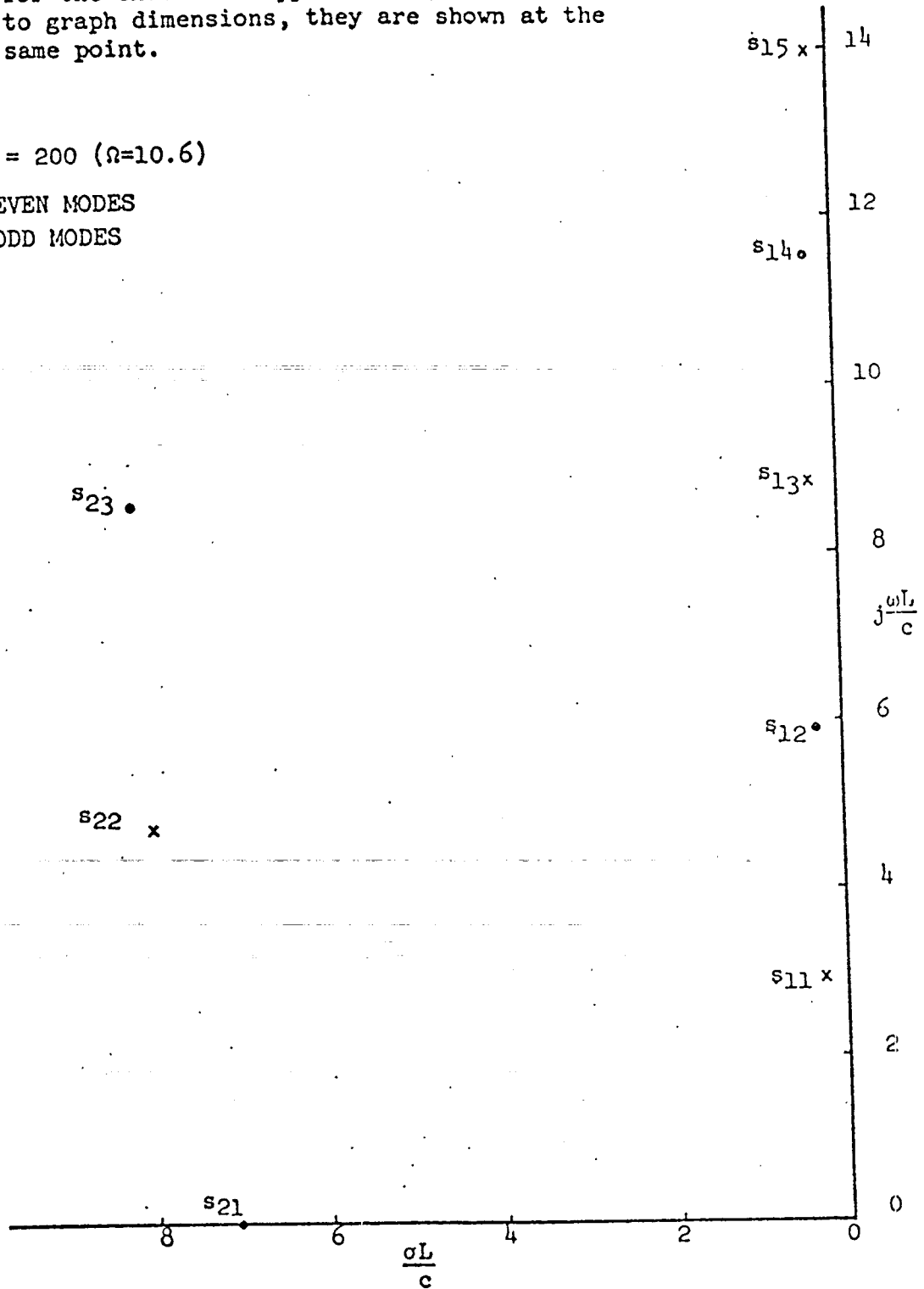
Figure 3-1.   Singularity Locations of the Free Space Case with L/a=200
              - Approximate and Exact Kernels

Table 3-1. Location of the Singularities for the Free Space Case where
L/a = 200. (Note: Approximate and Exact Kernels yield
essentially the same values for a very thin wire scatterer.)

SINGULARITY	LOCATION
S_{11}	-0.2575+j2.9093
S_{12}	-0.3570+j5.9346
S_{13}	-0.3903+j8.8286
S_{14}	-0.3676+j11.5061
S_{15}	-0.1920+j15.9934
S_{21}	-7.1023+j0.0031
S_{22}	-8.0816+j4.7632
S_{23}	-8.1417+j8.4358

EXACT KERNEL - EVEN MODES
APPROXIMATE KERNEL - EVEN MODES

EXACT KERNEL - ODD MODES
APPROXIMATE KERNEL - ODD MODES
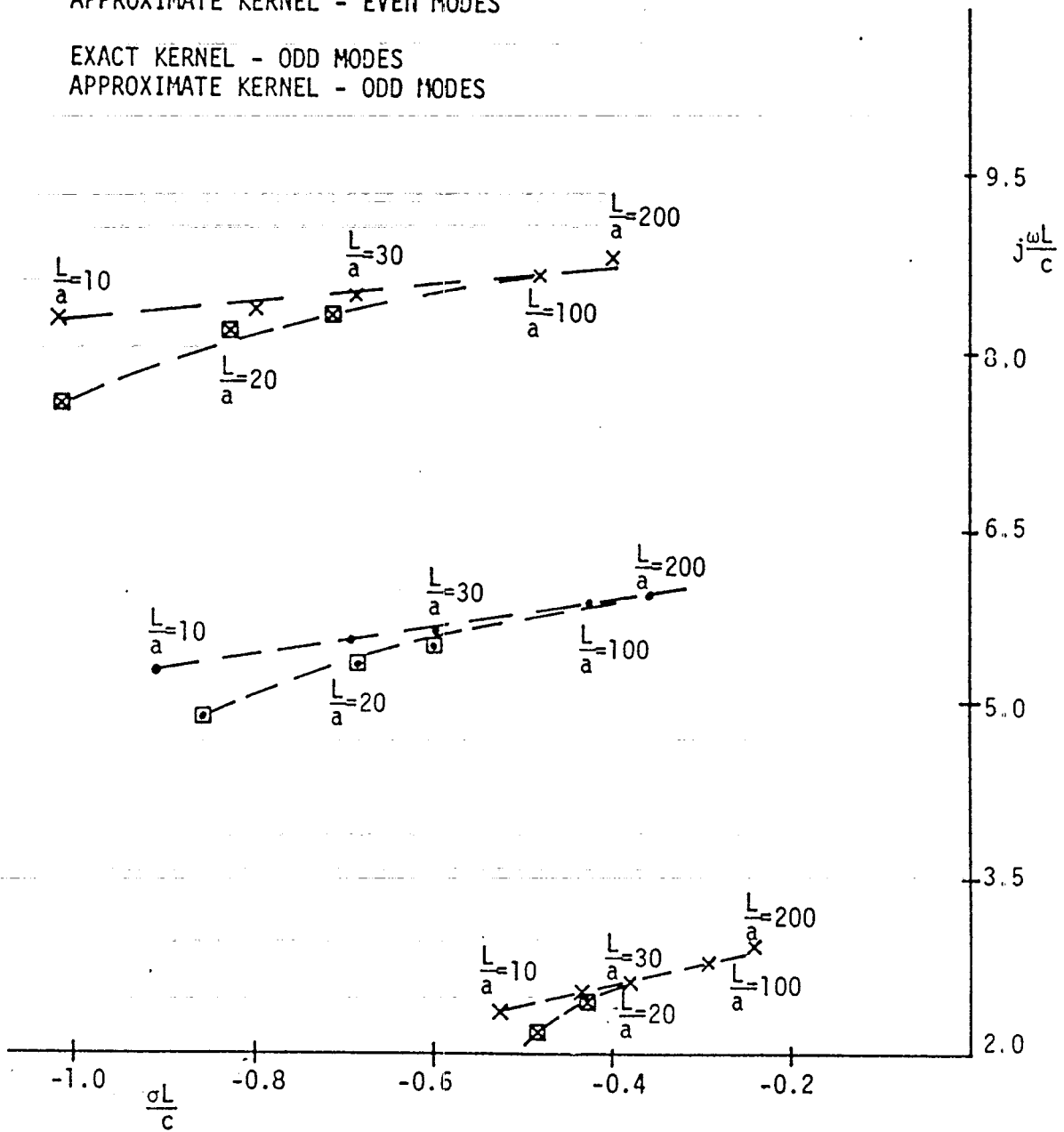
Figure 3-2.   Trajectories of the Singularities Associated with the First
Three Resonances of the Scatterer Itself for the Free Space
Case as a Function of L/a - Approximate and Exact Kernels.

Table 3-2. Trajectories of Singularities Associated with the First
Three Resonances of the Scatterer in Free Space as a
Funcation of L/a.

| L/a | Ω | Singularity Locations | | | Solution Method |
		S_{11}	S_{12}	S_{13}	
200	10.60	-0.2575+j2.9093	-0.3570+j5.9346	-0.3903+j8.8286	"approximate"
		-0.2576+j2.9096	-0.3557+j5.9368	-0.3858+j8.8338	"exact"
100	9.21	-0.2970+j2.8499	-0.4230+j5.8550	-0.4702+j8.7407	"approximate"
		-0.2973+j2.8517	-0.4212+j5.8612	-0.4633+j8.7533	"exact"
30	6.80	-0.3903+j2.6524	-0.5990+j5.5646	-0.6995+j8.4030	"approximate"
		-0.3946+j2.6742	-0.5990+j5.6232	-0.6804+j8.5088	"exact"
20	5.99	-0.4279+j2.5377	-0.6815+j5.3829	-0.8167+j8.1833	"approximate"
		-0.4380+j2.5847	-0.6879+j5.5098	-0.7866+j8.4120	"exact"
10	4.61	-0.4893+j2.2499	-0.8464+j4.8964	-1.0790+j7.5747	"approximate"
		-0.5340+j2.3878	-0.9065+j5.3055	-1.0085+j8.3377	"exact"

60

Note: When the difference between exact and approximate kernel singularity locations is small, they are shown as one point.

L/a = 200 (Ω ≐ 10.6)

× s_{11} SINGULARITY - EXACT KERNEL
⊠ s_{11} SINGULARITY - APPROXIMATE KERNEL
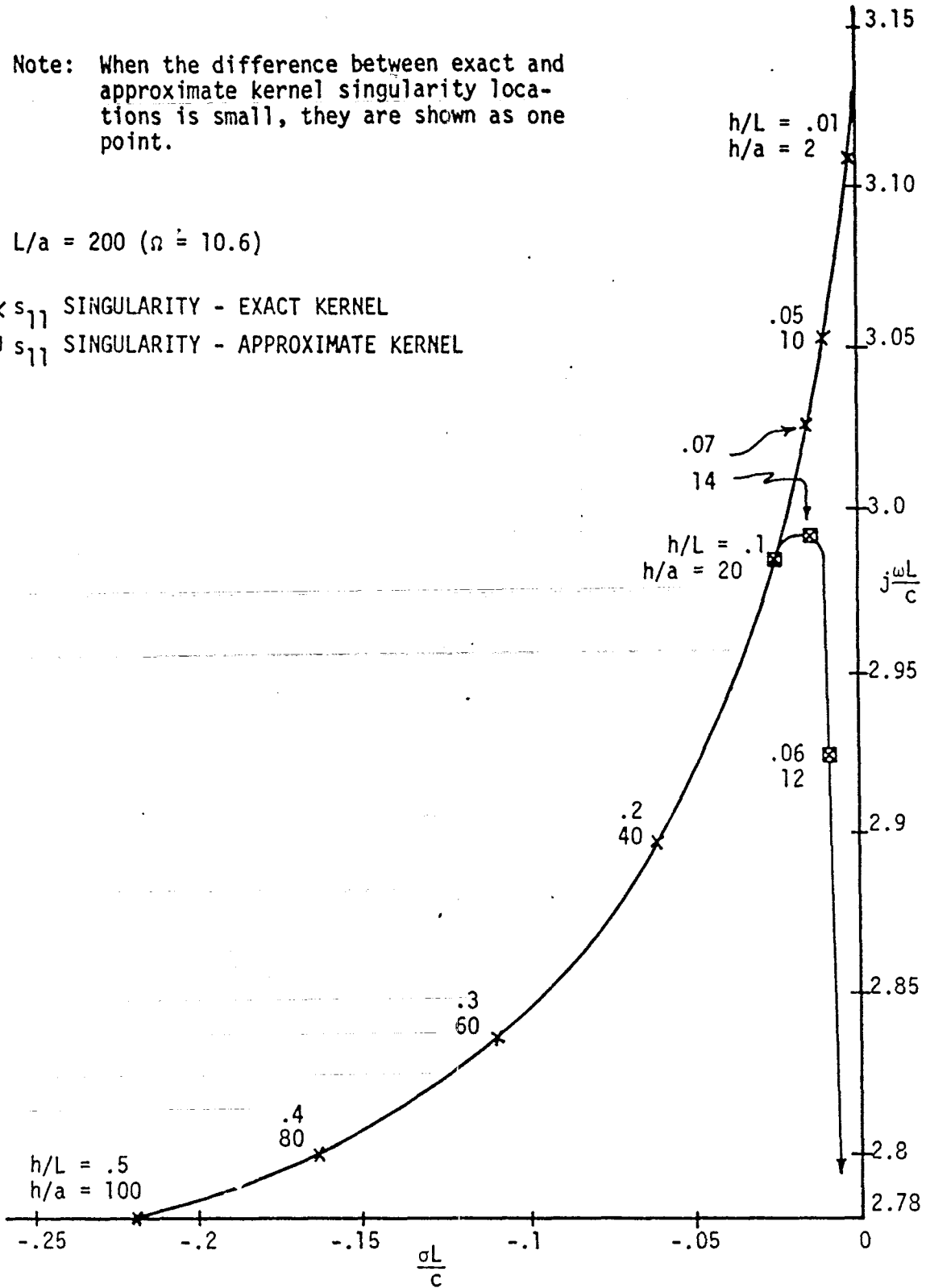
Figure 3-3. Trajectory of the Singularity Associated with the First Resonance of the Scatterer Itself as a Function of h/L or h/a with L/a=200 - Approximate and Exact Kernels

Table 3-3: Trajectory of the Singularity Associated with the First
Resonance of the Scatterer Itself as a Function of h/L
or h/a with L/a = 200 - Approximate and Exact Kernels

L/a = 200   (Ω = 10.6)

h/L	h/a	s_{11} SINGULARITY LOCATION	
		APPROXIMATE KERNEL	EXACT KERNEL
.75	150	-.3755 + j2.8313	-.3769 + j2.8339
.6	120	-.2824 + j2.7804	-.2840 + j2.7811
.5	100	-.2212 + j2.7805	-.2228 + j2.7806
.4	80	-.1635 + j2.8001	-.1649 + j2.7998
.3	60	-.1099 + j2.8385	-.1113 + j2.8380
.2	40	-.0615 + j2.8987	-.0626 + j2.8982
.1	20	-.0217 + j2.9866	-.0225 + j2.9894
.07	14	-.0121 + j2.9928	-.0131 + j3.0257
.06	12	-.0087 + j2.9256	-.0104 + j3.0391
.05	10	-.0042 + j2.5959	-.0079 + j3.0532
.01	2	_____	-.0009 + j3.1150

L/a = 100 (Ω=9.21)

x s_{11} SINGULARITY – EXACT KERNEL
⊠ s_{11} SINGULARITY – APPROXIMATE KERNEL

h/L = .05
h/a = 5

.06
6

.07
7

.1
10

.06
6

.2
20

.3
30

.4
40

h/L = .5
h/a = 50

$j\frac{\omega L}{c}$

$\frac{\sigma L}{c}$
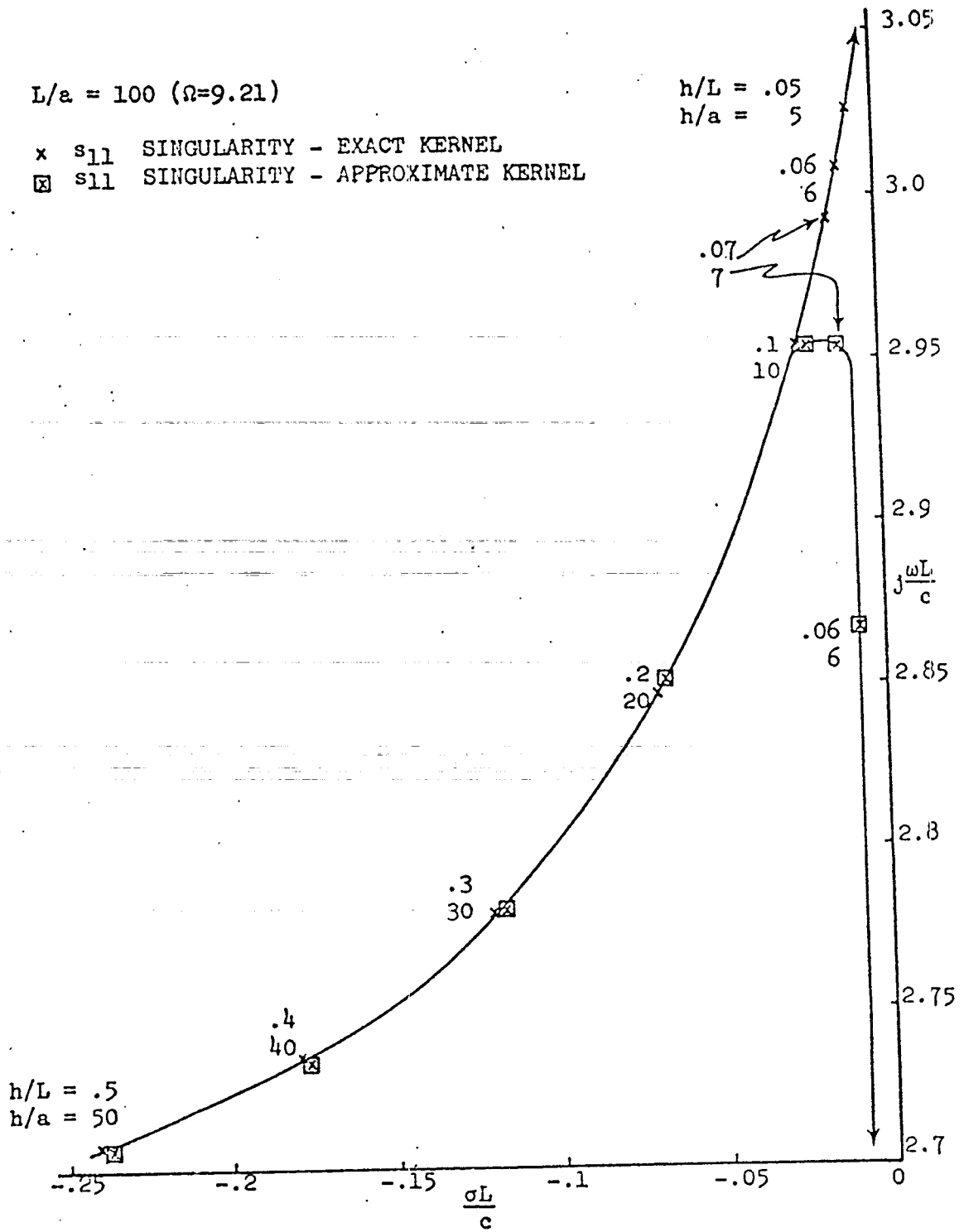
Figure 3-4.   Trajectory of the Singularity Associated with the First
Resonance of the Scatterer Itself as a Function of h/L
or h/a with L/a = 100 – Approximate and Exact Kernels

63

Table 3-4. Trajectory of the Singularity Associated with the First
Resonance of the Scatterer Itself as a Function of h/L
or h/a with L/a = 100 - Approximate and Exact Kernels

$L/a = 100$ ($\Omega = 9.21$)

h/L	h/a	s_{11} SINGULARITY LOCATION	
		APPROXIMATE KERNEL	EXACT KERNEL
.5	50	$-.2375 + j2.7063$	$-.2411 + j2.7064$
.4	40	$-.1767 + j2.7340$	$-.1799 + j2.7331$
.3	30	$-.1202 + j2.7804$	$-.1232 + j2.7787$
.2	20	$-.0689 + j2.8501$	$-.0715 + j2.8476$
.1	10	$-.0256 + j2.9514$	$-.0275 + j2.9514$
.07	7	$-.0146 + j2.9554$	$-.0170 + j2.9933$
.06	6	$-.0103 + j2.8660$	$-.0138 + j3.0088$
.05	5	$-.0040 + j2.4108$	$-.0107 + j3.0256$
.02	2	_____	$-.0035 + j3.0821$

L/a = 30   (Ω = 6.80)

× s_{11} SINGULARITY - EXACT KERNEL

⊠ s_{11} SINGULARITY - APPROXIMATE KERNEL

$j\frac{\omega L}{c}$

2.9

2.8

2.7

2.6

0.06
1.8

0.08
2.4

0.1
3

0.2
6

0.3
9

h/L = 0.4
h/a = 12

-0.3 $\frac{\sigma L}{c}$ -0.2   -0.1   0.0
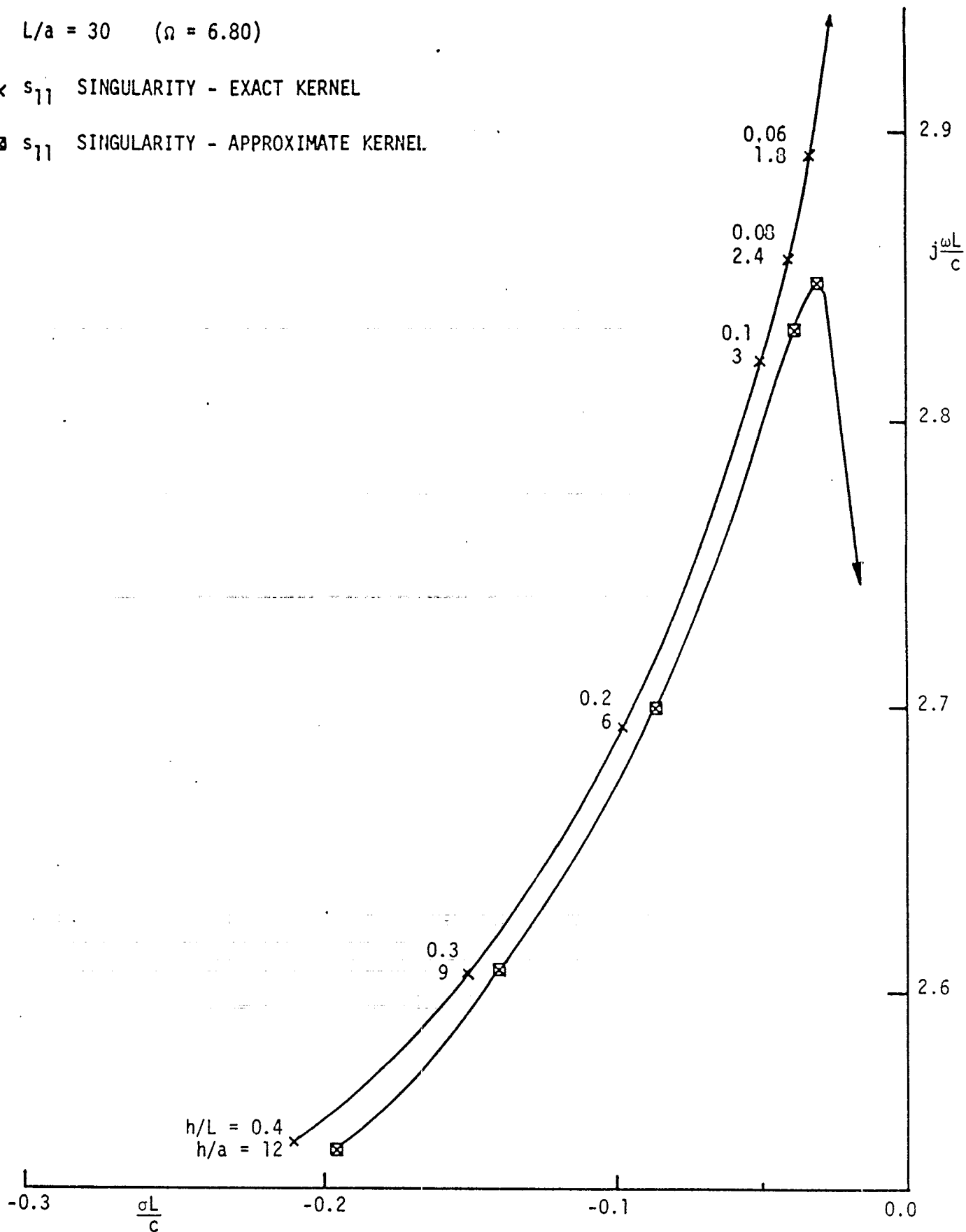
Figure 3-5. Trajectory of the Singularity Associated with the First Resonance of the Scatterer Itself as a Function of h/L or h/a with L/a = 30 - Approximate and Exact Kernels

65

Table 3-5. Trajectory of the Singularity Associated with the First Resonance of the Scatterer Itself as a function of h/L or h/a with L/a = 30 - Approximate and Exact Kernels.

$L/a = 30$ $(\Omega = 6.80)$

h/L	h/a	s_{11} SINGULARITY LOCATION	
		APPROXIMATE KERNEL	EXACT KERNEL
0.4	12	$-0.1957 + j2.5422$	$-0.2098 + j2.5448$
0.3	9	$-0.1387 + j2.6077$	$-0.1505 + j2.6066$
0.2	6	$-0.0850 + j2.7000$	$-0.0957 + j2.6924$
0.1	3	$-0.0362 + j2.8329$	$-0.0454 + j2.8208$
0.08	2.4	$-0.0271 + j2.8500$	$-0.0363 + j2.8547$
0.06	1.8	-----	$-0.0277 + j2.8936$
0.04	1.2	-----	$-0.0173 + j2.9397$
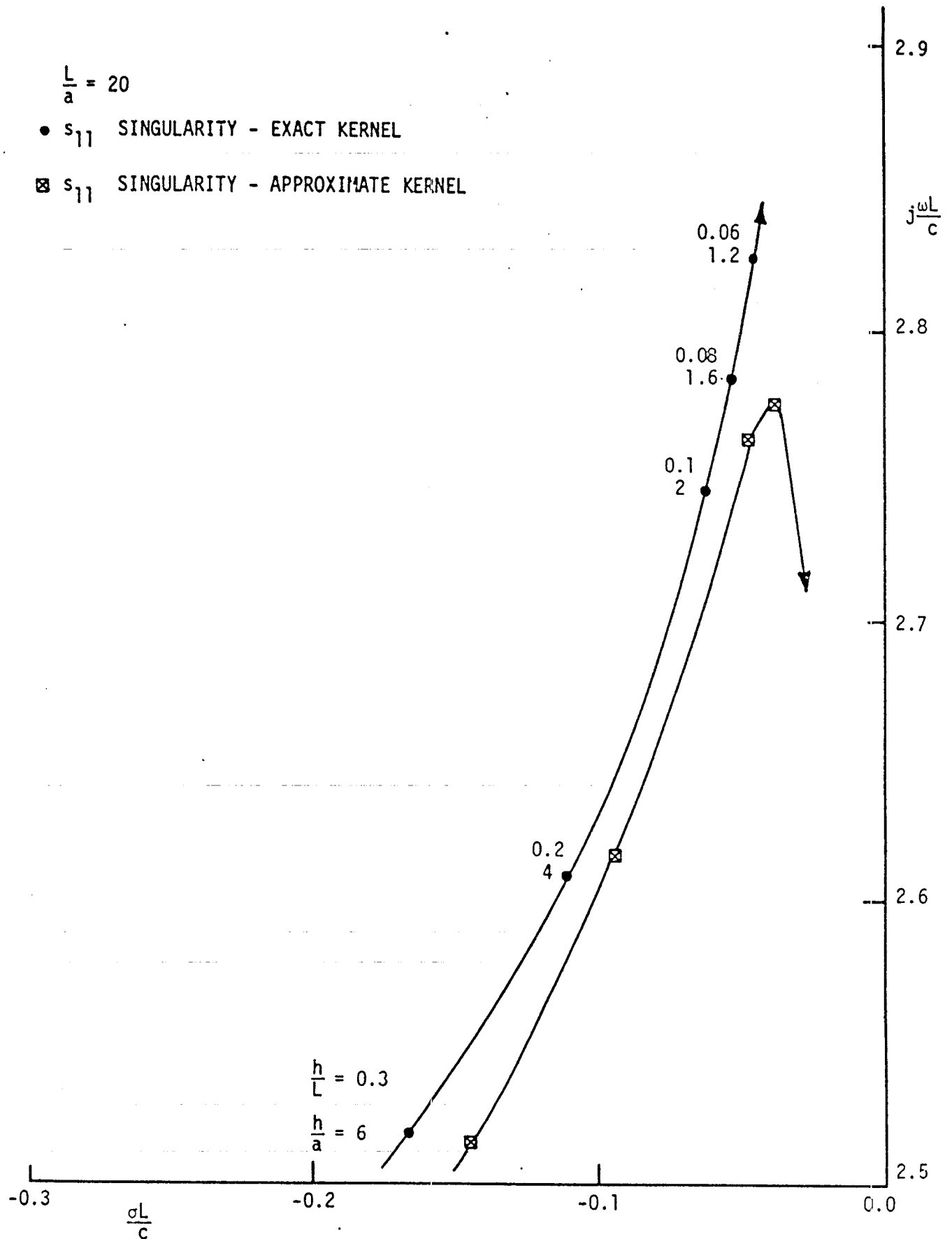
Figure 3-6. Trajectory of the Singularity Associated with the First Resonance of the Scatterer Itself as a function of h/L or h/a with L/a = 20 - Approximate and Exact Kernels

Table 3-6. Trajectory of the Singularity Associated with the First
Resonance of the Scatterer Itself as a Function of h/L
or h/a with L/a = 20 - Approximate and Exact Kernels.

L/a = 20   (Ω = 5.99)

h/L	h/a	s_{11} SINGULARITY LOCATION	
		APPROXIMATE KERNEL	EXACT KERNEL
0.4	8	-0.198 + j2.443	-0.2211 + j2.454
0.3	6	-0.143 + j2.516	-0.1644 + j2.519
0.2	4	-0.091 + j2.617	-0.1085 + j2.611
0.1	2	-0.041 + j2.763	-0.0563 + j2.747
0.08	1.6	-0.031 + j2.776	-0.0463 + j2.784
0.06	1.2	-----	-0.0359 + j2.829

L/a = 10 (Ω = 4.60 5)

x s_{11} SINGULARITY – EXACT KERNEL

⊠ s_{11} SINGULARITY – APPROXIMATE KERNEL

h/L = .2
h/a = 2

2.5

2.4

$j\frac{\omega L}{c}$

2.3

.3
3

.4
4

2.2

.5
5

.6
6

2.1

h/L = .75
h/a = 7.5

2.0

-.5   -.4   -.3 $\frac{\sigma L}{c}$ -.2   -.1   0
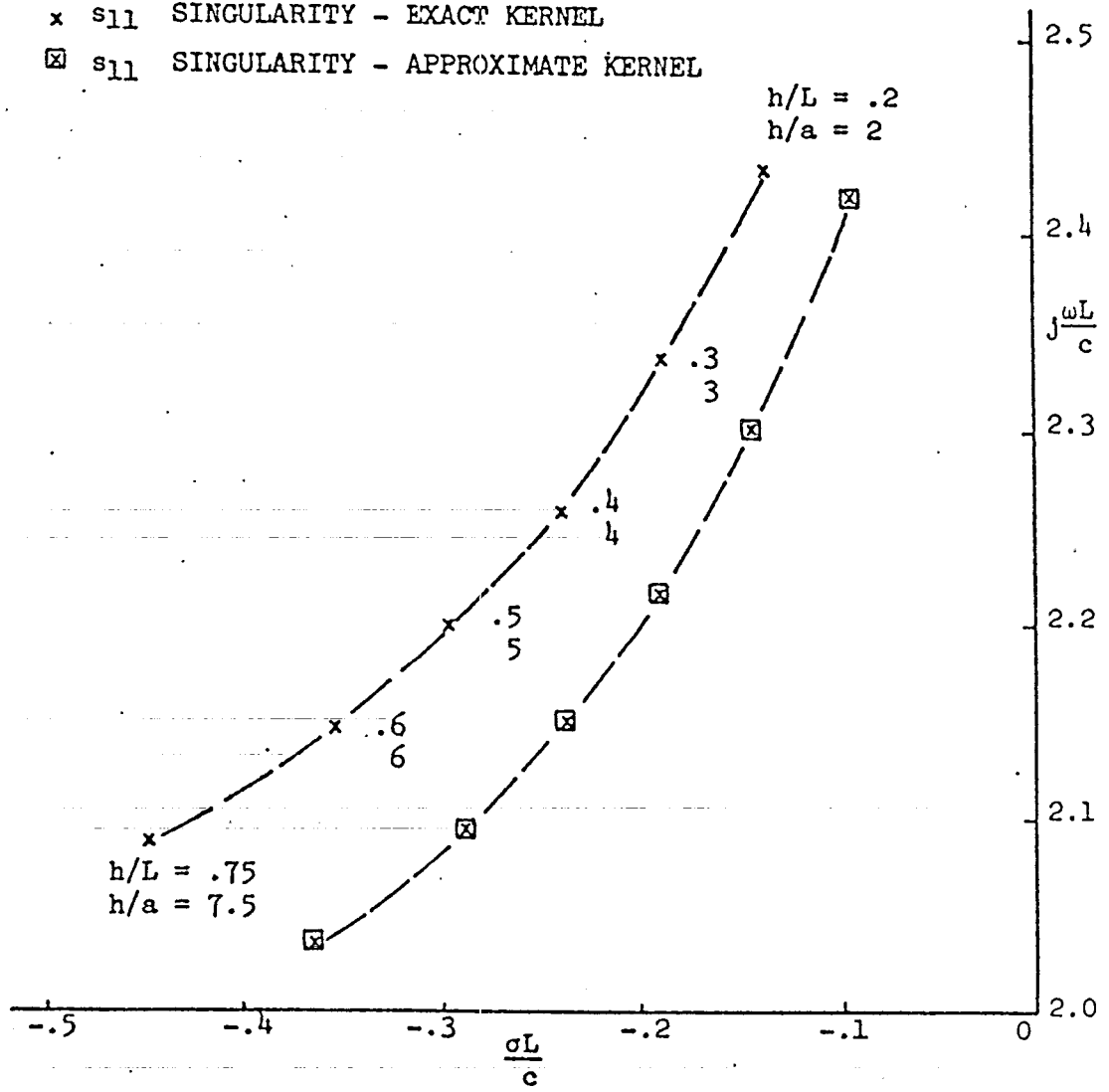
Figure 3-7:   Trajectory of the Singularity Associated with the First
Resonance of the Scatterer Itself as a Function of h/L
or h/a with L/a = 10 – Approximate and Exact Kernels

Table 3.7 Trajectory of the Singularity Associated with the First Resonance of the Scatterer Itself as a Function of h/L or h/a with L/a = 10 - Approximate and Exact Kernels

L/a = 10   (Ω = 4.605)

h/L	h/a	s_{11} SINGULARITY LOCATION APPROXIMATE KERNEL	EXACT KERNEL
.75	7.5	-.3694 + j2.0327	-.4506 + j2.088c
.6	6	-.2905 + j2.0955	-.3565 + j2.1491
.5	5	-.2414 + j2.1482	-.2995 + j2.1982
.4	4	-.1939 + j2.2144	-.2452 + j2.2576
.3	3	-.1473 + j2.3004	-.1923 + j2.3330
.2	2	-.1007 + j2.4190	-.1401 + j2.4345

Note: When the difference between exact and approximate kernel singularity locations is small, they are shown as one point.

L/a = 200 (Ω = 10.6)

$\bullet$ s_{12} SINGULARITY - EXACT KERNEL

$\boxed{\bullet}$ s_{12} SINGULARITY - APPROXIMATE KERNEL

h/L = .5
h/a = 100

.05
10

.06
12

.07
14

.1
20

.06
12

.4
80

.2
40

.3
60

$j\dfrac{\omega L}{c}$

6.1
6.05
6.0
5.95
5.9
5.85
5.8
5.75

-.5   -.4   -.3   -.2   -.1

$\dfrac{\sigma L}{c}$
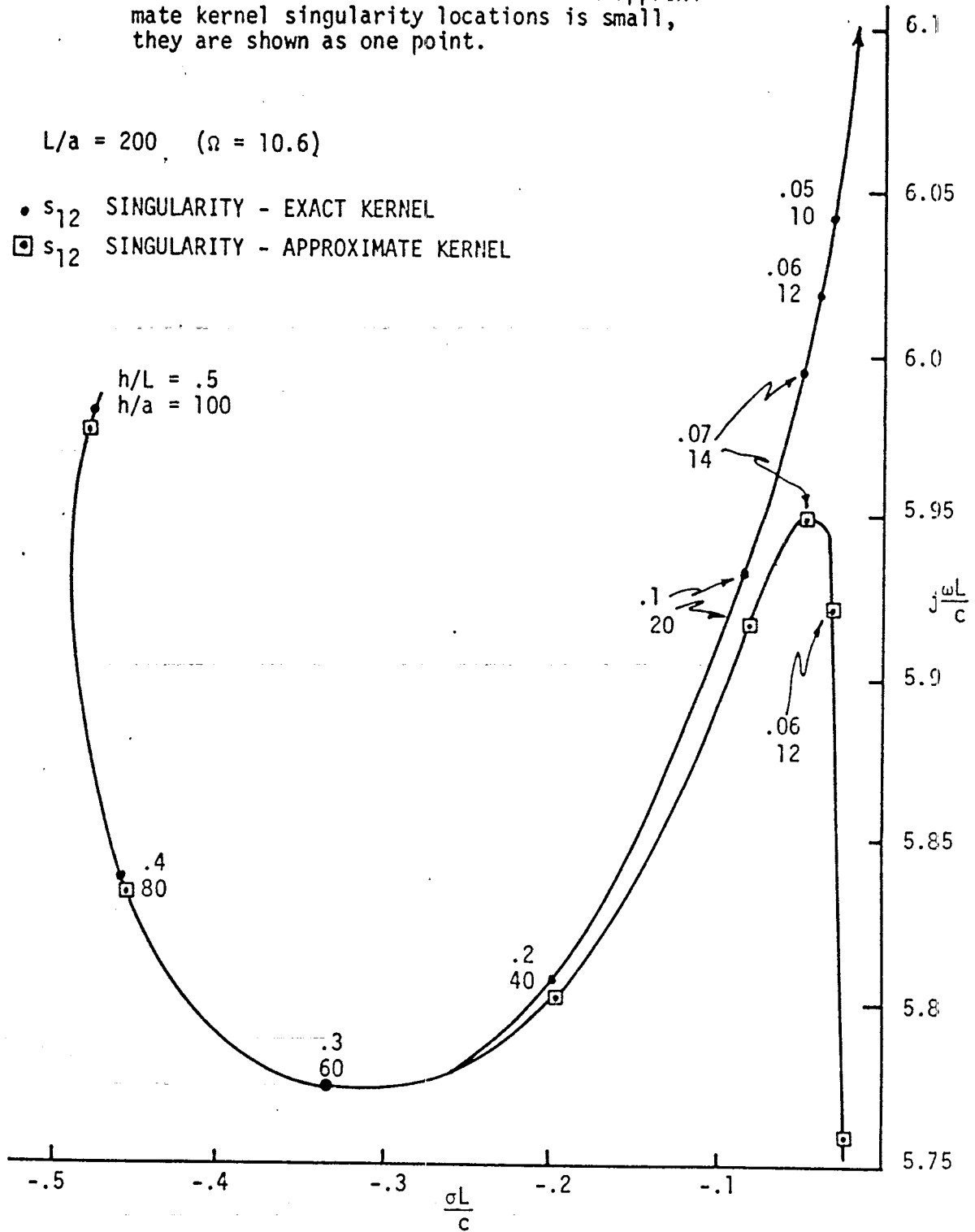
Figure 3-8.   Trajectory of the Singularity Associated with the Second Resonance of the Scatterer Itself as a Function of h/L or h/a with L/a = 200 - Approximate and Exact Kernels

71

Table 3-8 Trajectory of the Singularity Associated with the Second Resonance of the Scatterer Itself as a Function of h/L or h/a with $L/a = 200$ – Approximate and Exact Kernels

$L/a = 200$　$(\Omega = 10.6)$

h/L	h/a	s_{12} SINGULARITY LOCATION APPROXIMATE KERNEL	EXACT KERNEL
.75	150	$-.2919 + j5.9401$	$-.2914 + j5.9404$
.6	120	$-.3633 + j6.0304$	$-.3591 + j6.0308$
.4	80	$-.4589 + j5.8343$	$-.4583 + j5.8404$
.3	60	$-.3385 + j5.7736$	$-.3395 + j5.7783$
.2	40	$-.2014 + j5.8041$	$-.2022 + j5.8092$
.1	20	$-.0774 + j5.9184$	$-.0767 + j5.9339$
.07	14	$-.0468 + j5.9498$	$-.0456 + j5.9945$
.06	12	$-.0369 + j5.9207$	$-.0364 + j6.0178$
.05	10	$-.0254 + j5.760$	$-.0279 + j6.0428$
.01	2	_____	$-.0041 + j6.1552$
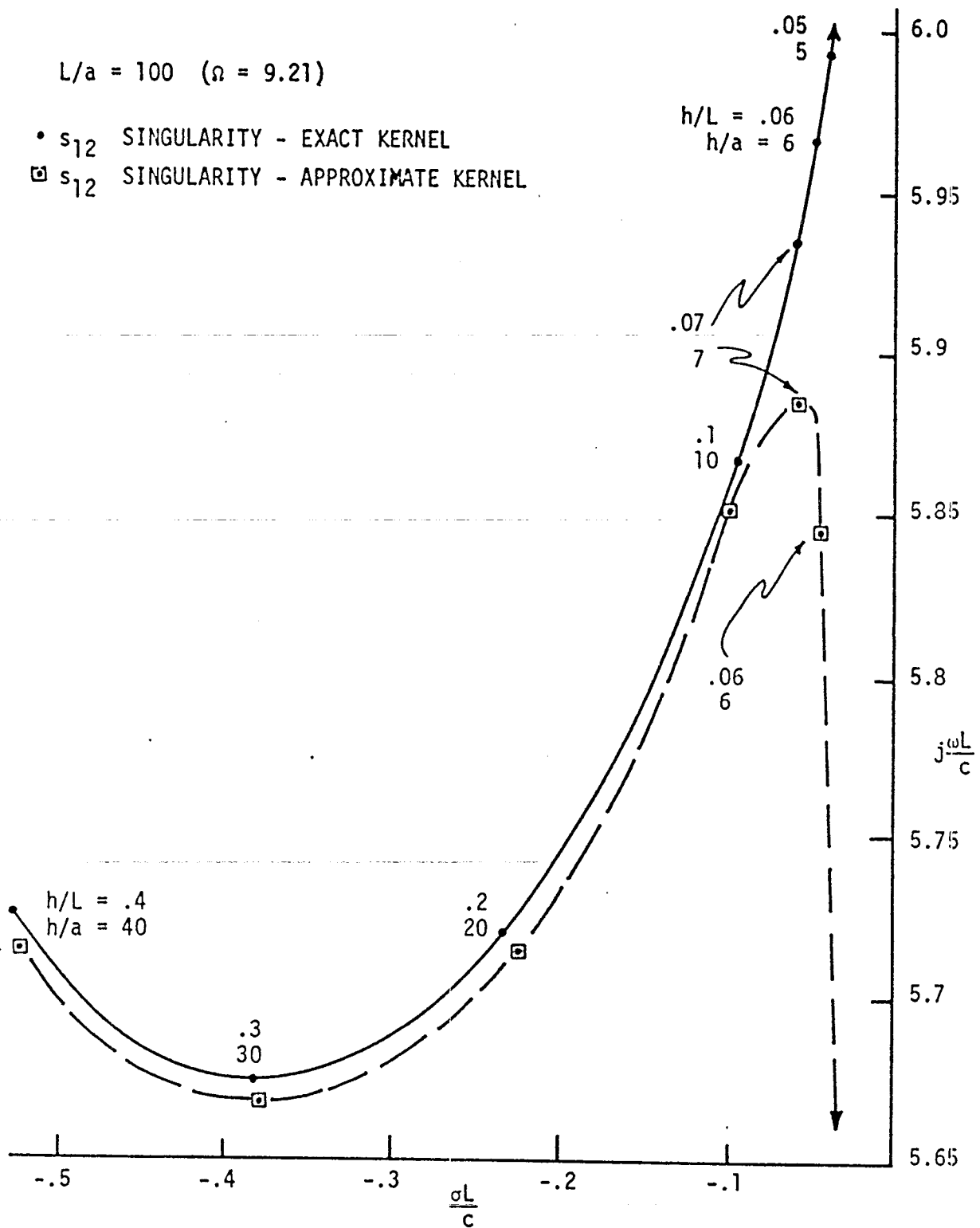
Figure 3-9. Trajectory of the Singularity Associated with the Second Resonance of the Scatterer Itself as a Function of h/L or h/a with L/a = 100 - Approximate and Exact Kernels

Table 3-9. Trajectory of the Singularity Associated with the Second
Resonance of the Scatterer Itself as a Function of h/L
or h/a with L/a = 100 – Approximate and Exact Kernels

L/a = 100   (Ω = 9.21)

h/L	h/a	s_{12} SINGULARITY LOCATION	
		APPROXIMATE KERNEL	EXACT KERNEL
.5	50	$-.5876 + j5.8812$	$-.5807 + j5.8969$
.4	40	$-.5263 + j5.7139$	$-.5304 + j5.7262$
.3	30	$-.3791 + j5.6668$	$-.3848 + j5.6737$
.2	20	$-.2271 + j5.7154$	$-.2323 + j5.7201$
.1	10	$-.0909 + j5.8521$	$-.0938 + j5.8664$
.07	7	$-.0563 + j5.8860$	$-.0583 + j5.9367$
.06	6	$-.0444 + j5.8451$	$-.0475 + j5.9673$
.05	5	$-.0295 + j5.6256$	$-.0375 + j5.9931$
.02	2	_____	$-.0124 + j6.0958$
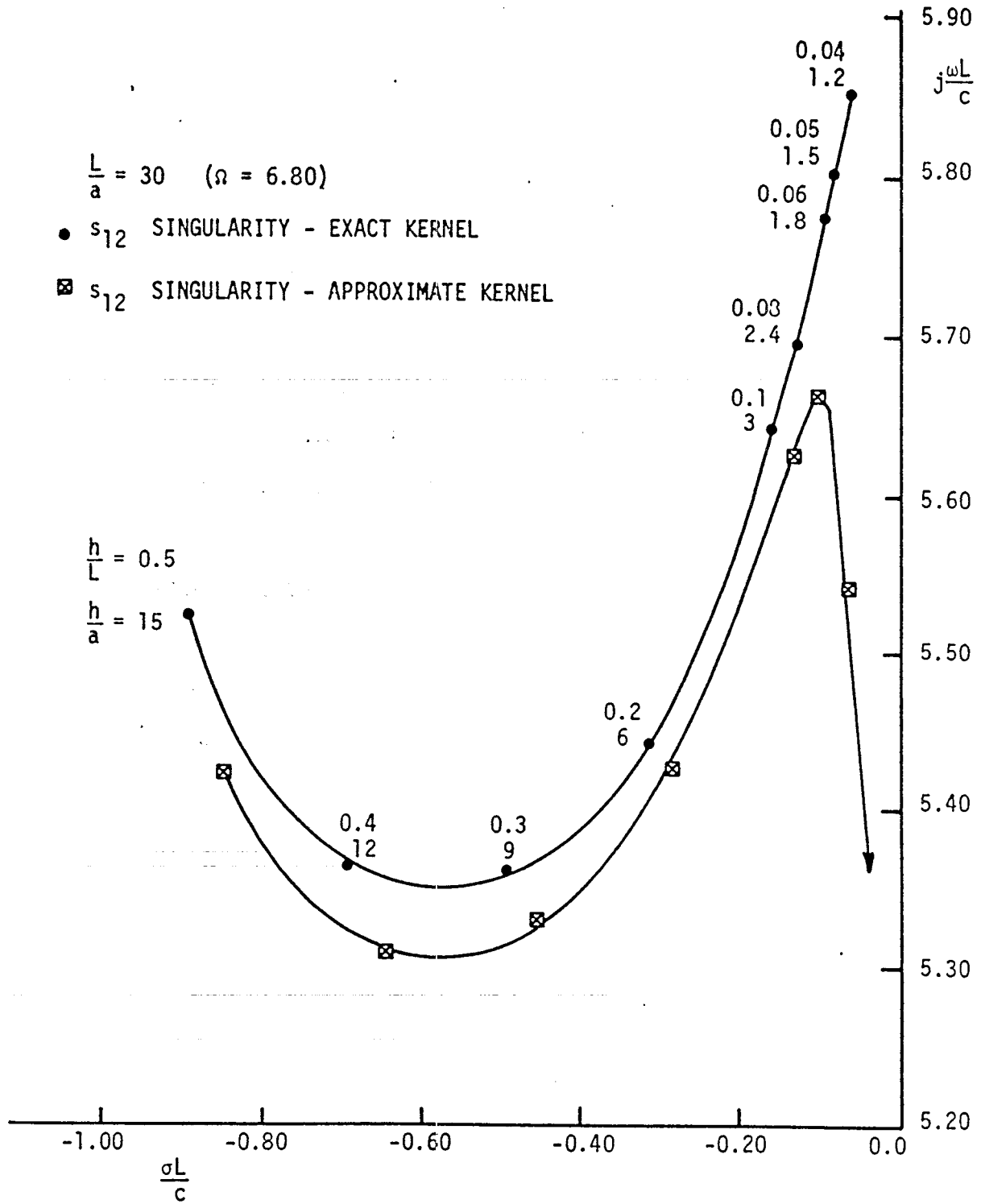
Figure 3-10. Trajectory of the Singularity Associated with the Second
Resonance of the Scatterer Itself as a Function of h/L or
h/a with L/a = 30 - Approximate and Exact Kernels

Table 3-10. Trajectory of the Singularity Associated with the
Second Resonance of the Scatterer as a Function
of h/L and h/a with L/a = 30.

L/a = 30   (Ω = 6.80)

h/L	h/a	S_{12} Singularity Location	
		Approximate Kernel	Exact Kernel
0.5	15	-0.8431+j5.4258	-0.8888+j.5.5322
0.4	12	-0.6403+j5.3128	-0.6857+j5.3652
0.3	9	-0.4535+j5.3299	-0.4917+j5.3602
0.2	6	-0.2826+j5.4324	-0.3138+j5.4481
0.1	3	-0.1275+j5.6261	-0.1515+j5.6406
0.08	2.4	-0.0989+j5.6614	-0.1212+j5.6983
0.06	1.8	-0.0646+j5.5414	-0.0916+j5.7669
0.04	1.2	-0.0064+j4.9373	-0.0619+j5.8585

$\dfrac{L}{a} = 20 \qquad (\Omega = 5.99)$

● s_{12} SINGULARITY – EXACT KERNEL

▨ s_{12} SINGULARITY – APPROXIMATE KERNEL

$\dfrac{h}{L} = 0.5$

$\dfrac{h}{a} = 10$

$j\dfrac{\omega L}{c}$

$\dfrac{\sigma L}{c}$
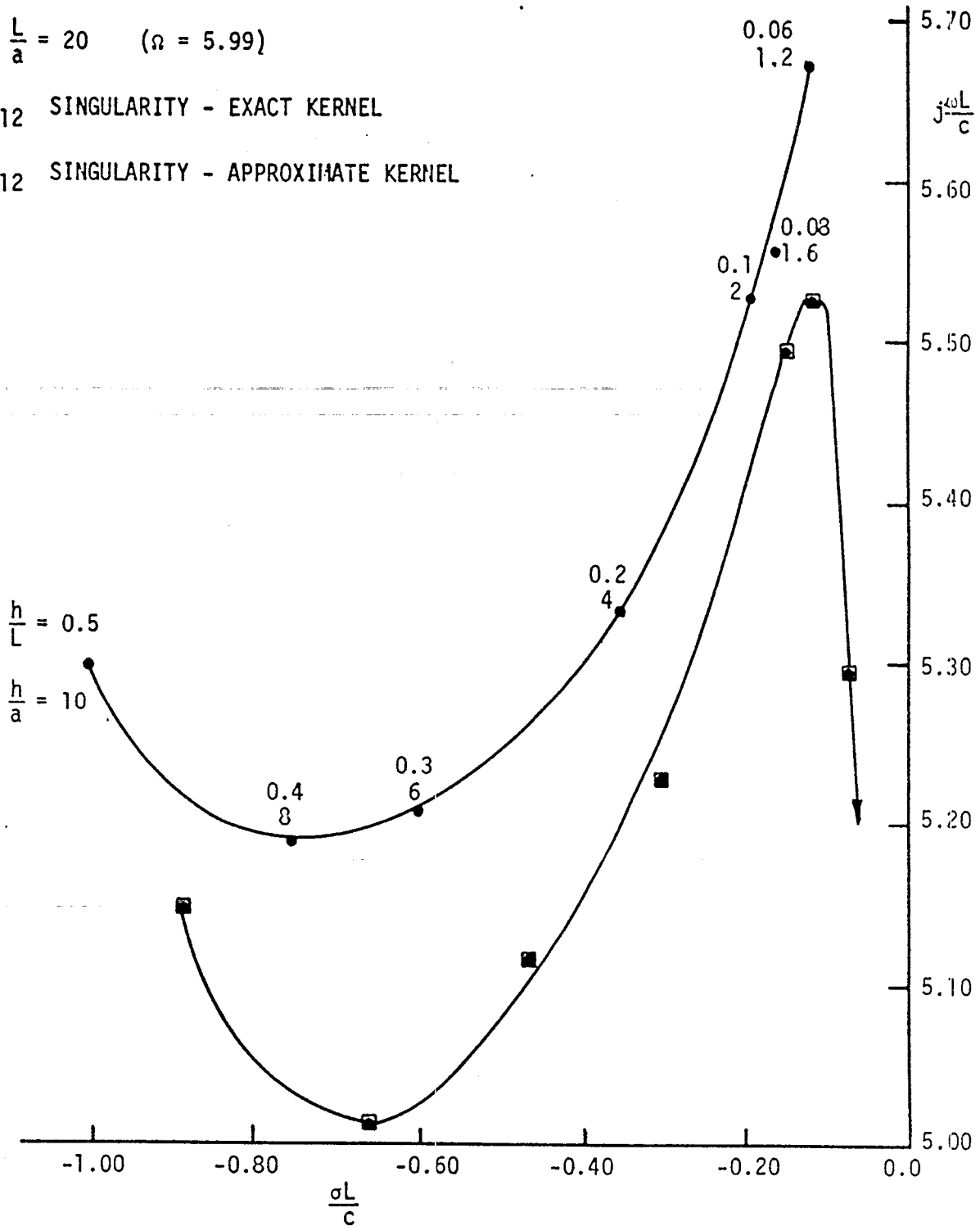
Figure 3-11. Trajectory of the Singularity Associated with the Second Resonance of the Scatterer Itself as a Function of h/L or h/a with L/a = 20 – Approximate and Exact Kernels

Table 3-11.   Trajectory of the Singularity Associated
with the Second Resonance of the Scatterer
as a Function of h/L and h/a with L/a = 20.

L/a = 20   (Ω = 5.99)

h/L	h/a	S_{12} Singularity Location	
		Approximate Kernel	Exact Kernel
0.5	10	-0.8848+j5.1403	-1.005+j5.296
0.4	8	-0.6617+j5.0947	-0.7459+j5.185
0.3	6	-0.4738+j5.1454	-0.5995+j5.208
0.2	4	-0.3032+j5.2737	-0.3558+j5.3131
0.1	2	-0.1452+j5.4913	-0.1851+j5.5265
0.08	1.6	-0.1146+j5.5214	-0.1509+j5.5936
0.06	1.2	-0.0711+j5.2959	-0.1131+j5.6887

L/a = 10 (Ω=4.605)

• s_{12} SINGULARITY - EXACT KERNEL

⊡ s_{12} SINGULARITY - APPROXIMATE KERNEL
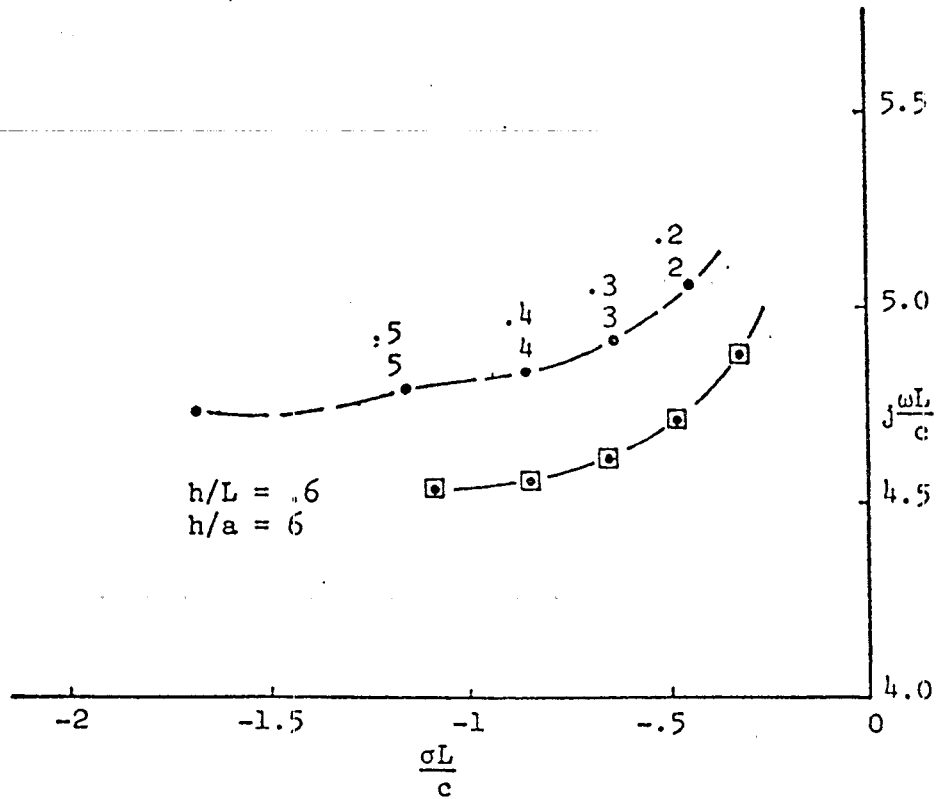
Figure 3-12. Trajectory of the Singularity Associated with the Second Resonance of the Scatterer Itself as a Function of h/L or h/a with L/a = 10 - Approximate and Exact Kernels

79

Table 3-12. Trajectory of the Singularity Associated with the Second
Resonance of the Scatterer Itself as a Function of h/L
or h/a with L/a = 10 - Approximate and Exact Kernels

L/a = 10   (Ω = 4.605)

h/L	h/a	s_{12} SINGULARITY LOCATION	
		APPROXIMATE KERNEL	EXACT KERNEL
.6	6	$-1.1060 + j4.5349$	$-1.7024 + j4.7277$
.5	5	$-.8479 + j4.5388$	$-1.1620 + j4.8091$
.4	4	$-.6571 + j4.5976$	$-.8720 + j4.8323$
.3	3	$-.4915 + j4.7092$	$-.6524 + j4.9144$
.2	2	$-.3366 + j4.8886$	$-.4560 + j5.0709$
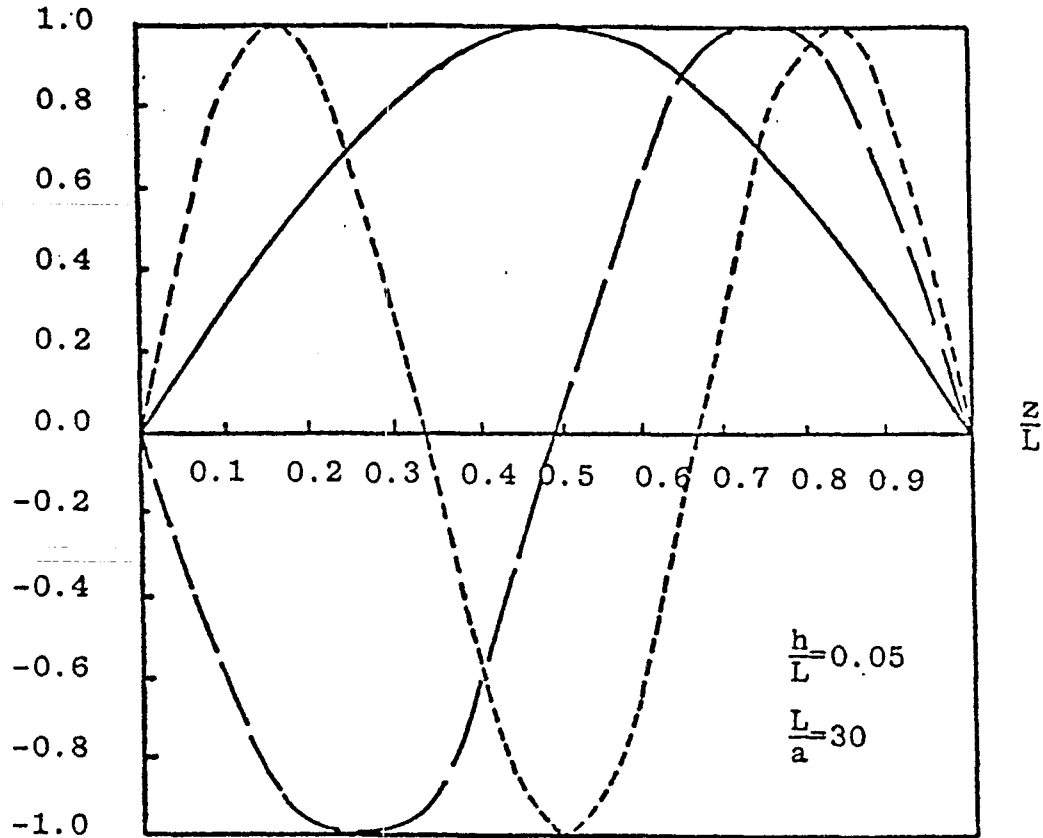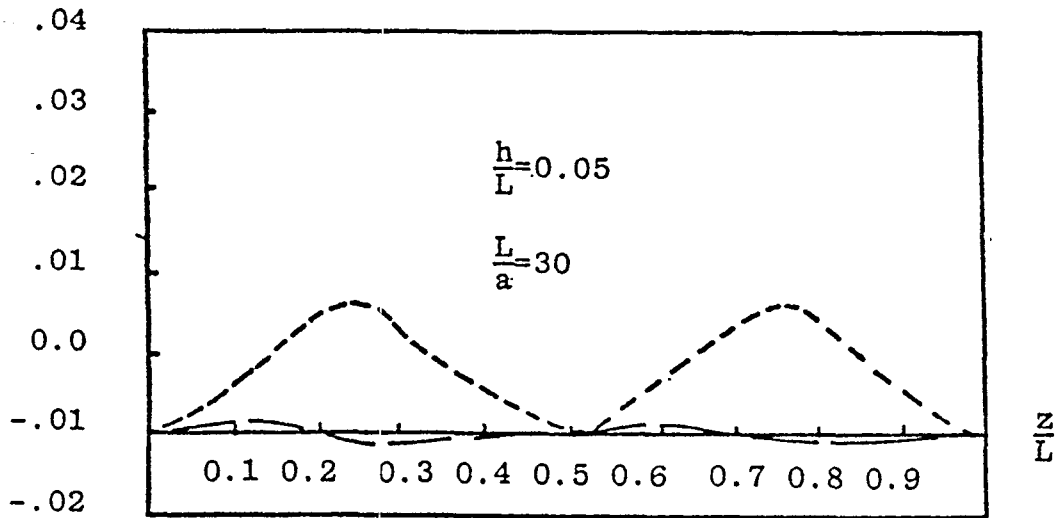
Figure 3-13 Real and Imaginary Parts of the First Three Normalized Natural Modes with h/L = 0.05, L/a = 30, and h/a =1.5

COUPLING COEFFICIENTS
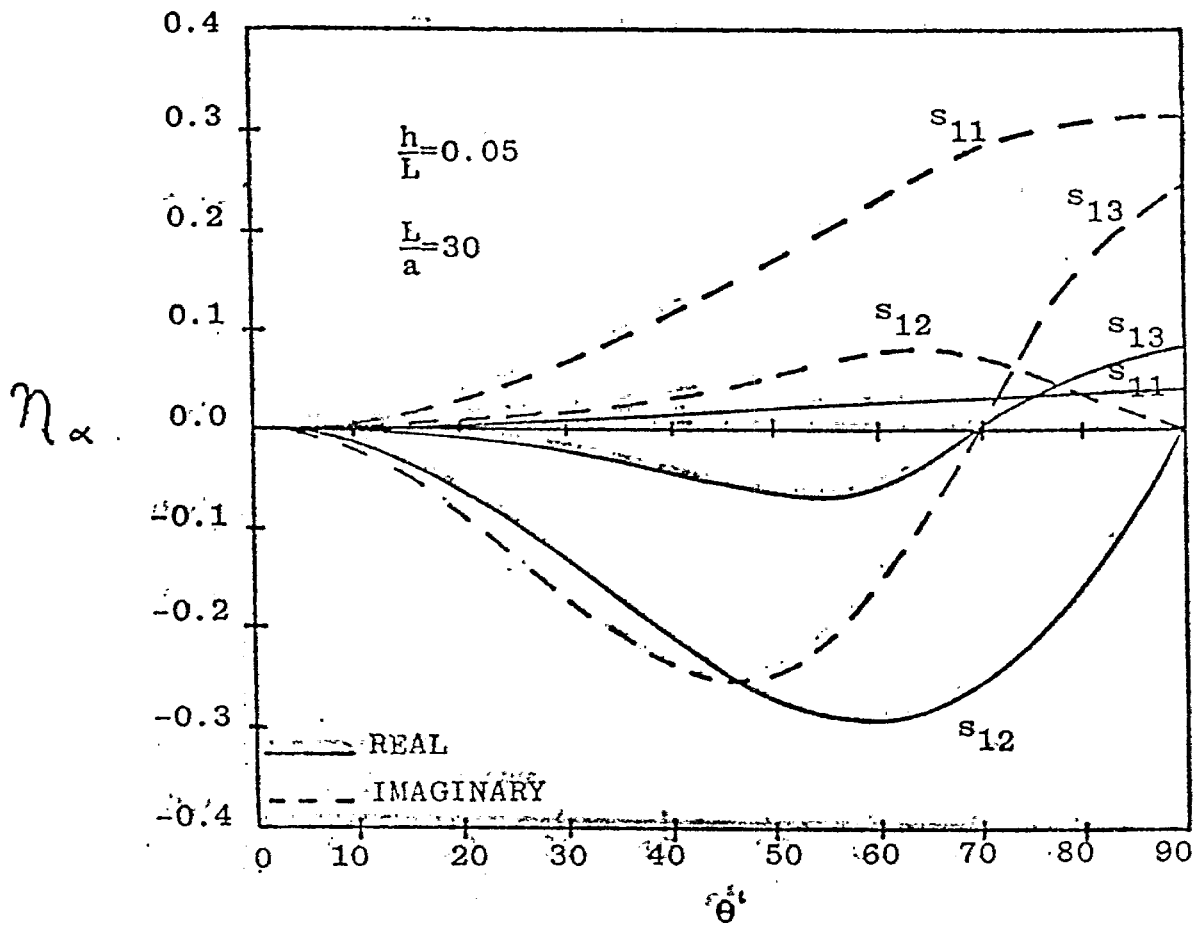
Figure 3-14 Real and Imaginary Parts of the Coupling Coefficients as a function of θ^i for the first three natural frequencies for $L/a = 30$, $h/L = 0.05$, and $h/a = 1.5$

COUPLING COEFFICIENTS
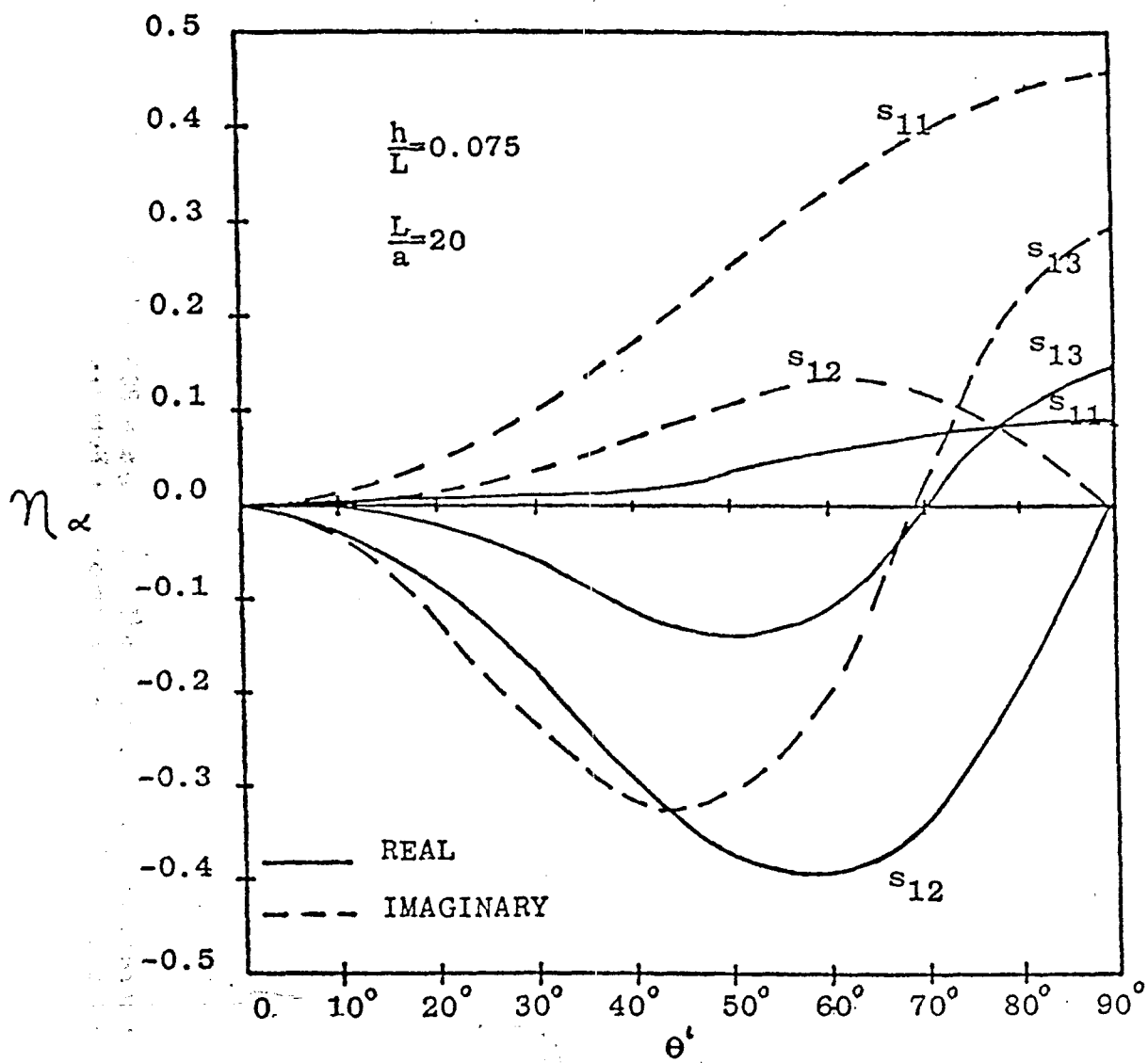
Figure 3-15 Real and Imaginary Parts of the Coupling Coefficients as a function of θ^i for the first three natural frequencies for L/a = 20, h/L = 0.075, and h/a = 1.5
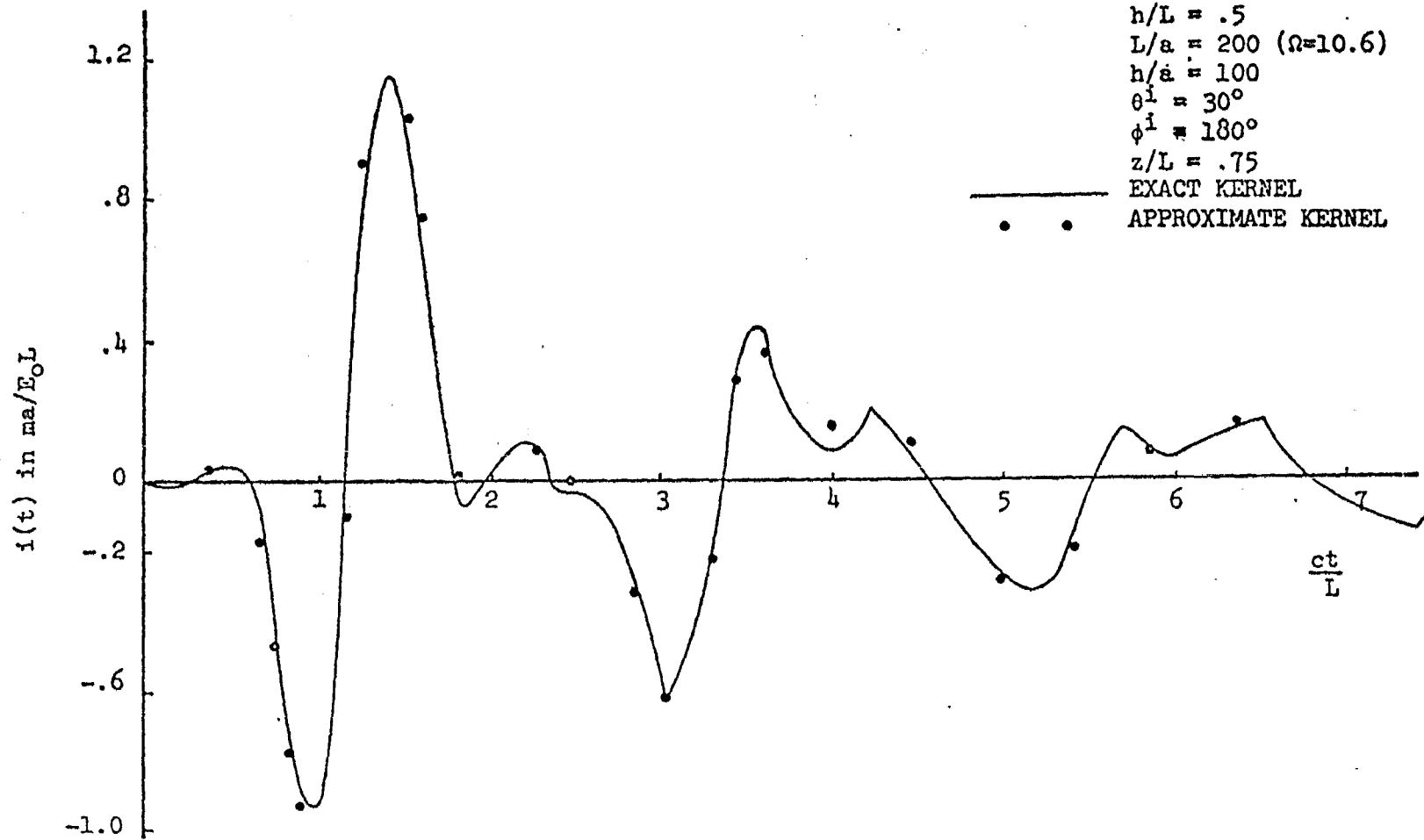
Figure 3-16. Current on Cylinder with h/L = .5, L/a = 200, h/a = 100, θ^i = 30°, ϕ^i = 180°, at z/L = .75 - Exact and Approximate Kernels
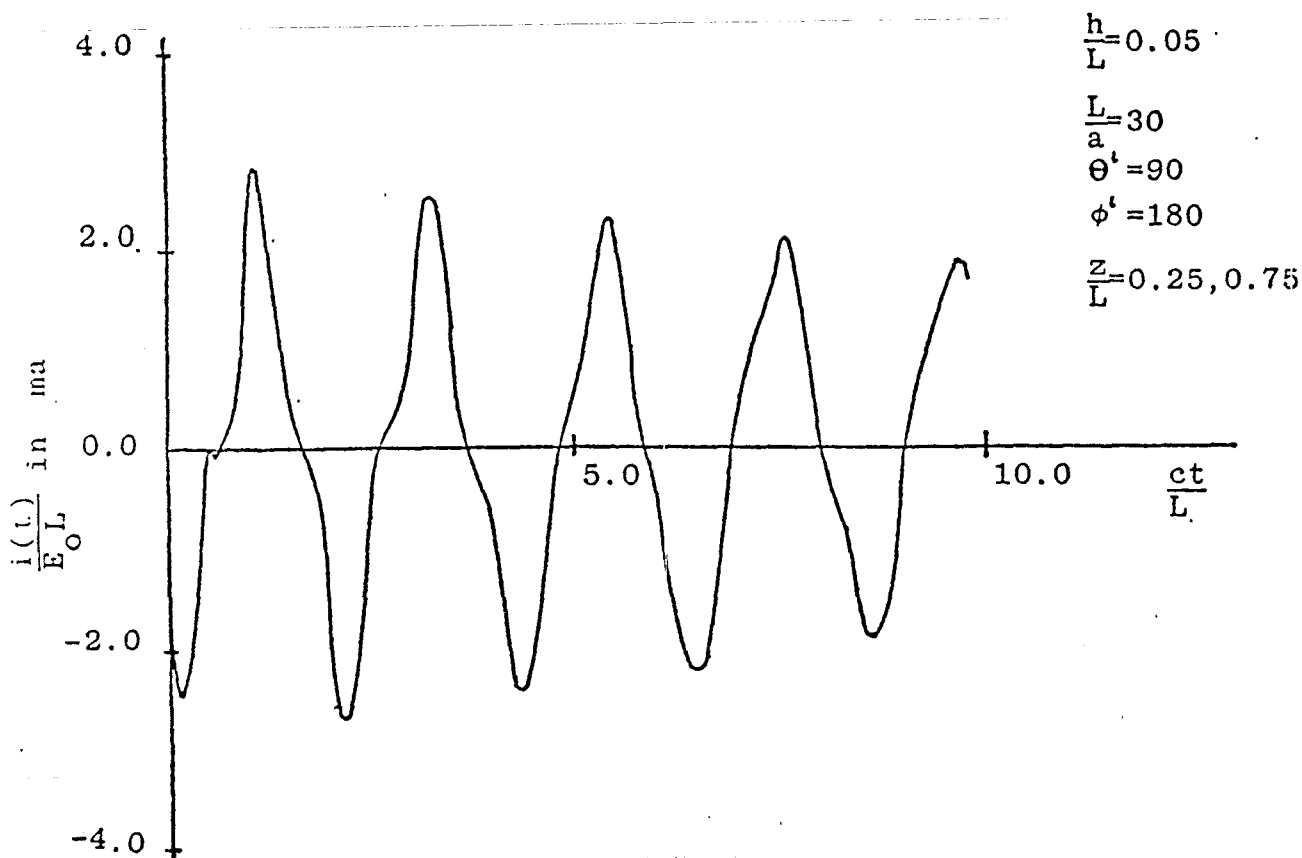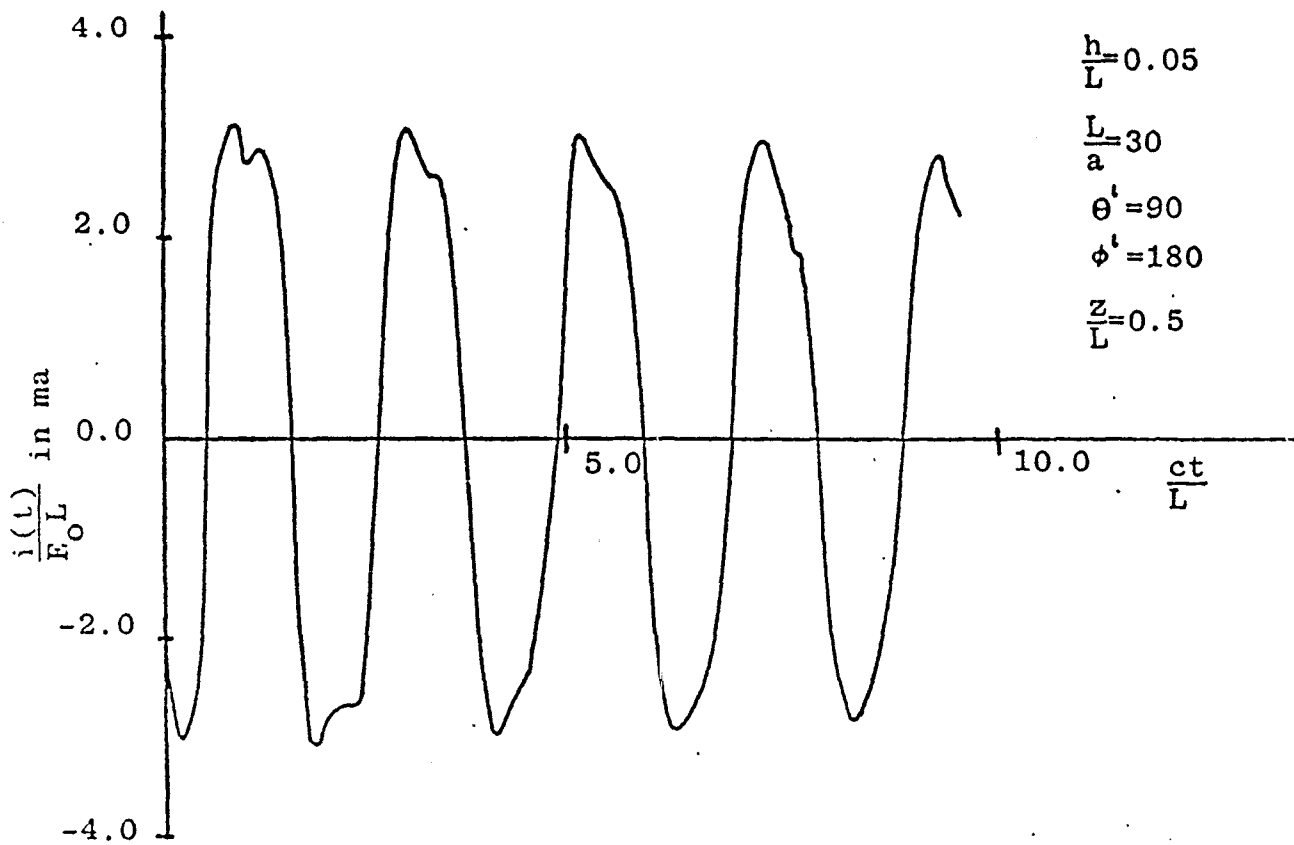
Figure 3-17. Current on Cylinder with h/L = 0.05, L/a = 30, h/a = 1.5, θ^i = 90° and ϕ^i = 180° at z/L = 0.25, 0.5, 0.75.
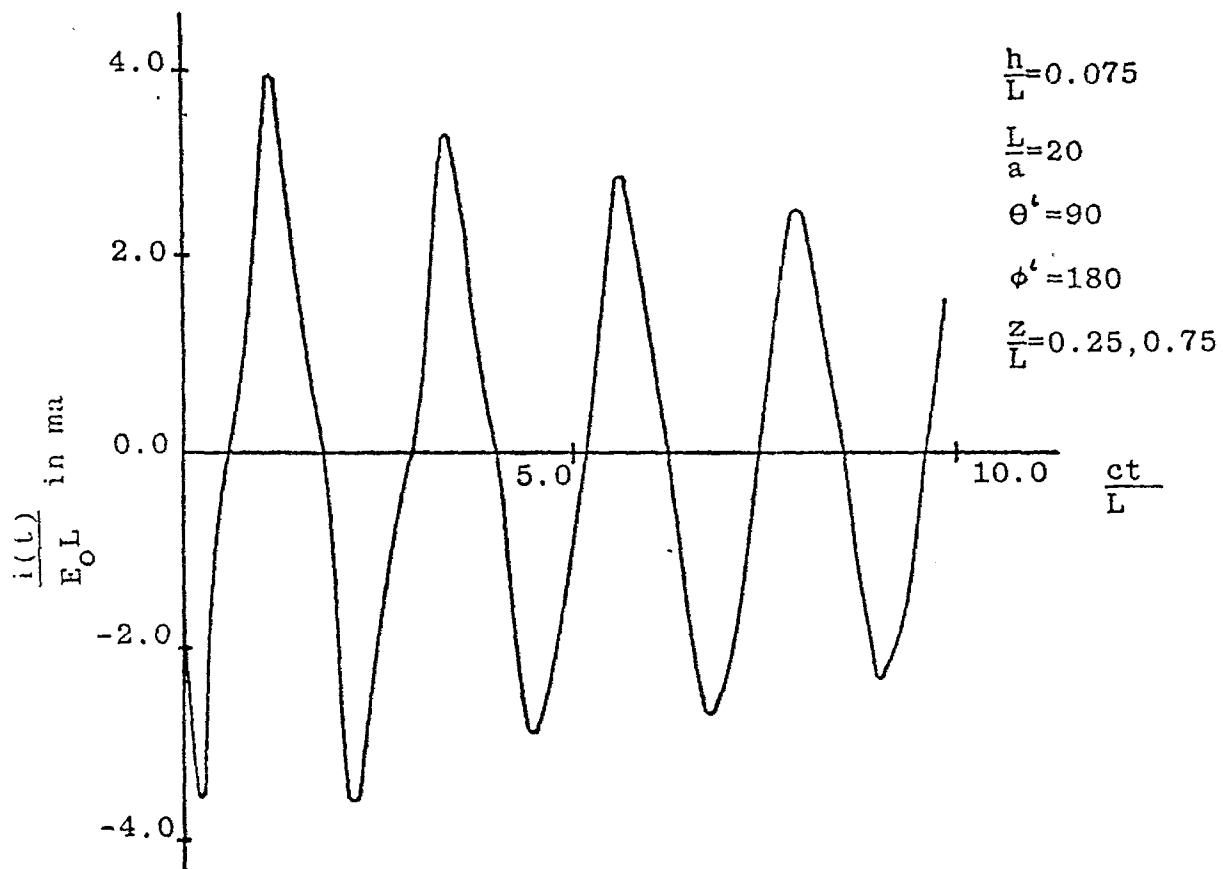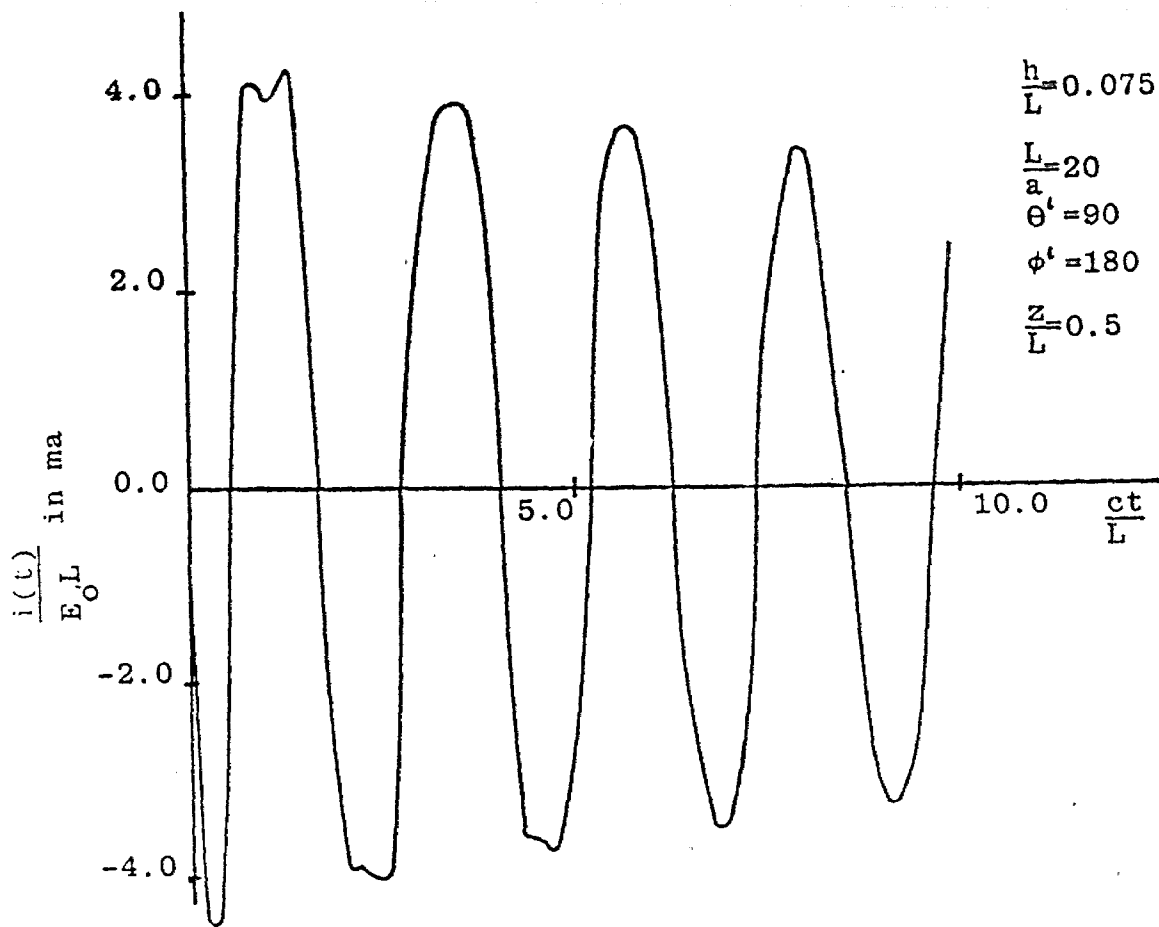
Figure 3-18. Current on Cylinder with h/L = 0.075, L/a = 20, h/a = 1.5, θ^i = 90° and ϕ^i = 180° at z/L = 0.25, 0.5, 0.75.
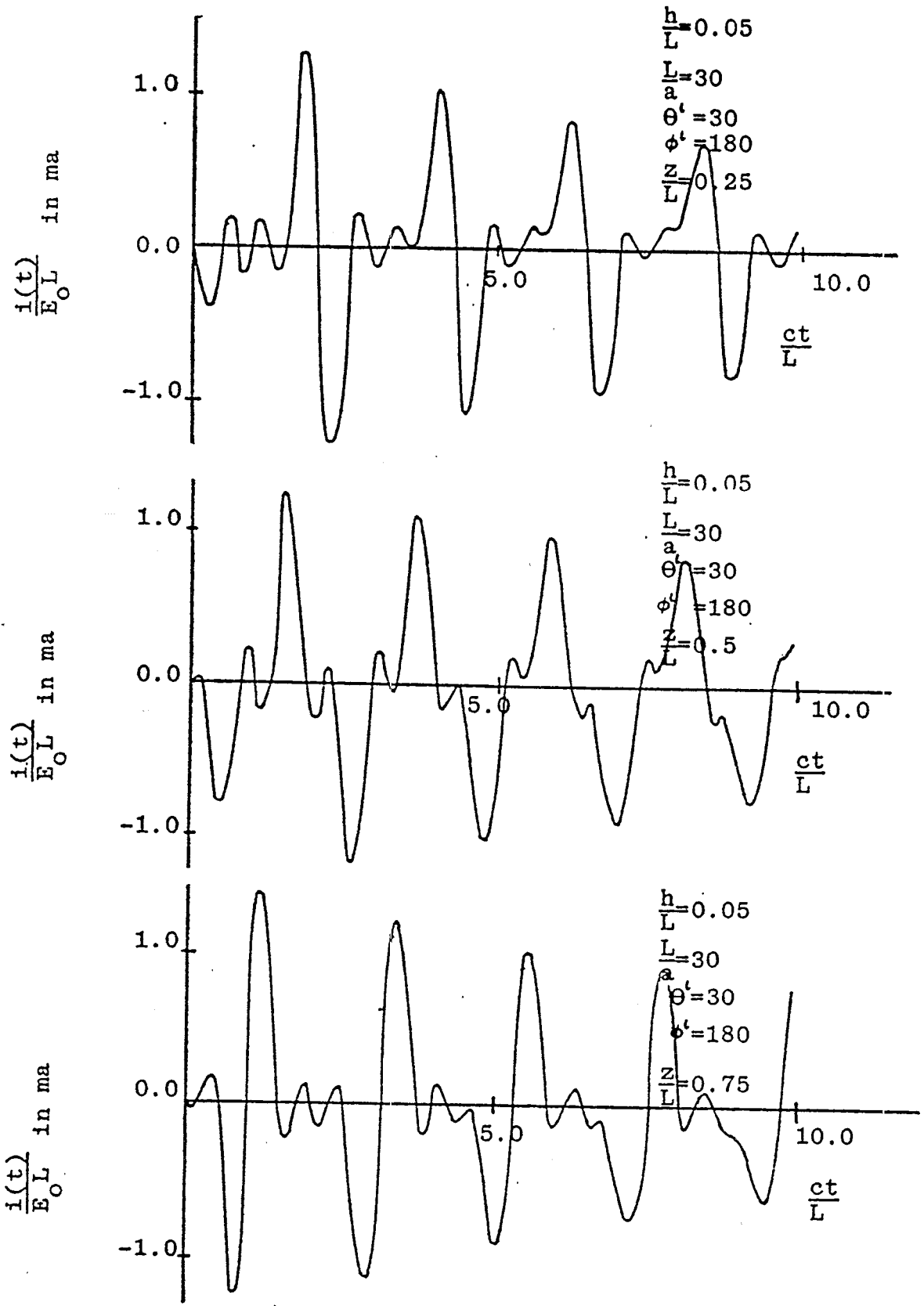
Figure 3-19. Current on Cylinder with h/L = 0.05, L/a = 30, h/a = 1.5,
$\theta^1 = 30°$ and $\phi^1 = 180°$ at z/L = 0.25, 0.5, 0.75.

IV. CONCLUSIONS

The use of an assumed circumferential variation for the axial currents induced on a thin cylinder, near a perfectly conducting ground plane, enhances the validity of analysis. "Thin-wire" approximations produce reasonable results when the thin cylindrical scatterer is more than one-tenth of its length above the ground plane. As the thin cylinder is brought near to the ground plane, the assumption of only axial variation of the currents begins to breakdown.

With the thin scatterer in free space or far removed from the ground plane, the computer time consumed in locating singularities through this formulation is roughly three times that required by Shumpert's [1] computer code. As the cylinder approaches the ground plane, the computer time required increases markedly. Nevertheless, when the scatterer is close, one cannot use "thin-wire" approximations - the exact kernel with allowance for nonuniform circumferential variation of the axial current is necessary. The usefulness of this formulation, due to the increased complexity and calculation time required, must be evaluated in light of the particular scattering problem being solved.

As noted previously, the assumed circumferential variation of the axial current is linked to a transmission line mode (TEM) approximation. The addition of higher order modes would improve the accuracy of the data obtained. However, the improvement in accuracy versus the increase in time and effort required would necessitate careful study.

REFERENCES

1. T. H. Shumpert, "EMP Interaction with a Thin Cylinder Above a Ground Plane Using the Singularity Expansion Method," Air Force Weapons Laboratory, Albuquerque, N. Mex., Interaction Note 182, June, 1973.

2. K. R. Umashankar and D. R. Wilton, "Analysis of an L-Shaped Wire Over a Conducting Ground Plane Using the Singularity Expansion Method," Air Force Weapons Laboratory, Albuquerque, N. Mex., Interaction Note 174, March 1974.

3. K. R. Umashankar and D. R. Wilton, "Transient Scattering by a Thin Wire in Free Space and Above Ground Plane Using the Singularity Expansion Method," University of Mississippi, University, Mississippi, Interaction Note 236, August 1974.

4. F. M. Tesche, "Numerical Determination of the Step Wave Response of a Thin-Wire Scattering Element Arbitrarily Located Above a Perfectly Conducting Ground Plane," Northrop Corporate Labs, Sensor and Simulation Note 141, February 1972.

5. H. J. Schmitt, C. W. Harrison, Jr., and C. S. Williams, Jr., "Calculated and Experimental Response of Thin Cylindrical Antennas to Pulse Excitation," IEEE Trans. Antennas Propagat., Vol. AP-14, pp. 120-127, March 1966.

6. R. W. P. King, Fundamental Electromagnetic Theory, Dover Publications, New York, N. Y., pp. 435-441, 1963.

7. William A. Imbriale and Paul G. Ingerson, "On Numerical Convergence of Moment Solutions of Moderately Thick Wire Antennas Using Sinusoidal Basis Functions," IEEE Trans. Antennas Propagat., Vol. AP-21, pp. 363-366, May 1973.

8. David C. Chang, "On the Electrically Thick Cylindrical Antenna," Radio Science, Vol. 2, pp. 1043-1060, September 1967.

9. R. F. Harrington, Field Computation by Moment Methods, MacMillan Co., New York, N. Y., pp. 62-81, 1968.

10. K. K. Mei, "On the Integral Equations of Thin Wire Antennas," IEEE Trans. Antennas Propagat., Vol. AP-13, pp. 374-378, May 1965.

11. R. Mittra (Editor), Computer Techniques for Electromagnetics, Pergamon Press, New York, N. Y., 1973.

12. R. W. P. King, The Theory of Linear Antennas, Harvard University Press, Cambridge, Mass., pp. 848-855, pp. 264-267, 1956.

13. R. W. Latham, K. S. H. Lee, "Pulse Radiation and Synthesis by an Infinite Cylindrical Antenna," Northrop Corporate Labs, Sensor and Simulation Note 73, February 1969.

14. B. A. Howarth, "Multiple-Scattering Resonances Between Parallel Conducting Cylinders," Can. J. Phys., Vol. 51, pp. 2415-2427, December 1973.

15. C. Leonard Bennett, Jr., and Walter L. Weeks, "Transient Scattering from Conducting Cylinders," IEEE Trans. Antennas Propagat., Vol. AP-18, pp. 627-633, September 1970.

16. R. F. Millar, "The Scattering of a Plane Wave by a Row of Small Cylinders," Can. J. Phys., Vol. 38, pp. 272-289, 1960.

17. G. O. Olaofe, "Scattering by Two Cylinders," Radio Sci., Vol. 5, pp. 1351-1360, November 1970.

18. R. F. Harrington, Time-Harmonic Electromagnetic Fields, McGraw-Hill, New York, N. Y., 1961.

19. Albert W. Adey, "Scattering of Electromagnetic Waves by Long Cylinders," Electronic and Radio Engineer, Vol. 35, pp. 149-158, April 1958.

20. Mogen G. Andreasen, "Scattering from Parallel Metallic Cylinders with Arbitrary Cross Sections," IEEE Trans. Antennas Propagat., Vol. AP-12, pp. 746-754, November 1964.

21. Victor Twersky, "Multiple Scattering of Radiation by an Arbitrary Planar Configuration of Parallel Cylinders and by Two Parallel Cylinders," J. Appl. Phy., Vol. 23, pp. 407-414, April 1952.

22. Cheng C. Kao, "Measurements of Surface Currents on a Finite Circular Tube Illuminated by Electromagnetic Wave," IEEE Trans. Antennas Propagat. (Commun.), Vol. AP-18, pp. 569-573, July 1970.

23. Cheng C. Kao, "Electromagnetic Scattering from a Finite Tubular Cylinder: Numerical Solutions," Radio Sci., Vol. 5, pp. 617-624, March 1970.

24. Cheng C. Kao, "Three-Dimensional Electromagnetic Scattering from a Circular Tube of Finite Length," J. App. Phys., Vol. 40, pp. 4723-4740, November 1969,

25. W. E. Williams, "Diffraction by a Cylinder of Finite Length," Proc. Cambridge Phil. Soc., Vol. 52, pp. 322-335, 1956.

26. J. J. Bowman, T. B. A. Senior and P. L. E. Uslenghi (Editors), Electromagnetic and Acoustic Scattering by Simple Shapes, North-Holland Publishing Co., Amsterdam, Holland, 1969.

27. John D. Kraus and Keith R. Carver, Electromagnetics, McGraw-Hill, New York, N. Y., pp. 81-86, 1973.

28. R. F. Harrington, "Matrix Methods for Fields Problems," Proc. IEEE, Vol. 55, pp. 136-149, February 1967.

29. P. C. Waterman, "Matrix Formulation of Electromagnetic Scattering," Proc. IEEE, Vol. 53, pp. 805-812, August 1965.

30. Lennart Marin, R. W. Latham, "Analytical Properties of the Field Scattered by a Perfect Conducting, Finite Body," Northrop Corporate Labs, Interaction Note 92, January 1972.

31. Carl E. Baum, "On the Singularity Expansion Method for the Case of First Order Poles," Air Force Weapons Laboratory, Albuquerque, N. Mex., Interaction Note 129, October 1972.

32. Carl E. Baum, "Use of Locally Quasi-Static Modes on Thin Structures to Expand the Electromagnetic Response," personal communication, 1975.

33. Carl E. Baum, "On the Singularity Expansion Method for the Solution of Electromagnetic Interaction Problems," Air Force Weapons Laboratory, Albuquerque, N. Mex., Interaction Note 88, December 1971.

34. Lennart Marin, "Natural-Mode Representation of Transient Scattering from Rotationally Symmetric, Perfectly Conducting Bodies and Numerical Results for a Prolate Spheroid," Northrop Corporate Labs, Interaction Note 119, September 1972.

35. Lennart Marin, R. W. Latham, "Analytical Properties of the Field Scattered by a Perfect Conducting, Finite Body," Northrop Corporate Labs, Interaction Note 92, January 1972.

36. F. M. Tesche, "Application of the Singularity Expansion Method to the Analysis of Impedance Loaded Linear Antennas," Dikewood Corporation, Sensor and Simulation Note 177, May 1973.

37. F. M. Tesche, "On the Singularity Expansion Method as Applied to Electromagnetic Scattering from Thin Wires," Dikewood Corporation, Interaction Note 102, April 1972.

38. R. W. P. King, Fundamental Electromagnetic Theory, Dover Publications, New York, N.Y., pp. 305-311, 1963.

39. S. Ramo, J. R. Whinnery, and J. Van Duzer, Fields and Waves in Communication Electronics, John Wiley and Sons, Inc., New York, N. Y., pp. 650-651, 1965.

40. C. D. Taylor, "On the Circumferential Current and Charge Distributions of Circular Cylinders Near a Ground Plane", Air Force Weapons Laboratory, Albuquerque, N. Mex., Interaction Note 138, March 1973.

41. J. Van Bladel, Electromagnetic Fields, McGraw-Hill, New York, N. Y., p. 492, 1964.

42. E. C. Jordan and K. G. Balmain, Electromagnetic Waves and Radiating Systems, Prentice-Hall, Inc., Englewood Cliffs, N. J., pp. 133-136, 1968.

43. F. M. Tesche, "Evaluation of the Surface Integral In the E-Field Integral Equations for Wire Antennas," Air Force Weapons Laboratory, Albuquerque, N. Mex., Mathematics Note 29, September 1973.

44. J. W. Dettman, Mathematical Methods in Physics and Engineering, McGraw-Hill, New York, N. Y., 1969.

45. Ian H. Sneddon, The Use of Integral Transforms, McGraw-Hill, New York, N. Y., 1972.

46. Olav Einarsson, "A Comparison Between Tube-Shaped and Solid Cylindrical Antennas," IEEE Trans. Antennas Propagat., Vol. AP-14, pp. 31-37, January, 1966.

47. P. J. Davis and Philip Rabinowitz, Methods of Numerical Integration, Academic Press, New York, N. Y., 1975.

48. M. E. Van Valkenburg, Network Analysis, Prentice-Hall, Englewood Cliffs, N. J., 1964.

49. H. B. Dwight, Tables of Integrals and Other Mathematical Data, MacMillan Co., Toronto, Canada, 1969.

50. Samuel Selby (Editor), Standard Mathematical Tables, Chemical Rubber Co., Cleveland, Ohio, 1968.

APPENDIX A

EVALUATION OF A PARTICULAR SINGULAR INTEGRAL

This appendix deals with the evaluation of a particular singular integral, namely

$$T = \int_{-\frac{\Delta}{2}}^{\frac{\Delta}{2}} \int_{0}^{2\pi} \frac{1}{1 + (a/h)\cos\phi} \, \frac{e^{-\gamma r}}{r} \, d\phi \, dz \,, \tag{A1.1}$$

where

$$r = [z^2 + d^2 \sin^2 \tfrac{\phi}{2}]^{1/2} \,. \tag{A1.2}$$

As shown by Tesche [43], in order to accurately treat the integration the singularity can be integrated analytically. Interchanging the order of integration and rearranging the form gives

$$T = \int_{0}^{2\pi} \frac{1}{1 + (a/h)\cos\phi} \int_{-\frac{\Delta}{2}}^{\frac{\Delta}{2}} \frac{e^{-\gamma r}}{r} \, dz \, d\phi \,. \tag{A1.3}$$

Expanding $e^{-\gamma r}$ in a Taylor series about $r=0$,

$$e^{-\gamma r} = 1 - \gamma r + \frac{r^2}{2!} \gamma^2 - \frac{r^3}{3!} \gamma^3 + \dots (-1)^n \frac{r^n}{n!} \gamma^n \dots \tag{A1.4}$$

and retaining only the first two terms (this truncation places restrictions on the problem, which are mentioned on page 47) yields

$$e^{-\gamma r} \simeq 1 - \gamma r \tag{A1.5}$$

Thus,

$$T \simeq \int_0^{2\pi} \frac{1}{1 + (a/h)\cos \phi} \int_{-\frac{\Delta}{2}}^{\frac{\Delta}{2}} \left(\frac{1}{r} - \gamma\right) dz \, d\phi$$

$$= \int_0^{2\pi} \frac{1}{1 + (a/h)\cos \phi} \left\{ \int_{-\frac{\Delta}{2}}^{\frac{\Delta}{2}} \frac{1}{r} \, dz - \gamma \int_{-\frac{\Delta}{2}}^{\frac{\Delta}{2}} dz \right\} \, d\phi \qquad (A1.6)$$

$$T = -\gamma\Delta \int_0^{2\pi} \frac{1}{1 + (a/h)\cos \phi} \, d\phi + \int_0^{2\pi} \frac{1}{1 + (a/h)\cos \phi} \, \cdot$$

$$\left[\int_{-\frac{\Delta}{2}}^{\frac{\Delta}{2}} \frac{1}{r} \, dz \right] d\phi \qquad , \qquad (A1.7)$$

with r given by (A1.2). Tesche [43] used Dwight's equation (200.01) [49] to give

$$\int_{-\frac{\Delta}{2}}^{\frac{\Delta}{2}} \frac{1}{r} \, dz = 2 \ln \left[\frac{\Delta}{4a} + [(\frac{\Delta}{4a})^2 + \sin^2 \frac{\phi}{2}]^{1/2} \right] -$$

$$2 \ln (\sin \phi/2). \qquad (A1.8)$$

Thus,

$$T \simeq -\gamma\Delta \int_0^{2\pi} \frac{1}{1 + (a/h)\cos \phi} \, d\phi + 2 \int_0^{2\pi} \frac{1}{1 + (a/h)\cos \phi} \, \cdot$$

$$\left\{ \ln \left[\frac{\Delta}{4a} + \left[(\frac{\Delta}{4a})^2 + \sin^2 \phi/2 \right]^{1/2} \right] - \ln[\sin \phi/2] \right\} \, d\phi$$

$$(A1.9)$$

$$T \simeq -\gamma\Delta \int_0^{2\pi} \frac{1}{1 + (a/h)\cos \phi} \, d\phi + 2 \int_0^{2\pi} \frac{1}{1 + (a/h)\cos \phi} \, \cdot$$

$$\ln \left(\frac{\Delta}{4a} + [(\frac{\Delta}{4a})^2 - \sin^2 \phi/2]^{1/2} \right) \, d\phi$$

$$-2 \int_0^{2\pi} \frac{1}{1 + (a/h)\cos \phi} \, \ln[\, \sin (\phi/2)] \, d\phi. \qquad (A1.10)$$

94

Provided $(a/h)^2 < 1$, which is satisfied (see Figure 2-1), any standard integral table [50] (for instance equation 509, page 425 of this reference) gives

$$\int_0^{2\pi} \frac{1}{1 +(a/h)\cos \phi} \, d\phi = 2\pi[1-(a/h)^2]^{-1/2} \quad . \tag{A1.11}$$

Therefore,

$$T \simeq \frac{-2\pi\gamma\Delta}{[1-(a/h)^2]^{1/2}} + 2 \int_0^{2\pi} \frac{1}{1 +(a/h)\cos \phi} \ln \left(\frac{\Delta}{4a} + [(\frac{\Delta}{4a})^2 + \right.$$

$$\left. \sin^2 \phi/2]^{1/2} \right) d\phi \quad -2 \int_0^{2\pi} \frac{1}{1 +(a/h)\cos \phi} \cdot$$

$$\ln[\sin \phi/2] \, d\phi \quad . \tag{A1.12}$$

The second term on the right-hand side of this equation is non-singular and easily determined by machine integration, but the last term on the right-hand side has a singularity. Let

$$A = 2 \int_0^{2\pi} \frac{\ln (\sin \phi/2)}{1 +(a/h)\cos \phi} \, d\phi \quad . \tag{A1.13}$$

From Dwight [49], page 140, equation (603.2),

$$\ln|\sin x| = -\ln 2 - \cos 2x - \frac{\cos 4x}{2} - \frac{\cos 6x}{3} \quad \ldots \tag{A1.14}$$

for $\sin x \neq 0$.

Let $x = \phi/2$ for ϕ between 0 and 2π, such that

$$|\sin x| = |\sin \phi/2| = \sin \phi/2 \tag{A1.15}$$

and

$$\ln(\sin \phi/2) = -\ln 2 - \sum_{n=1}^{\infty} 1/n \cos n\phi \quad . \quad (A1.16)$$

This allows A to be expressed as

$$A = 2 \int_0^{2\pi} \frac{(-\ln 2)}{1 + (a/h)\cos \phi} \, d\phi + 2 \int_0^{2\pi} \frac{-\sum_{n=1}^{\infty} 1/n \cos n\phi}{1 + (a/h)\cos \phi} \, d\phi \quad (A1.17)$$

$$A = \frac{-4\pi \ln 2}{[1-(a/h)^2]^{1/2}} - 2 \sum_{n=1}^{\infty} 1/n \int_0^{2\pi} \frac{\cos n\phi}{1 + (a/h)\cos \phi} \, d\phi \quad . \quad (A1.18)$$

Continuing with the last term on the right-hand side,

$$\int_0^{2\pi} \frac{\cos n\phi}{1 + (a/h)\cos \phi} \, d\phi = \int_0^{\pi} \frac{\cos n\phi}{1 + (a/h)\cos \phi} \, d\phi + \int_{\pi}^{2\pi} \frac{\cos n\phi}{1 + (a/h)\cos \phi} \, d\phi \quad . \quad (A1.19)$$

Consider the last term on the right-hand side of (A1.19). The transformation, $\phi = \beta$ yields

$$\int_{\pi}^{2\pi} \frac{\cos n\phi}{1 + (a/h)\cos \phi} \, d\phi = \int_{-2\pi}^{-\pi} \frac{\cos n\beta}{1 + (a/h)\cos \beta} \, d\beta \quad . \quad (A1.20)$$

Letting $\theta = \beta + 2\pi$ results in

$$\int_{\pi}^{2\pi} \frac{\cos n\phi}{1 + (a/h)\cos \phi} \, d\phi = \int_0^{\pi} \frac{\cos n(\theta - 2\pi)}{1 + (a/h)\cos (\theta - 2\pi)} \, d\theta; \quad (A1.21)$$

and since $\cos [n(\theta - 2\pi)] = \cos n\theta$,

$$\int_{\pi}^{2\pi} \frac{\cos n\phi}{1 + (a/h)\cos \phi} \, d\phi = \int_0^{\pi} \frac{\cos n\theta}{1 + (a/h)\cos \theta} \, d\theta \quad . \quad (A1.22)$$

Therefore (A1.19) can be expressed as

$$\int_0^{2\pi} \frac{\cos n\phi}{1 + (a/h)\cos \phi} \, d\phi = 2 \int_0^{\pi} \frac{\cos n\phi}{1 + (a/h)\cos \phi} \, d\phi \quad . \quad (A1.23)$$

From Dwight [49], page 219, equation (858.536) is

$$\int_0^{\pi} \frac{\cos n\phi}{1 + (a/h)\cos \phi} \, d\phi = \frac{\pi \left[[1-(a/h)^2]^{1/2}-1 \right]^n}{(a/h)^n[1-(a/h)^2]^{1/2}} \quad , \quad (A1.24)$$

for $0 < a/h < 1$, $n = 0,1,\ldots$.

Substituting this expression into (A1.23) and then placing (A1.23) back into (A1.17),

$$A = -4\pi \ln(2)[1-(a/h)^2]^{-1/2}$$

$$-2 \sum_{n=1}^{\infty} 1/n \left(\frac{2\pi \left[[1-(a/h)^2]^{1/2}-1 \right]^n}{(a/h)^n[1-(a/h)^2]^{1/2}} \right)$$

$$A = \frac{-4\pi}{\sqrt{1-(a/h)^2}} \left[\ln 2 + \sum_{n=1}^{\infty} 1/n(h/a)^n \left[\sqrt{1-(a/h)^2}-1 \right]^n \right] \quad . \quad (A1.25)$$

Simple manipulation shows that

$$1/n(h/a)^n[\sqrt{1-(a/h)^2}-1]^n = 1/n \left[\sqrt{(h/a)^2-1} - h/a \right]^n \quad .$$

Let

$$b = \sqrt{(h/a)^2-1} - h/a \quad , \quad (A1.26)$$

such that

$$A = \frac{-4\pi}{\sqrt{1-(a/h)^2}} \left[\ln 2 + \sum_{n=1}^{\infty} 1/n \, b^n \right] \quad . \quad (A1.27)$$

Since $a < h < \infty$ (see Figure 2-1)

97.

$$\lim_{h \to a} b = -1$$

and by L' Hospital's rule

$$\lim_{h \to \infty} b = \lim_{h \to \infty} - \frac{(a/h)}{\sqrt{1-(a/h)^2}} = 0.$$

Conclude that for $a < h < \infty$, $-1 < b < 0$. Let $c = -b$, such that $0 < c < 1$, then

$$A = \frac{-4\pi}{\sqrt{1-(a/h)^2}} \left[\ln2 + \sum_{n=1}^{\infty} \frac{(-1)^n}{n} c^n \right] . \tag{A1.28}$$

From [50], page 432, a logarithmic series has the form of

$$\ln(1+x) = x - 1/2x^2 + 1/3x^3 - 1/4x^4 + \dots , \tag{A1.29}$$

for $-1 < x < 1$. Thus,

$$-\ln(1+c) = -c + 1/2c^2 - 1/3c^3 + 1/4c^4 - \dots . \tag{A1.30}$$

since $0 < c < 1$. With

$$-\ln(1+c) = \sum_{n=1}^{\infty} \frac{(-1)^n}{n} c^n ,$$

(A1.28) is written as

$$A = \frac{-4\pi}{\sqrt{1-(a/h)^2}} \left[\ln2 - \ln(c+1) \right] , \tag{A1.31}$$

with

$$c = h/a \left[1 - [1-(a/h)^2]^{1/2} \right] . \tag{A1.32}$$

Using this expression for A, originally defined by (A1.13), in the equation for T (A1.12) gives the final result

$$T \simeq \frac{-2\pi\gamma\Delta}{\sqrt{1 - (a/h)^2}} + 2 \int_0^{2\pi} \frac{1}{1 + (a/h)\cos\phi} \cdot$$

$$\ln\left\{ \frac{\Delta}{4a} + \sqrt{\left(\frac{\Delta}{4a}\right)^2 + \sin^2\phi/2} \right\} d\phi +$$

$$\frac{4\pi}{\sqrt{1 - (a/h)^2}} \left\{ \ln 2 - \ln\left[h/a + 1 - \sqrt{(h/a)^2 - 1} \right] \right\}. \quad (A1.33)$$

This function can be easily evaluated numerically since the integrand is not singular.

99